



**FLORIDA HURRICANE LOSS MITIGATION  
PROGRAM  
2017 ANNUAL REPORT**

*January 1, 2018*

Prepared by  
Florida Division of Emergency Management

Rick Scott  
Governor

Wes Maul  
Director

## TABLE OF CONTENTS

Executive Summary.....	3
Background.....	4
Program Activities.....	6
Program Analysis.....	7
Program Goals and Recommendations.....	11
Appendix A: Annual Report for Mobile Home Tie Down Program	
Appendix B: Annual Report for Florida International University	

## EXECUTIVE SUMMARY

This document satisfies subsection 215.559 (6) Florida Statutes (F.S.), by providing a full report and accounting of activities and evaluation of such activities. The time period covered by this report is July 1, 2016- June 30, 2017 or State Fiscal Year (SFY) 2017. Based on section 215.559 (1), F.S., the Hurricane Loss Mitigation Program is established in the Division of Emergency Management. The Division receives an annual appropriation of \$10 million from the investment income of the Florida Hurricane Catastrophe Fund authorized under the Florida General Appropriation Act and Section 215.555 (7) (c), F.S. The Public Shelter Retrofit Program, Tallahassee Community College's (TCC) Mobile Home Tie-Down Program, Florida International University's (FIU) Hurricane Research Program and Mitigation Program, account for a combined \$6,500,000 or sixty-five (65%) percent of the SFY 2017 \$10 million appropriation. The remaining thirty-five (35%) percent is used to implement a residential wind retrofit program that includes both physical wind retrofits of Florida residences and public outreach for education about retrofits to citizens and local government officials and their staff. In compliance with the appropriation language for SFY 2017, these funds were distributed as required.

The Shelter Retrofit Program and TCC's Mobile Home Tie-Down Program have separate reporting requirements as stated in Section 252.385, F.S., and Section 215.559 (2) (a), F.S., respectively. A separate report from FIU is also required. The Shelter Retrofit Program Report is prepared annually and separately submitted to the Governor and the Legislature pursuant to Section 252.385, F.S. The TCC and FIU reports are attached.

## BACKGROUND

In the aftermath of Hurricane Andrew, the Florida Legislature created a series of programs to stabilize the economy and insurance industry. These programs consist of the following:

- Citizens Property Insurance Corporation (formed from a merger of the Florida Windstorm Underwriting Association and the Florida Residential Property and Casualty Joint Underwriting Association), the state insurance plan for residents unable to obtain a conventional homeowners insurance policy;
- The Florida Hurricane Catastrophe Fund, section 215.555 F.S., a re-insurance fund established to limit insurance exposure after a storm;
- The Bill Williams Residential Safety and Preparedness Act, which in 1999 created the Hurricane Loss Mitigation Program, section 215.559 F. S., with an annual appropriation of \$10 million.

Based on Section 215.559 (1) F. S., the Hurricane Loss Mitigation Program is established in the Division of Emergency Management. The Division receives an annual appropriation of \$10 million from the investment income of the Florida Hurricane Catastrophe Fund authorized under the Florida General Appropriation Act and Section 215.555 (7) (c) F. S. The purpose of the \$10 million annual appropriation is to provide funding to local governments, State agencies, public and private educational institutions, and nonprofit organizations to support programs that improve hurricane preparedness, reduce potential losses in the event of a hurricane, and to provide research and education on how to reduce hurricane losses.

The funds are also to be used for programs that will assist the public in determining the appropriateness of particular upgrades to structures and in the financing of such upgrades, or to protect local infrastructure from potential damage from a hurricane. Section 215.559 F.S., establishes minimum funding levels for specific program areas and creates an Advisory Council to make recommendations on developing programs.

### **Specific Program Areas and Funding Levels**

**Shelter Retrofits** - According to Section 215.559 (2) (a) F. S., \$3 million of the annual \$10 million appropriation for the Hurricane Loss Mitigation Program is directed to retrofit existing public facilities to enable them to be used as public shelters. An annual report of the state's shelter retrofit program, entitled the Shelter Retrofit Report, is prepared annually and separately submitted to the Governor and the Legislature pursuant to section 252.385 F.S. The remaining \$7 million of the \$10 million appropriation is allocated according to different subsections in Section 215.559, F. S., as described below.

**Tallahassee Community College (TCC)** - As required by section 215.559 (2) (a) F. S., TCC is given an annual allocation of \$2.8 million or 40 percent of the remaining \$7 million. The funds are administered by TCC and are to be used to mitigate future losses for mobile homes, and to provide tie-downs to mobile home in communities throughout the State of Florida. Please see Appendix A for TCC's 2016-2017 Annual Report.

**Florida International University (FIU)** - As required by Chapter 215.559 (3), F. S., FIU is allocated \$700,000, or 10 percent of the remaining \$7 million. The funds are administered by FIU and dedicated to hurricane research at the Type I Center of the State University System to support hurricane loss reduction devices and techniques. Please see Appendix B for FIU's 2016-2017 Annual report.

**Residential Construction Mitigation Program(RCMP)** – Previously, the Division allocated to remaining \$3.5 million for the Residential Construction Mitigation Program ("RCMP"), which provided grant funding to governmental entities, nonprofit organizations, and qualified for-profit organizations as a means to improve the resiliency of residential structures within their communities. The RCMP utilized a benefit-cost analysis (BCA) for each of the submitted projects in order to determine whether the mitigation retrofits were cost-effective.

The Division has recently been approved to change the RCMP into the Hurricane Loss Mitigation Program (HLMP). Although this year's report does not reflect this change, moving forward the Division will allocate \$3.5 million for construction mitigation efforts that will "prevent or reduce losses or reduce the cost of rebuilding after a disaster" - provided that the construction:

- Involves a structure; and,
- Does not supplant any other mitigation grant program funded by or through the Division.

Current mitigation grant programs funded by or through the Division that involve structures include:

- Elevating residential structures; and,
- Tearing down residences and converting the real property into perpetual greenspace;

Therefore, no HLMP construction mitigation proposal shall duplicate either of the two mitigation grant programs outlined above. The changing of the RCMP into the HMLP provides a more compressive approach to mitigation measures. The HMLP is free to explore other avenues of mitigation than just wind mitigation measures.

**Outreach Program** – HMLP outreach program is designed to educate and inform Florida homeowners and local governments about construction mitigation techniques that prevent or reduce losses by minimizing the damage to property during a disaster. The program funds the development and utilization of outreach materials focused on wind mitigation retrofit techniques and training for local governments. This material includes community workshops, printed materials, training, seminars, hands-on demonstrations, and webinars. The HMLP program continues to consider and review additional outreach methods and new technologies to improve program content and delivery. One such focus, is the HMLP section of the

floridadisaster.org website. This section provides detailed information on HLMP programs as well as links to applications, deadlines and all required documents that a grant recipient would need throughout the grant process. The site also has a link to a comprehensive Hurricane Retrofit Guide. This guide helps citizens better understand the risks of wind damage and informs them on mitigation options for community resiliency.

## **PROGRAM ACTIVITIES**

### **July 1, 2016- June 30, 2017**

**RCMP Wind Mitigation-** Due to RFP-DEM-14-15-043 not being issued until June 22, 2015 and the awarded agreements not being distributed to the recipients until December of 2015 and January of 2016, the Division made the choice to extend the SFY 2016 agreements beyond the initial period of performance to June 30, 2017. To make these extensions possible, the Division had to use 2016-2017 allocation to fund prior agreements for an additional year. Three recipients completed their funding by June 30, 2017 but used SFY 2017 funds. These were the City of North Lauderdale, the City of Pompano Beach and Centro-Campesino. The Cities of Bunnell, Bradenton, Flagler Beach, Cape Coral, Edgewater, Hallandale Beach, Miami, and Deltona were extended to June 30, 2017. Flagler, Pasco, Taylor, Manatee, and Miami-Dade Counties were extended to June 30, 2017.

In June 2016, the Division issued a Request for Proposal (RFP) for projects funded during the SFY 2017 for the annual appropriate amount of \$3.5 million as appropriated by 215.559, Florida Statute. A review panel appointed by the Division selected eligible applicants based on priority, need, benefit, and alignment with local mitigation strategy projects. Based on this evaluation process, the Division contracted with 24 grant recipients to conduct wind mitigation retrofits to homes in the cities of North Miami, Panama City, Coral Springs, Pompano Beach, and North Lauderdale and in the counties of St. Lucie, Broward, and Franklin as well as the non-profit entities West Florida Regional Planning Council (Washington and Holmes Counties), Ability Housing Northwest Florida (Duval County), the ARC (Pinellas County), LASER (Lake County), Hope for Housing (Duval County), Grace and Truth (Duval County), Empowerment (Duval County) and Rebuild Northwest Florida (Escambia and Santa Rosa Counties). The Division received a total of forty-one applicants for this grant cycle. The project agreements were funded with an initial period of performance closeout date of June 30, 2017. Agreements were distributed to the recipients between December 2016 and January 2017.

**RCMP Outreach-** Due to recent outreach success, the Division decided to keep outreach in house. The division focused mainly on the floridadisaster.org website for public outreach. This site provides citizens and potential recipients all the information and forms needed to apply to the RCMP program. It also includes an additional hurricane retrofit guide to help citizens make informed decisions on how to prepare their homes from potentially hazardous weather. During the SFY 2017, the Division hosted four workshops that were open to the public, as well as non-profits and local governments. The purpose of these workshops was to build a higher recipient

base and educate localities about the RCMP program and the changes between the RCMP and HLMP. Outreach and education activities yielded 41 applications for the SFY 2017.

## PROGRAM ANALYSIS

<b><i>PROJECTS COMPLETED IN SFY 2016 WITH SFY 2017 FUNDS</i></b>					
<b>Project Designation</b>	<b>Project Name</b>	<b>Contract Award</b>	<b>Actual Expenditures</b>	<b>% Budget Complete</b>	<b># of Homes</b>
RCMP 16-003	North Lauderdale	\$ 194,000.00	\$ 191,763.55	98.85%	14
RCMP 16-016	Pompano Beach	\$ 194,000.00	\$ 194,000.00	100.00%	27
RCMP 16-020	Centro-Campesino	\$ 194,000.00	\$ 194,000.00	100.00%	9
<b>TOTALS</b>		<b>\$ 582,000.00</b>	<b>\$ 579,763.55</b>	<b>99.62%</b>	<b>50</b>

*Figure 1a*

<b><i>SFY 2016 ROLL OVER PROJECTS</i></b>					
<b>Project Designation</b>	<b>Project Name</b>	<b>Contract Award</b>	<b>Actual Expenditures</b>	<b>% Budget Complete</b>	<b># of Homes</b>
RCMP16-002	City of Bunnell	\$ 194,000.00	\$ 160,923.60	82.95%	7
RCMP16-005	City of Bradenton	\$ 194,000.00	\$ 130,008.68	67.01%	11
RCMP16-006	Flagler County	\$ 229,000.00	\$ 229,000.00	100.00%	14
RCMP16-007	City of Palm Coast	\$ 194,000.00	\$ 167,546.50	86.36%	6
RCMP16-008	City of Flagler Beach	\$ 194,000.00	\$ 187,760.38	96.78%	8
RCMP16-009	City of Cape Coral	\$ 194,000.00	\$ 185,895.75	95.82%	9
RCMP16-010	City of Edgewater	\$ 194,000.00	\$ 7,808.38	4.02%	WD
RCMP16-015	Taylor County	\$ 250,000.00	\$ 237,908.02	95.16%	16
RCMP16-016	City of Pompano Beach	\$ 194,000.00	\$ 194,000.00	100.00%	11
RCMP16-018	City of Hallandale Beach	\$ 194,000.00	\$ 22,473.33	11.58%	8
RCMP16-019	City of Miami	\$ 194,000.00	\$ 27,756.20	14.31%	2
RCMP16-021	City of Deltona	\$ 194,000.00	\$ 11,073.17	5.71%	WD
RCMP16-022	Manatee County	\$ 194,000.00	\$ 159,607.47	82.27%	9
RCMP16-023	Miami-Dade CAHSD	\$ 194,000.00	\$ 194,000.00	100.00%	10
<b>TOTALS</b>		<b>\$ 2,807,000.00</b>	<b>\$ 1,915,761.48</b>	<b>68.25%</b>	<b>111</b>

*Figure 1b*

**SFY 2017 RCMP PROJECTS**

<b>Project Designation</b>	<b>Project Name</b>	<b>Contract Award</b>	<b>Actual Expenditures</b>	<b>% Budget Complete</b>	<b># of Homes</b>
RCMP 17-002	St. Lucie County	\$ 237,279.77	\$ 237,279.77	100.00%	11
RCMP 17-003	West FL RPC	\$ 194,000.00	\$ 89,011.16	45.88%	8
RCMP 17-004	Broward County	\$ 194,000.00	\$ 193,595.20	99.79%	9
RCMP 17-005	City of North Miami	\$ 194,000.00	\$ 193,637.86	99.81%	10
RCMP 17-006	Ability Housing NWFL	\$ 194,000.00	\$ 157,646.65	81.26%	8
RCMP 17-008	ARC	\$ 194,000.00	\$ 118,732.40	61.20%	6
RCMP 17-010	City of Panama City	\$ 194,000.00	\$ 142,805.77	73.61%	8
RCMP 17-011	LASER	\$ 194,000.00	\$ 180,659.32	93.12%	7
RCMP 17-012	Franklin County	\$ 260,059.25	\$ 260,059.25	100.00%	12
RCMP 17-013	Hope for Housing	\$ 194,000.00	\$ 161,589.41	83.29%	9
RCMP 17-014	Grace and Truth	\$ 194,000.00	\$ 144,630.51	74.55%	6
RCMP 17-016	City of Coral Springs	\$ 194,000.00	\$ 133,377.45	68.75%	5
RCMP 17-018	NW Jacksonville CDC	\$ 194,000.00	\$ 131,280.90	67.67%	7
RCMP 17-020	FAIR	\$ 194,000.00	\$ 160,000.00	82.47%	
RCMP 17-021	Empowerment	\$ 194,000.00	\$ 120,717.92	62.23%	6
RCMP 17-022	City of Pompano Beach	\$ 394,000.00	\$ 394,000.00	100.00%	18
RCMP 17-023	City of North Lauderdale	\$ 242,765.96	\$ 242,765.96	100.00%	27
RCMP 17-024	University of Florida	\$ 194,000.00	\$ 50,000.00	25.77%	
RCMP 17-025	Rebuild NWFL	\$ 195,270.82	\$ 195,270.82	100.00%	56
<b>TOTALS</b>		<b>\$ 4,045,375.80</b>	<b>\$ 3,307,060.35</b>	<b>81.75%</b>	<b>213</b>

*Figure 1c*

**Benefit Cost Analysis by SFY**

<b>Project Designation</b>	<b>APPLICANT NAME</b>	<b>BCA Generated Benefits</b>	<b>Cost</b>	<b>ROI</b>	<b>Notes</b>
RCMP16-000	TCC	\$ -	\$ -	0%	NO BCA generated
RCMP16-001	FIU	\$ -	\$ -	0%	Research Grant
RCMP16-002	City of Bunnell	\$ 74,839.00	\$ 160,923.60	-53%	
RCMP16-003	North Lauderdale	\$ 168,712.00	\$ 191,763.55	-12%	
RCMP16-004	Tamarac	\$ -	\$ -	0%	No Project
RCMP16-005	City of Bradenton	\$ 129,112.00	\$ 160,923.60	-20%	
RCMP16-006	Flagler County	\$ 309,040.20	\$ 229,000.00	35%	
RCMP16-007	City of Palm Coast	\$ 163,923.00	\$ 167,546.50	-2%	
RCMP16-008	City of Flagler Beach	\$ 166,749.00	\$ 187,760.38	-11%	
RCMP16-009	City of Cape Coral	\$ 210,557.00	\$ 185,895.75	13%	
RCMP16-010	City of Edgewater	\$ -	\$ 7,808.38	0%	Voluntarily WD 2/7/2017
RCMP16-011	Pasco County	\$ 48,979.00	\$ 111,687.00	-56%	
RCMP16-012	City of Davie			0%	Project not initiated on 4/15/16. Project Closed.
RCMP16-014	City of Delray Beach	\$ -		0%	Project not initiated on 4/15/16. Project Closed.
RCMP16-015	Taylor County	\$ 21,962.00	\$ 237,908.02	-91%	
RCMP16-016	Pompano Beach	\$ 248,640.00	\$ 194,000.00	28%	
RCMP16-017	Citrus County			0%	Voluntarily Withdrew
RCMP16-018	City of Hallandale Beach	\$ 158,797.00	\$ 159,362.60	0%	
RCMP16-019	City of Miami	\$ 122,093.00	\$ 27,756.20	340%	
RCMP16-020	Centro-Campesino	\$ 264,744.00	\$ 194,000.00	36%	
RCMP16-021	City of Deltona		\$ 11,073.17	0%	
RCMP16-022	Manatee County	\$ 171,543.00	\$ 159,607.47	7%	
RCMP16-023	Miami Dade CAHSD	\$ 523,770.00	\$ 194,000.00	170%	
<b>Totals</b>		\$ 2,783,460.20	\$ 2,581,016.22		
<b>ROI 2015-2016</b>				<b>8%</b>	

Figure 2a

Project Designation	APPLICANT NAME	BCA Generated Benefits	Cost	ROI	Notes
RCMP17-000	TCC	\$ -	\$ -	0%	NO BCA generated
RCMP17-001	Florida Int. University	\$ -	\$ -	0%	Research Grant
RCMP17-002	St. Lucie County	\$ 161,550.71	\$ 237,279.77	-32%	
RCMP17-003	West FL Regional Plan Council	\$ 73,312.00	\$ 89,011.16	-18%	
RCMP17-004	Broward County	\$ 325,935.00	\$ 193,595.20	68%	
RCMP17-005	City of North Miami	\$ 472,233.75	\$ 193,637.86	144%	
RCMP17-006	Ability Housing of NE FL	\$ 98,953.00	\$ 157,646.65	-37%	
RCMP17-007	Lakeview Center	\$ -	\$ -	0%	Voluntarily WD
RCMP17-008	The ARC Tampa Bay	\$ 123,233.00	\$ 118,732.40	4%	
RCMP17-009	Jefferson County	\$ -	\$ -	0%	Voluntarily WD
RCMP17-010	Panama City	\$ 95,758.00	\$ 142,805.77	-33%	
RCMP17-011	LASER	\$ 29,723.17	\$ 180,659.32	-84%	
RCMP17-012	Franklin County	\$ 222,136.00	\$ 260,059.25	-15%	
RCMP17-013	Hope for Housing	\$ 48,448.00	\$ 161,589.41	-70%	
RCMP17-014	Grace and Truth, CDC	\$ 65,558.00	\$ 144,630.51	-55%	
RCMP17-015	Habitat NE Jacksonville	\$ -	\$ -	0%	Voluntarily WD
RCMP17-016	City of Coral Springs	\$ 150,788.00	\$ 133,377.45	13%	
RCMP17-017	City of New Smyrna Beach			0%	Voluntarily WD
RCMP17-018	NW Jacksonville CDC	\$ 40,962.00	\$ 131,280.90	-69%	
RCMP17-019	Dixie County	\$ -	\$ -	0%	Voluntarily WD
RCMP17-020	FAIR	\$ -	\$ -	0%	Voluntarily WD
RCMP17-021	Empowerment Academy	\$ 88,253.00	\$ 120,717.92	-27%	
RCMP17-022	City of Pompano Beach	\$ 311,838.55	\$ 394,000.00	-21%	
RCMP17-23	City of North Lauderdale	\$ 316,557.00	\$ 242,765.96		
RCMP17-25	Rebuild NWFL	\$960,315	\$ 195,270.82		
<b>Totals</b>		<b>\$ 3,585,554.18</b>	<b>\$ 3,097,060.35</b>		
<b>ROI 2016-2017</b>				<b>15.77%</b>	
<b>2 Year Totals</b>		<b>\$ 6,369,014.38</b>	<b>\$ 5,678,076.57</b>		
<b>Current SFY's Year ROI</b>				<b>12.17%</b>	

Figure 1b

**Analysis Discussion-** The total expenditures to contract reward ratio for the SFY 2016 is 73.64 percent. This number was generated by adding the total expenditures from Figures 1a and 1b together and dividing by the sum of total contract rewards of Figure 1a and 1b. When compared to the ratio of awards spent from the SFY 2017 (81.75% Figure 1c) this shows an increase of percentage of funds spent of 11%. This means that 11% more of the allocated funds are being used to provide retrofitting for citizens. If you take 11% of the \$3.5 million dollars allocated to the RCMP then you can see a potential increase of \$385,000 dollars spent. That is an increase of nearly two grant recipient's project lists per year. Moving to Figure 2, the Return on Investment (ROI) for SFY 2016 was 8% (Figure 2a). Figure 2b shows an ROI of 15.77 for SFY 2017. This results in a percent change of 97.13%. This number indicates that the RCMP yielded 93% more returns per dollar spent than it did in the previous year.

## **PROGRAM GOALS AND RECOMMENDATIONS**

The Division of Emergency Management is committed to developing programs to educate the public on ways to reduce the impact of a disaster. The Hurricane Loss Mitigation Program educates the public and local communities on wind-mitigation programs that will increase structural survivability for residences and to aid Florida homeowners in obtaining a financial discount for insurance. Through a comprehensive outreach campaign, additional communities will have an opportunity to participate in the grant program.

The Division has the following goals to increase participation in the program:

- Moving forward, the Division would like to focus on more community based mitigation that the previous RCMP did not allow. The Division will enhance its scope of work to include other storm related mitigation efforts that can be undertaken within the confines of State Statute 215.555. This widening of the scope of work aims to better promote storm mitigation and structural resiliency.
- Induction of more pamphlets and physical material to better educate citizens and localities about the HLMP.
- Provide fresh strategies on the Florida Division of Emergency Management's new website in support of local government's mitigation efforts.
- Include information on the new website's "Rebuild and Recover" tab so that citizens may learn more about mitigation activities they can do independently to protect their properties.
- Develop and maintain public education campaign materials to promote the program with a goal to increase the number of applications for SFY 2018 by 10%, or an additional 5 applicants. A 10% increase will mean a total applicant pool for SFY 2018 of 46 applicants.

- Conduct a minimum of four, Community Education Visits (CEV) across the state to promote a partnership strategy that includes the whole community. This whole community strategy seeks to bring together representatives from county government, municipal government, local non-profit entities, and qualified for-profit entities. These meetings will target local officials for education about program implementation and grant management success.
- Conduct a minimum of 75 Recipient Assistance Visits (RAV), to build a relationship with recipients of RCMP grant awards. By implementing a one on one, direct customer service strategy, program management seeks to provide every avenue of success for the local grant recipient.
- Re-engage the Division's relationship with other Mitigation units including Hazard Mitigation Grant Program (HMGP), Floodplain and External Affairs in outreach events, seminars, and conferences with the aim and purpose of cross-promoting mitigation resources across the State of Florida.
- The Division will continue to identify new partnerships and continue with existing partners on research into ways to reduce the impact of disasters.

**Discussion-** In SFY 2016 Program management, in concert with the recipients, became aware that without extending the current agreements, the Program would have experienced a significant failure rate in performance. Only five recipients would have spent their grant funds. Program management and Division leadership made the decision to use future allocation to extend what agreements could be extended in order for the maximum amount of funding to be expended. This decision led to the RCMP actively managing 43 recipients during SFY 2017. This decision led to an inclusion of 12 more recipients into SFY 2017. The Division has successfully allocated the required funds for all 43 projects and is closing said projects without extensions.

2016-2017 ANNUAL REPORT

TALLAHASSEE COMMUNITY COLLEGE

MOBILE HOME TIE DOWN PROGRAM

The Mobile Home Tie-Down Program continued to be a popular and a successful program during the 2016-2017 fiscal year. There were a number of necessary changes to the program this year which constituted a delay in our usual starting time frame of July of the proposed year and instead began in January six months later. The program hired a new Program Coordinator, Albert Wynn as the College's Point of Contact and Program Manager. Contract negotiations as a result of the necessary changes took place between the Department of Emergency Management and Tallahassee Community College to ensure a cohesive assessment of oversight over the Mitigation Program. As a result of such oversight, some of the policies governing the program in years past changed to allow more homeowners to participate. The proposed and thus effective changes are thus: 1. 60% eligibility requirement is no longer in effect. 2. Individual Homeowner Component will be implemented. 3. Multiple Vendors will be chosen for this and future years of the program. All changes were made to allow for more homeowners to participate and to increase the visibility of the grant among Floridians and Vendors looking to be involved with the Hurricane Residential Mitigation Program. As a result, even with the shortened timeframe, One thousand two-hundred and seventy-three (1,273) Florida homeowners participated in the program this past year. The program was successfully completed in eight (8) mobile home communities across six (6) different Florida counties. In all One-million nine-hundred eighty-six thousand, nine-hundred and seventy-five dollars (1,986,975) were expensed on the grant spending 81% of the allocated funds.

	PARK NAME	ADDRESS	CITY	COUNTY	# OF HOMES
1	CROSSWINDS MHP	4125 Park St. N	St. Petersburg	Pinellas	139
2	HONEYMOON MHP	1100 Curlew Rd	Dunedin	Pinellas	160
3	TANGLEWOOD	345 E. Weatherbee Rd	Ft. Pierce	St. Lucie	80
4	WOODDALE MHP	37945 Bentley Dr.	Zephyrhills	Pasco	65
5	COLONY COVE MHP	101 Amsterdam Ave	Ellenton	Manatee	606
6	CHULA VISTA MHP	1734 Wheelhouse Cir	Ruskin	Hillsborough	88
7	LONE PINE RIDGE MHP	77 Lone Pine Ave	Dunedin	Pinellas	87
8	ARCADIA MHP	1 Maine St.	Arcadia	Desoto	48
9					1273

Upon completion of a community The Florida Department of Highway Safety and Motor Vehicles (D.H.S.M.V), Division of Motor Vehicles, Manufactured Housing Section completes a random inspection of a minimum of 10% of the homes. This is to verify the items were actually installed by the vendor and installed according to the manufacturer's specifications.

As is the case every year, critical assistance and advisement was provided by the Federation of Mobile Home Owners (FMO) and Florida Manufactured Housing Association, Inc. in sending out our Community Interest Verification form. This begins the process of intake and eligibility for the program.

The intake and eligibility process began as site visits were scheduled and completed at nine (9) communities throughout the year. These communities were evaluated and the following deliverables were completed during this process:

- Interviews with management and/or homeowner association representatives.
- Visual inspections of all homes within the community.
- Intake training for the homeowners association representatives.

Since Communities are no longer required to have 60% participation of the eligible units. Tallahassee Community College began accruing a listing of all interested Communities and Individuals for the completion of the scope of work and participation into the program. Site visits are no longer the responsibility of the vendor for eligibility evaluation but the sole responsibility of the College. TCC visited Ninety-four (94) communities within the shortened span for this year for the evaluation of parks for participation in the program.

During the 2016-2017 program year nine (9) resident meetings were conducted by the Program Contractors. These meetings were conducted with homeowner's association board members, volunteers and, on many occasions, all residents of a particular community. Additionally, Tallahassee Community College, Windstorm Mitigation Inc. (contractor), and the partnership of DSI/Frier Home Sales Inc. responded to over four hundred (400) resident inquiries during this program year.

### **Moving Forward.**

***Individual Component.*** The process for implementing the Individual Component is complete and will begin within the new contract year of HMLP 18. As part of this effort TCC is developing a website for participant intake and will be functional sometime in the coming month.

***Quality Control Inspector.*** To ensure every resident receives quality services from the grant. TCC is looking to contract services with a Quality Control Inspector. This person's responsibilities will be to inspect 30% of the Individual Homeowner's serviced by the program as a way to ensure a quality product is being provided to the homeowner and provided by the vendor. FLHSMV is providing the services to assist TCC in vetting the vendors interested in participating in the program as part of our quality control.

***Program Webinar.*** There will be a Pre-Bid Conference on July 13<sup>th</sup> to ensure the vision, expectation of the program is communicated clearly too all participants. This will be a recorded session for future use and reference.

Please refer any questions relating to this report or the Program in general to:

Albert Wynn  
MHTDP Program Coordinator  
Tallahassee Community College  
444 Appleyard Drive  
Tallahassee, FL 32304  
850.201.8508  
[wynna@tcc.fl.edu](mailto:wynna@tcc.fl.edu)



*A Resource for the State of Florida*

# **HURRICANE LOSS REDUCTION FOR HOUSING IN FLORIDA**

## **FINAL REPORT**

**For the Period November 10, 2016 to June 30, 2017**

*A Research Project Funded by:*  
**The State of Florida Division of Emergency Management  
Through Contract #17-RC-A7-11-23-05-293**

*Prepared by*  
The International Hurricane Research Center (IHRC)  
Florida International University (FIU)

July 31, 2017

# Final Report

## Table of Contents

Executive Summary	Section 1
Holistic Testing to Determine the Efficacy of a Retrofit Techniques for Residential Buildings and Assessing the Aerodynamics of Elevated Homes (PI: Dr. Arindam Gan Chowdhury and Dr. Peter Irwin)	Section 2
Investigation and Incorporation of WOW Testing Outputs in the Florida Public Hurricane Loss Model (PI: Dr. Jean Paul-Pinelli and Dr.Kurt Gurley)	Section 3
Hurricane Resilient Residential Building Construction: Wind-induced Dynamic Effect on Photovoltaic Systems and Wind Driven Rain Intrusion on Interior Zones of Residential Construction (PI: Dr. Ioannis Zisis)	Section 4
Education and Outreach Programs to Convey the Benefits of Various Hurricane Loss Mitigation Devises and Techniques (PI: Erik Salna)	Section 5

## **Section 1**

### **Executive Summary**

Four major efforts were identified by the International Hurricane Research Center (IHRC) for the Residential Construction Mitigation Program (RCMP) Fiscal Year 2016-2017 funding in the areas of structural mitigation analysis, socioeconomic research, data dissemination to stakeholders and education and outreach. In keeping with the comprehensive agenda of the research topics for this project, the IHRC organized a multidisciplinary team of researchers, students and support staff to complete the stated objectives. The following is a summary of research findings:

#### **Holistic Testing to Determine the Efficacy of a Retrofit Techniques for Residential Buildings and Assessing the Aerodynamics of Elevated Homes (PI: Arindam Gan Chowdhury and Peter Irwin)**

##### ***Fiber Reinforced Polymer Retrofit Technique for Residential Buildings***

Non-intrusive Fiber Reinforced Polymer (FRP) connections were considered as replacements or retrofitting alternatives for intrusive metal connectors for roof-to-wall connections in residential buildings. The FRP connection system is advantageous as it is nonintrusive and corrosion resistant. The results of the Wall of Wind (WOW) testing showed that the uplift load capacity of the FRP connection is adequate for resisting wind induced loads at high wind speeds (up to 115 mph, which represents Category 3 hurricane condition). The WOW tests were also used to experimentally validate the theoretically calculated failure wind speed for the connection. A close agreement was obtained between the theoretical and experimental failure wind speeds. It was concluded that the failure wind speed for FRP roof-to-wall connection for any given roof configuration can be accurately estimated based on component level testing of the uplift capacity of the connection and comparing that with the wind loading estimated from ASCE 7-10. The research results also showed the efficacy of alternative non-intrusive inter-component connections for new buildings and retrofitting of older residential buildings to reduce their vulnerability to hurricane wind forces. The effective design and development of non-intrusive roof-to-wall connections can significantly reduce property losses in tropical storms and hurricanes, thus positively impact the economy of the State of Florida and increase safety of its residents.

##### ***Assessment of Aerodynamic Loads on Elevated Homes***

Elevated homes are common in many coastal communities to minimize the impact of storm surge on the residences. Many other structures, including as mobile homes, trailers, and homes built on crawl space foundations, have an air gap between the floor level and the ground. However, the aerodynamics effects of elevating a structure above the ground are not well addressed in the current building codes. To provide more information for these situations, large-scale experiments were conducted at FIU's WOW facility on a representative single-story residential gable roof house. The primary testing was conducted on a 1:5 scale model of the test building for four different elevation conditions: 1) no building elevation, 2) 2-ft equivalent full-scale elevation, 3) 7-ft equivalent full-scale elevation, and 4) 12-ft equivalent full-scale elevation. The 1:5 model was instrumented with four multi-axis load cells and 363 pressure taps

to capture the aerodynamic forces and bending moments transferred to the ground and the fluctuating pressure distributions on all surfaces of the building model. Additional pressure testing was conducted on a 1:60 scale model of the structure installed at the 7-ft equivalent full-scale elevation to check for Reynold's number effects in the testing.

Results showed that the largest wind loads exerted on the building are the lateral force in the along-wind direction, the vertical uplift force, and the overturning moment about the lateral axis. It was found that the along-wind shear force increases with increasing stilt height, the uplift force reduces with increasing stilt height, and the primary overturning moment increases with increasing stilt height. Strong suction pressures were found on the roof surface, the side and leeward walls, and the underside of the building model for all wind angles tested. The reduction in net uplift with increasing stilt height appears to be the result of offsetting suction pressures acting simultaneously on the roof and floor surfaces of the elevated building. Thus designers should consider the strong suction pressures acting beneath the floor to ensure that an adequate design of the floor's structural system is achieved for performance during high wind events. Careful design of the floor-to-stilt and the stilt-to-foundation connections must be considered to ensure that the building is able to resist strong bending moments exerted at these locations. The effect of Reynolds number needs to be investigated using a partial turbulence simulation approach.

### **Investigation and Incorporation of WOW Testing Outputs in the Florida Public Hurricane Loss Model (PI: Dr. Jean Paul-Pinelli and Kurt Gurley)**

One of the key components of a better mitigated and therefore more disaster-resilient Florida involves recovery and reconstruction funding for homeowners, and a key element of that funding derives from insurance coverage, which is increasingly driven by cost considerations. The Florida Public Hurricane Loss Model (FPHLM) which has been supported by the State through the Office of Insurance Regulation (OIR), provides a means of evaluating hazard insurance rate requests independently of the proprietary models used by private insurers. The model is continually refined to both satisfy the standards issued by the Florida Commission on Hurricane Loss Projection Methodology, and incorporate the current state-of-knowledge in the methodologies employed by the meteorological, engineering, actuarial, statistical, and computer science teams.

Recently completed Wall of Wind (WOW) Florida Department of Emergency Management (DEM) projects (FY 2015–2016) address elements of low-rise and high-rise building performance, in particular the wind loads on high-rise balcony glass handrail systems (GHRS) and the exterior wall adjacent to the balcony. The incorporation of these experimental results within the FPHLM were investigated.

The results indicate that the modifications under investigation could influence FPHLM loss outputs. Sliding glass doors are not the only significant contributor to mid high rise losses. Windows and entry doors are also vulnerable components, and water ingress from all openings represent a significant portion of calculated losses. Additionally, the cost and vulnerability of the GHRS itself has not yet been included in this investigation (GHRS is ~ \$250/linear foot). That is, the reduced vulnerability of the sliding glass door may be offset by the increase in loss due to damage to the

GHRIS. With this in mind, future refinements will focus on an explicit glass hand rail vulnerability model. This will be very sensitive to the WOW experimental results currently under analysis at multiple scales. The ongoing analyses of the model scale effects on results are part of an ongoing PhD dissertation at FIU and will continued to be examined.

## **Hurricane Resilient Residential Building Construction: Wind-induced dynamic Effect on Photovoltaic Systems and Wind Driven Rain Intrusion on Interior Zones of Residential Construction (PI: Dr. Ioannis Zisis)**

### ***Wind-induced Dynamic Effect on Photovoltaic Systems***

Reduction in construction and installation costs of photovoltaic (PV) panels and inverters has led to widespread use of residential rooftop PV modules. Propagation of solar energy harvesting and development of more efficient PV systems have increased the attention toward the structural design aspect of these systems and in particular the design for wind forces. Over the past decade, numerous studies have been performed and guidelines for estimating wind loads on industrial and residential structures have started to be included in some building codes and wind standards. Photovoltaic (PV) module vibrations under wind action have been found to be significant during full-scale tests while current design standards and building codes do not address this unfavorable behavior. Preliminary studies showed that the effect of PV-system vibration should be considered in the design of mounting structure. The  $<1$  Hz fundamental natural frequency criterion used in current standards to determine whether wind-induced dynamic effects should be considered or not, may not be applicable to PV systems. The goal of this study was to expand the understanding of the dynamic behavior of PV systems exposed to wind-induced loads. More specific, the study examined vibration on the PV panels and supporting system due to turbulent action of wind.

Three models were tested at the Wall of Wind (WOW) facility at FIU, including a full-scale real PV panel array (i.e. flexible model), a full-scale rigid panel array (i.e. wood model) and a large scale rigid panel array (i.e. plexiglass model). The main achievements of this study included the following:

- The mean force coefficient (CF) results obtained from the flexible model tests appear to be independent of the wind speed. The peak CF values show some discrepancies for specific wind directions.
- No significant differences were found between the CF values obtained from the flexible versus the rigid model tests. For specific wind directions, the flexible model experiences considerably higher CF values when compared to the rigid model pressure tap results.
- When the CF values are calculated using the pressure tap data the results indicate a good match between the large-scale and full-scale mean values. The peak CF values show significant discrepancies which are though reduced when the partial turbulence simulation is used.
- The resonant response of the PV array at the first natural frequency (approx. 10 Hz) is very close to the module's fundamental natural frequency of 10.5 Hz which was established by the hammer tests.
- The implementation of the Mechanical Admittance Function (MAF) resulted in mixed findings. Although it improved the agreement in certain wind directions, it also resulted in higher discrepancies for several cases.
- The findings compare well with the current wind standard recommendations. The best agreement is established when the CF values are estimated using the pressure data.

This study is expected to provide valuable information for the development of wind design guidelines for residential scale PV panel arrays. The majority of the current building codes and wind standards that include design guidelines for PV systems are based predominantly on tests that considered scaled models of large commercial PV array systems on flat industrial size buildings. These configurations are significantly different than a typical low-rise building therefore the current study is expected to add knowledge and assist in the development of more accurate design recommendation for residential scale PV installations. The State of Florida is in particular need for such guidelines as it is often impacted by strong wind events. Recent initiatives, such as the mandatory installation of PV panels in new residential construction in South Miami, demand for development of safe and efficient design tools for rooftop solar arrays. Furthermore, the findings related to the wind-induced vibration on the PV panels provide important insight on the dynamic response of the system. This type of information would not be possible to be extracted from small-scale rigid model tests and such knowledge will further improve our understanding of the wind-induced performance of solar arrays and assist in the development of more comprehensive building code guidelines.

### ***Wind Driven Rain Intrusion on Interior Zones of Residential Construction***

Considering the significant increase in the amount of economic losses caused by hurricanes during past few decades, there is a crucial need to accurately estimate vulnerability of buildings to hurricanes in coastal states like Florida. Although probabilistic simulation models can be used to predict the hurricane risk, their loss projection is not accurate enough due to simplifying assumption related to interior damage prediction. It has been shown that interior damages can make up 50% to 100 % of the total damage costs, so incorrect estimation of them can result in significant inaccuracy in the loss estimation models.

One of the main objectives of this project is to develop a framework for large-scale testing of low-rise building under wind driven rain (WDR). In the current study the experimental large-scale tests have shown that the water propagation path follows the anticipated internal air flow. The tests were successful in capturing this propagation into the ceiling and the interior compartments. In addition, the use of absorbing pads and thermal cameras provided reliable information on the water distribution on each wall of individual compartments.

These findings are extremely important and will be utilized to develop the necessary vulnerability curves that determine the performance state of different interior components in the building. The current study tested and modeled the interior and content damage mechanisms related to water ingress for the very first time. The acquired data will be further analyzed to develop benchmark test-based vulnerability models of hurricane induced interior and contents damage (and associated time related expenses) for typical low-rise residential coastal structures. The State of Florida will greatly benefit by the availability of such knowledge, as the information will be disseminated to the FIU, UF and FIT groups that are responsible for the Florida Public Hurricane Loss Model (FPHLM). The inclusion of the new interior, contents, and time related expenses models will enhance the existing FPHLM and increase its accuracy.

## **Education and Outreach Programs to Convey the Benefits of Various Hurricane Loss Mitigation Devises and Techniques (PI: Erik Salna)**

IHRC staff developed and coordinated educational partnerships, community events, and outreach programs. This work promoted hurricane-loss mitigation and the objectives of the RCMP and included the following:

### ***Hurricane Andrew Anniversary Museum Exhibit – May 19th, 2017***

The Museum of Discovery & Science (MODS), located in Fort Lauderdale, FL, assisted the IHRC in developing and coordinating a new *Hurricane Andrew Anniversary* exhibit, which included a video showing original TV news and weather reports before, during and after the storm. Local officials and media attended a ribbon-cutting ceremony to debut the new exhibit on May 19<sup>th</sup>. MODS averages 450,000 visitors annually, including thousands of local area school children.

### ***Hurricane (Science, Mitigation & Preparedness) Event: Eye of the Storm – May 20th, 2017***

The Museum of Discovery & Science (MODS), located in Fort Lauderdale, FL, assisted the IHRC in planning, coordinating and facilitating this public education event that showcased special hands-on, interactive activities and demonstrations teaching hurricane science, mitigation and preparedness. Over 2,000 people attended *Eye of the Storm* and 34 South Florida agencies and organizations participated.

### ***Hurricane Preparedness Spanish Website – June 15<sup>th</sup>, 2017***

The IHRC, in partnership with NOAA's National Hurricane Center (NHC), enhanced the Spanish language website (<https://hurricanes.fiu.edu/>) with new static and live content. The goal of the website is to help the Spanish-speaking community be better educated, informed and prepared for hurricanes, including safe-guarding their families, homes and businesses.

### ***NOAA Hurricane Awareness Tour – May 12th, 2017***

In conjunction with NOAA's National Hurricane Preparedness Week, IHRC joined the NOAA Hurricane Awareness Tour at the Miami-Opa Locka Executive Airport. The media conference was attended by almost 20 local, national and international media outlets. "Hurricane Hunter" aircraft and IHRC mitigation exhibit were on display and toured by close to 600 South Florida area students and approximately 400 public residents.



*A Resource for the State of Florida*

***SECTION 2***

**Holistic Testing to Determine the Efficacy of a  
Retrofit Techniques for Residential Buildings and  
Assessing the Aerodynamics of Elevated Homes**

A Report Submitted to:

The State of Florida Division of Emergency Management

*Prepared by:*

Arindam Gan Chowdhury, PhD.

Peter Irwin, PhD., PE

*Graduate Students*

Ziad Azzi

Ehssan Amir Sayyafi

Mohammadtaghi Moravej

The International Hurricane Research Center (IHRC)

Florida International University

July 2017

# 1. Fiber Reinforced Polymer Retrofit Technique for Residential Buildings

## Executive Summary

*Non-intrusive Fiber Reinforced Polymer (FRP) connections were considered as replacements or retrofitting alternatives for intrusive metal connectors for roof-to-wall connections in residential buildings. The FRP connection system is advantageous as it is nonintrusive and corrosion resistant. The results of the Wall of Wind (WOW) testing showed that the uplift load capacity of the FRP connection is adequate for resisting wind induced loads at high wind speeds (up to 115 mph, which represents Category 3 hurricane condition). The WOW tests were also used to experimentally validate the theoretically calculated failure wind speed for the connection. A close agreement was obtained between the theoretical and experimental failure wind speeds. It was concluded that the failure wind speed for FRP roof-to-wall connection for any given roof configuration can be accurately estimated based on component level testing of the uplift capacity of the connection and comparing that with the wind loading estimated from ASCE 7-10. The research results also showed the efficacy of alternative non-intrusive inter-component connections for new buildings and retrofitting of older residential buildings to reduce their vulnerability to hurricane wind forces. The effective design and development of non-intrusive roof-to-wall connections can significantly reduce property losses in tropical storms and hurricanes, thus positively impact the economy of the State of Florida and increase safety of its residents.*

## 1.1 Introduction and Background

The most frequently occurring natural hazards in the United States are related to wind. Hurricane-induced losses in the USA increased from US\$1.3 billion per year pre 1990 to US\$ 36 billion per year post 2000 [1]. The contributions of wind-related losses to overall hazard damage in the United States, averaged over a span of 5 years and 50 years, were around 89% and 69% respectively [2]. These numbers and their projection for the future show that designing buildings for wind loads is very crucial.

Roof to wall connections play a critical role in the behavior of wood-frame buildings when exposed to wind induced loadings. They contribute in resisting lateral loads and negative pressures (suctions) experienced by roofs [3]. The most common materials that these connectors are made of are steel or metal (such as in hurricane clips and straps). The fixing of these connectors require intrusion of screws or nails into the wooden members, which creates a pathway for water penetration and subsequently, deterioration of the wooden members [4]. Moreover, advanced research in wind engineering is considering the loading that occurs in three dimensions, versus just one. Traditionally, only one axis has been considered for the response of structures to pressures. However, it has been shown that triaxial loads provide more reliable and realistic data than their uniaxial counterparts. Under triaxial load tests, load capacities of metal connectors were found to be unsafe [5].

New alternatives to metal connectors as roof to wall connections are now being considered in the research community. Research findings from recent past showed that non-intrusive bonded connections have advantages over their intrusive (metal) counterparts. No intrusion into the structural members allows more stability and resistance to wind driven rain [6, 7]. Moreover, the

fundamental failure modes of hurricanes clips are the separation of the metal truss plate, truss rotation, and buckling of the clip; whereas non-intrusive connections' flexibility and direct contact with the timber members can avoid these failure modes, thus providing a safer solution [8]. This report investigates the use of Fiber Reinforced Polymers (FRP) as a non-intrusive roof to wall connection tested under simulated hurricane conditions. The current work focuses on large scale aerodynamic testing of the FRP connections subjected to simulated hurricane winds at the Wall of Wind facility. The main aim was to experimentally validate the theoretically calculated failure wind speed for the FRP connection.

## **1.2 Methodology**

### ***1.2.1 Wall of Wind Facility***

The Wall of Wind (WOW) is a full- and large-scale testing facility that was designed and built by wind engineering faculty and staff at the International Hurricane Research Center (IHRC) and the Department of Civil and Environmental Engineering at Florida International University (FIU). The WOW is comprised of a 12-fan system that is capable of generating wind speeds and turbulence characteristics similar to those observed during tropical cyclones. It can generate wind speeds up to those experienced in a Category 5 hurricane on a Saffir-Simpson scale. The 12-fan system is shown in Figure 1-1. Turbulence and boundary layer characteristics are generated using a set of triangular spires and roughness elements that are attached to the floor as shown in Figure 1-2.



**Figure 1-1 12-Fan Wall of Wind (WOW) at the Florida International University**

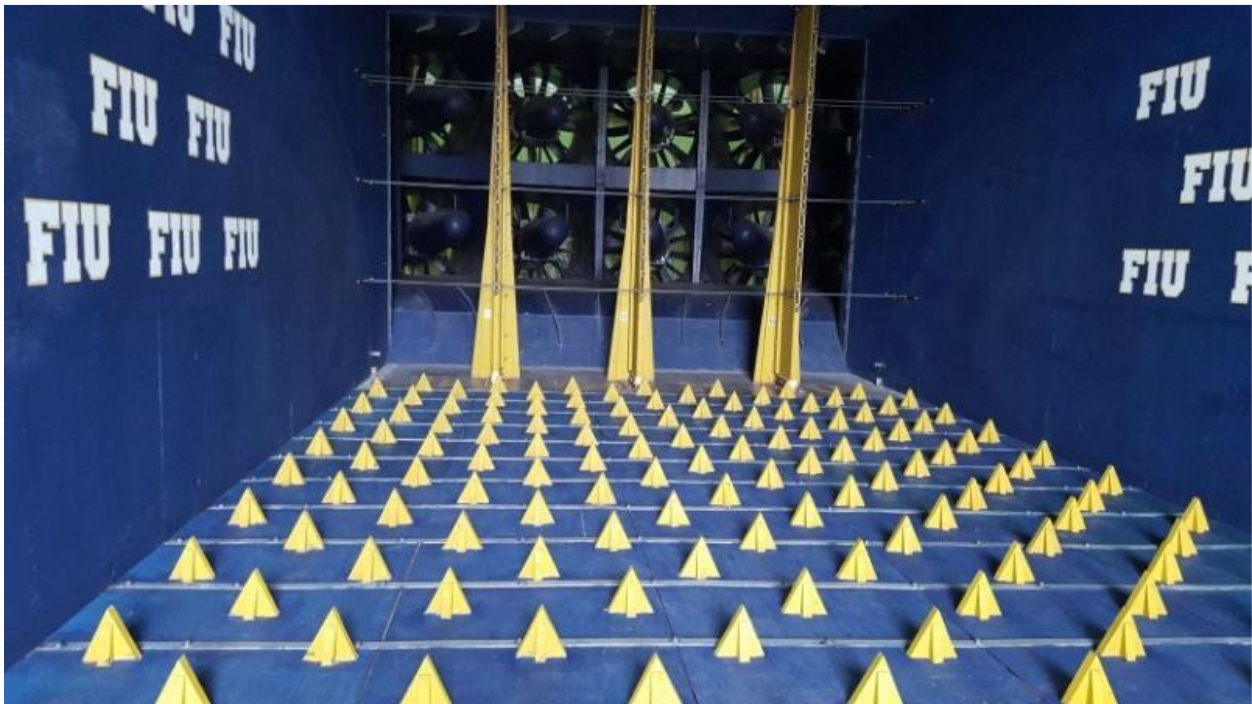


**Figure 1-2 Spires and Floor Roughness Elements**

The atmospheric boundary layer (ABL) mean wind speed profile and turbulence effects were simulated at the WOW. To measure the vertical wind speed profile throughout the entire boundary layer, a series of experiments were run. A turbulent flow Cobra probe, able to capture the 3 components of velocity and local static pressure, was utilized to accurately measure the different

wind speeds and turbulence at various heights. Figure 1-3 shows the mean wind speed profile at the WOW [9].

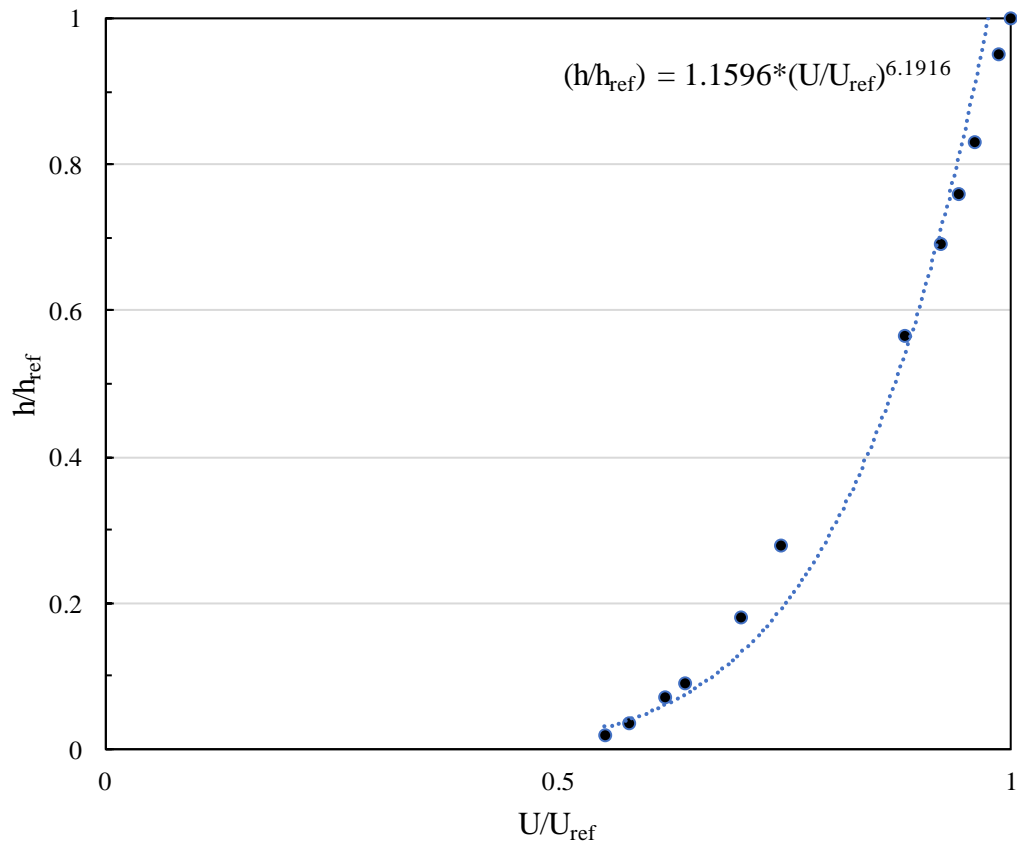


**Figure 1-3 Mean Wind Speed Profile at WOW**

### ***1.2.2 Building Model Description***

A residential building model, with FRP roof-to-wall connections, was tested at the WOW under simulated hurricane winds. The dimensions for the full-scale prototype testing specimen were length of 46.88-ft, width of 30.00-ft and height of 12.00-ft. The reduced scale (1:4) gable wood frame building had the following dimensions: length of 11.72-ft, width of 7.50-ft, and height of 3.00-ft. The building roof slope was approximately 14° or 3:12. Figure 1-4 shows an isometric drawing of the reduced scale model framing.

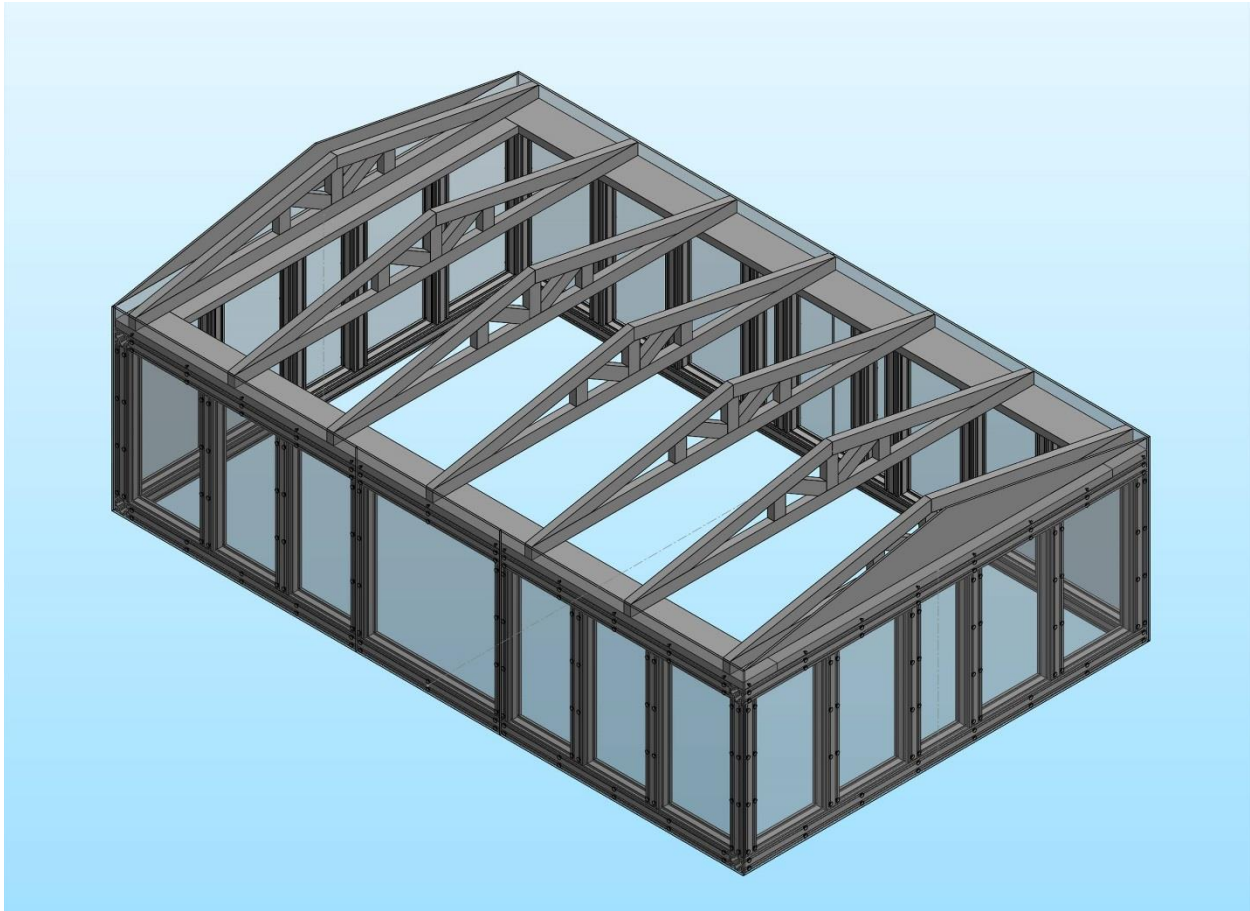


**Figure 1-4 Isometric Drawing of Building Model Framing**

Spruce-Pine-Fir #2 with nominal dimensions of 2×3-in and 2×6-in were used to construct the roof truss members and wall top plates, respectively. As for the roof sheathing materials, 3/8-in thick plywood sheets were screwed to the roof trusses. The walls on all four sides were constructed using aluminum studs connected together using screws and the sheathing was made out of nominal 3/8-in thick polycarbonate sheets attached to the vertical aluminum studs. The choice of aluminum and polycarbonate as materials for the walls provided more durability in the long run since the same walls were used for repeated trials. Furthermore, the use of polycarbonate as wall sheathing had another advantage since the enclosure configuration of the building could be altered by simply unscrewing one or more of the sheets. Different enclosures create different internal pressure scenarios that affect the net loading on the roof-to-wall connections. Figure 1-5 shows the reduced scale model after completion. In total, 7 trusses spaced at 24-in-on-center were used to construct the roof.



**Figure 1-5 Reduced-Scale Model Building**

The wooden top plate of the wall was screwed to the aluminum wall vertical studs. Roof trusses were connected to the wall top plate using two FRP connections on each end on the truss. Each FRP connection was made out of FRP sheet that was 3-in long by 1.5-in wide. The FRP sheet was glued using a resin to the wall (area: 1.5-in  $\times$  1.5-in) and the bottom chord of the roof truss (area: 1.5-in  $\times$  1.5-in), constituting the roof to wall connection adopted in this project. Figures 1-6 and 1-7 show typical views of a roof-to-wall connection using FRP sheets. Finally, the model was installed on the WOW 16-ft diameter turntable in order to expose the structure to different wind directions.



**Figure 1-6 FRP Sheet Application**



**Figure 1-7 Roof-to-Wall Connection on Each End of the Truss**

In Figures 1-6, galvanized clips are visible in the image. The clips were used temporarily in order to hold the truss straight as the FRP sheets underwent a minimum of 7 days of curing time to achieve maximum strength, as recommended by the manufacturer of the FRP and resin. The clips were removed after the 7 days of curing time, and were not in place during any of the wind tests.

### 1.2.3 Laws of Similitude

Since the model is a 1:4 scale of a full-scale prototype, certain parameters need to be taken into account in order to preserve the overall behavior of the building under dynamic loading. For that, a geometric scale factor is applied for geometric similitude. Similitude in dynamic behavior requires mass scaling between the prototype and model.

If a general quantity  $Q_P$  has been measured on the prototype, Equation 1-1 can be used for calculating the model quantity  $Q_M$ :

$$Q_M = Q_P \times \lambda_Q \quad (1-1)$$

where  $\lambda_Q$  is the scale factor.

The relationships between the model and prototype quantities strongly depend on the materials used for the construction of the model. In this project, prototype materials were used for the construction of the models. This means that materials normally used to construct the full-scale building were used to build the reduced scale model. Table 1-1 summarizes the resulting scale factors for the different engineering properties as well as the equations used.

**Table 1-1 Scale Factors Adopted**

Scale	Relationship	Scale Factor
Density	$\lambda_\rho = \frac{\rho_M}{\rho_P}$	1
Length	$\lambda_L = \frac{L_M}{L_P}$	$\frac{1}{4}$
Velocity	$\lambda_\vartheta = \frac{\vartheta_M}{\vartheta_P} = \sqrt{\lambda_L}$	$\sqrt{\frac{1}{4}} = \frac{1}{2}$
Mass	$\lambda_M = \lambda_P \times \lambda_L^3$	$\left(\frac{1}{4}\right)^3 = \frac{1}{64}$
Mass Moment of Inertia	$\lambda_I = \lambda_M \times \lambda_L^2$	$\frac{1}{64} \times \left(\frac{1}{4}\right)^2 = \left(\frac{1}{4}\right)^5 = \frac{1}{1,024}$
Time	$\lambda_T = \frac{T_M}{T_P} = \frac{\lambda_L}{\sqrt{\lambda_L}} = \sqrt{\lambda_L}$	$\sqrt{\frac{1}{4}} = \frac{1}{2}$
Force	$\lambda_F = \frac{F_M}{F_P} = \lambda_\vartheta^2 \times \lambda_L^2 = \lambda_L^3$	$\left(\frac{1}{4}\right)^3 = \frac{1}{64}$

For the construction of the model, the scaling factor for the mass was the governing factor for the design of the truss members and roof sheathing, controlling the type of wood used and the dimensions of the truss chords and the thickness of the roof sheathing.

#### **1.2.4 FRP Connection Testing**

To determine the uplift force that can be withstood by the FRP sheets with the resin connection provided by an industry partner, 9 samples were prepared and tested in the structures laboratory at FIU, Engineering Campus. Three samples for each scale factor were prepared and cured for 7 days. The preparation of the test specimens was conducted according to the specifications provided by the manufacturer of the FRP and resin. Figure 1-8, parts (a) – (c), show the correct application of the FRP sheet between two wooden members.

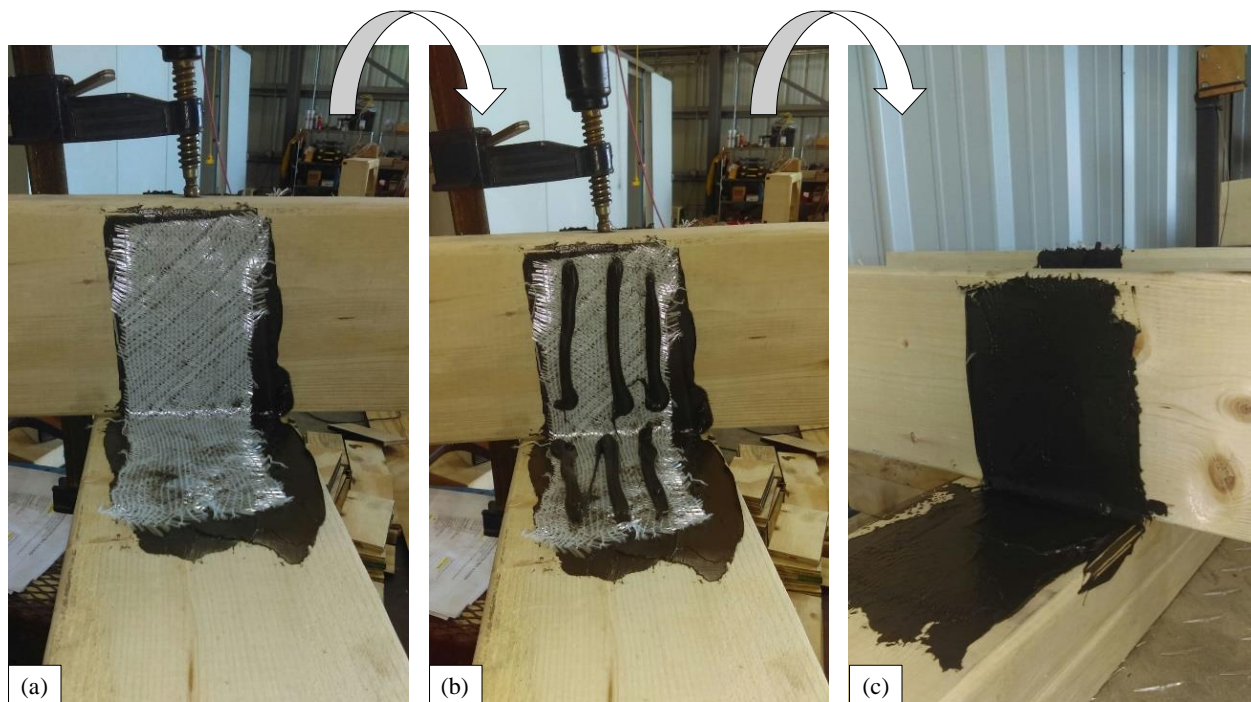


**Figure 1-8 FRP Application Process (a) Fiber Placed on First Resin Layer, (b) Second Resin Layer Placed on Top of Fiber, and (c) Completed FRP Roof-to-Wall Connection**

The dimensions of the FRP sheets used for the connections are: 6×3-in. surface area (3×3-in. glued to each structural member (roof and wall)); 3×1.5-in. surface area (1.5×1.5-in. glued to each structural member); 1.5×0.75-in. surface area (0.75×0.75-in. glued to each structural member).

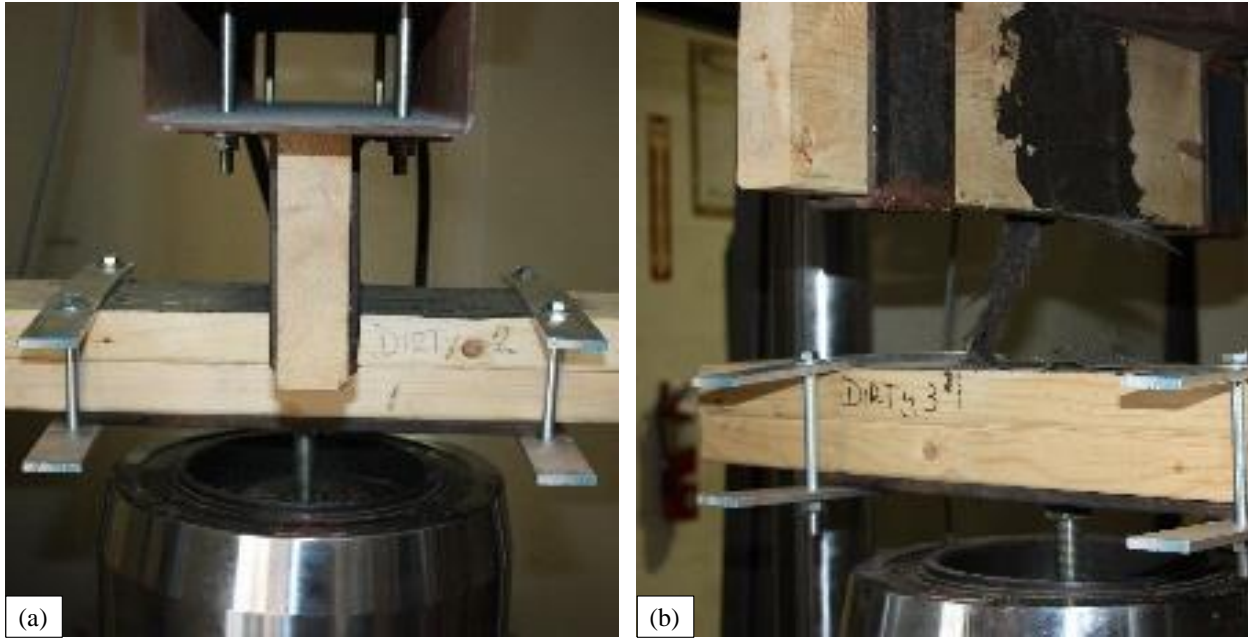


**Figure 1-9 (a) Test Specimen before Failure, (b) Test Specimen after Failure**

The objective of testing the specimens was to determine the pull-out force. Figure 1-9 parts (a) and (b) depict the actual specimen before and after failure, respectively. For simplicity and since the FRP sheets of 3×1.5-in surface area were used to construct the model for WOW testing, only the results for those tests are shown below. Figures 1-10, 1-11 and 1-12 show the behavior of the load with respect to time in all three FRP sheets tested. Table 1-2 summarizes the results.

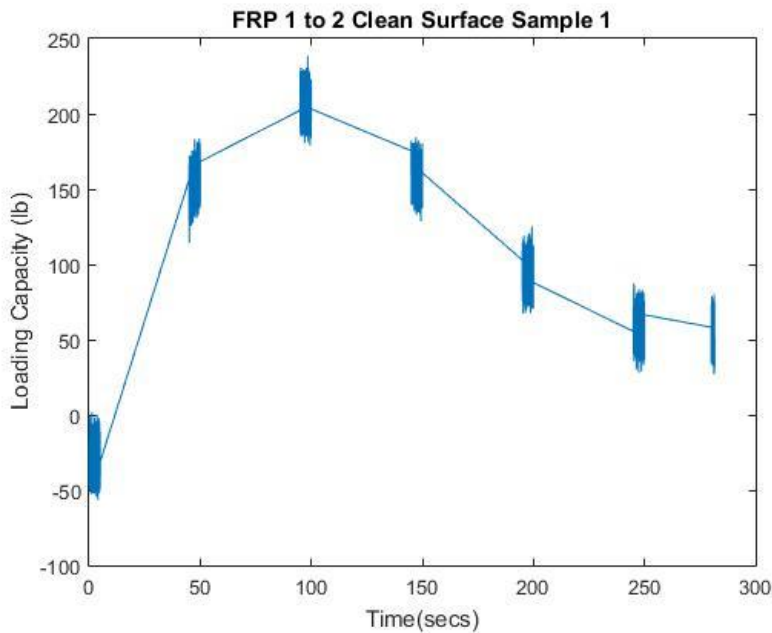


**Figure 1-10 1:2 FRP Sheet Sample 1**

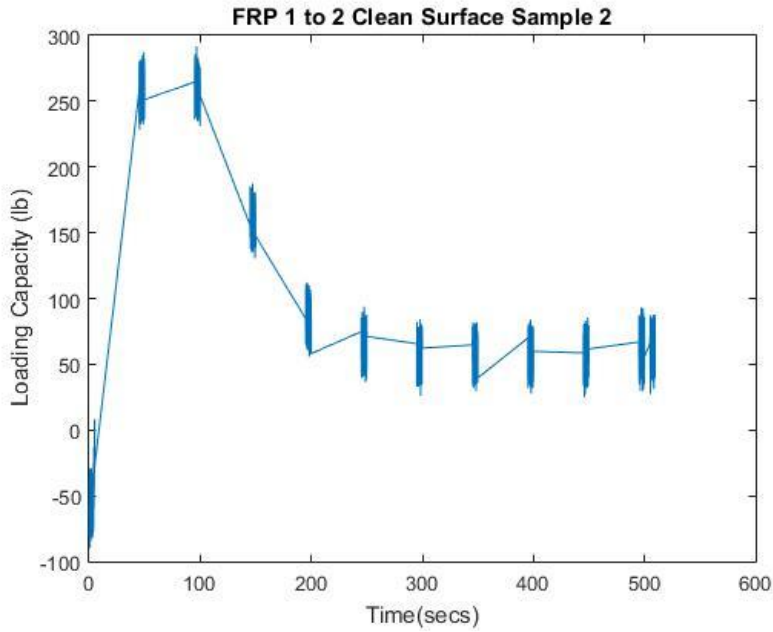


**Figure 1-11 1:2 FRP Sheet Sample 2**

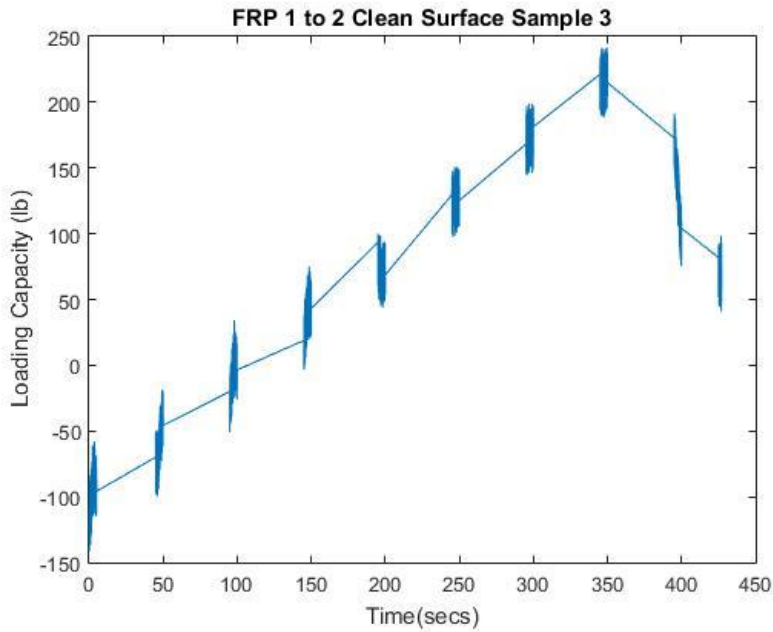


**Figure 1-12 1:2 FRP Sheet Sample 3**

**Table 1-2 Pull Out Results Obtained**

Sample Number	Maximum Force (lbs.)	Average Force (lbs.)
1	239	258
2	292	
3	242	

Based on the results of the pull tests, an uplift resistance of 260 pounds was used to estimate the failure wind speed for the FRP roof-to-wall connection when tested using the WOW reduced scale building model under testing conditions.

### 1.2.5 Estimation of Failure Wind Speed

A study was conducted to determine whether the calculated theoretical failure wind speed would match the one recorded experimentally at the WOW facility. The theoretical failure wind speed was based on the uplift resistance of the FRP connections as obtained in the structures laboratory and the wind loads estimated based on ASCE 7. The roof of the model building was made of 7 trusses, meaning that each FRP connection would carry a load coming from a tributary area of 0.75 ft × 3.75 ft (2.8125 ft<sup>2</sup>). In addition, roof total dead load including trusses and plywood sheathing was estimated at around 2.5 psf. This resulted in a compressive dead load of 7 lbs for each FRP sheet connection. The connection strength was estimated as 260 lbs from the component testing in the structures laboratory, which means that, theoretically, an uplift force of 267 lbs would be required to fail the roof-to-wall connection.

The aerodynamic pressure acting on the roof, causing failure of a connection, can be obtained according to Equation 1-2:

$$P = \frac{1}{2} \rho C_{p_{net}} \vartheta^2 \quad (1-2)$$

where  $P$  is the peak pressure in psf,  $\rho$  is the air density at the time of the test (0.00238 slugs/ft<sup>3</sup>),  $C_{p_{net}}$  is the net pressure coefficient defined as the difference between the external pressure coefficient and the internal pressure coefficient as described in equation 1-3 and  $\vartheta$  is the failure wind speed in ft/s.

$$C_{p_{net}} = C_{p_{external}} - C_{p_{internal}} \quad (1-3)$$

Based on ASCE 7-10, the peak external uplift pressure coefficient  $C_{p_{external}}$  is given as -2.6 and the peak internal pressure coefficient for an enclosed building is  $\pm 0.18$ . Taking a conservative design approach and assuming that the internal pressure is acting towards the roof, the net pressure coefficient would then be equal to -2.78.

Equation 1-2 can be rewritten as equation 1-4 in order to compute the maximum force required to fail a connection.

$$F = \frac{1}{2} \rho C_{p_{net}} \vartheta^2 A_T \quad (1-4)$$

where  $F$  is the uplift force in lbs (which can be equated to the failure load of 267 lbs) and  $A_T$  is the tributary area in ft<sup>2</sup> (2.8125 ft<sup>2</sup>) allocated to one FRP connection.

Equation 1-4 can be rewritten as Equation 1-5 to obtain the wind speed required to fail the FRP connection.

$$\vartheta = \sqrt{F / (\frac{1}{2} \rho C_{p_{net}} A_T)} \quad (1-5)$$

By solving Equation 1-5, the wind speed required for failure of the FRP roof-to-wall connection is approximately 116 mph. Table 3, below, summarizes the calculations.

**Table 1-3 Summary of Calculation of Failure Wind Speed**

# of Trusses	7
Tributary Area (ft × ft)	0.75 × 3.75
Tributary Area (ft <sup>2</sup> )	2.8125
Roof Dead Load (psf)	2.5
Roof Dead Load (lbs)	7.03
FRP Connection Uplift Strength (lbs)	260
Total Load to Fail the FRP Connection (lbs)	267.03
GC <sub>p</sub>	-2.6
GC <sub>pi</sub>	±0.18
Wind Pressure (psf) (Eq 1-2)	0.003304×V <sup>2</sup>
Wind Force (lbs) (Eq 1-4)	0.009292×V <sup>2</sup>
Failure Wind Speed (ft/s) for FRP Connection	169.52
Failure Wind Speed (mph) for FRP Connection	115.58

### ***1.2.6 Instrumentation on Building Model Tested at the WOW***

Cobra probes were used to measure the wind speeds at the mean roof height. Since the type of test for this portion of the research project is an aeroelastic destructive test, no pressure scanning instrumentation was installed on the model building. The main aim of the WOW test was to experimentally validate the theoretically calculated failure wind speed for the FRP connection. Video of each test was recorded to document the failure observations.

### ***1.2.7 WOW Test Protocol***

The protocol for this research project consisted of two consecutive main parts with different criteria, as discussed below:

- Part 1, where the turntable angle was fixed at a wind azimuth of 45° and the wind speed was uniformly increased from 60 mph to 100 mph at equal increments of 10 mph every 1 minute (sampling time was 60 seconds)
- Part 2, where the turntable was rotated from azimuths of 0° to 90° at equal increments of 9° every 1 minute (sampling time is 60 seconds). Testing speeds for Part 2 were 110 mph, 115 mph and 120 mph.

The building was kept under fully enclosed conditions for the duration of the test and the simulated conditions were for an open terrain with no obstructions. Tables 1-4 and 1-5, below, summarize the test protocols for Parts 1 and 2 described above, respectively. Note that the wind speeds presented in the following tables belong to the mean wind speeds estimated at mean roof height of the model building. The mean wind speeds in the WOW are measured at a height of 10.5-ft.

**Table 1-4 Part 1 of the Test Protocol**

Description	Duration (min)	WOW Throttle %	Approximate Wind Speed (mph)	Wind Direction (deg.)	Condition	Exposure
Destructive Testing	1	50	60	45	Enclosed	Open
		58	70			
		67	80			
		75	90			
		83	100			

**Table 1-5 Part 2 of the Test Protocol**

Description	Duration (min)	WOW Throttle %	Approximate Wind Speed (mph)	Wind Direction (deg.)	Condition	Exposure
Destructive Testing	1	92	110	0° to 90° at 9° increments	Enclosed	Open
		96	115	0° to 90° at 9° increments		
		100	120	0° to 90° at 9° increments		

### 1.3 Results and Discussion

During the WOW tests, protocols 1 and 2 were followed and experiments were conducted one after the other until failure of the model occurred. Failure occurred during the last phase of Part 2 testing protocol described above. Figures 1-13, 1-14, and 1-15 show the respective states of the model before, during, and after the roof failure. The model failed at a wind direction of during Part 2 of the test protocol.



**Figure 1-13 Model before Failure**



**Figure 1-14 Model during Failure**



**Figure 1-15 Model after Failure**

From Figure 1-15, the wind speed recorded at WOW at the exact time of failure is 147.4 mph. This value is recorded at a height of 10.5-ft. The model building had a mean roof height of 3-ft. Using Equation 1-6 below obtained for the mean wind speed profile shown in Figure 1-3, the failure speed at a height of 3-ft was estimated as:

$$\frac{h}{h_{ref}} = 1.1596 \times \left(\frac{\vartheta}{\vartheta_{ref}}\right)^{6.1916} \quad (1-6)$$

where  $h = 3$ -ft,  $h_{ref} = 10.5$ -ft and  $\vartheta_{ref} = 147.4$  mph.

Equation 1-6 can be re-written into Equation 1-7 in order to find the required experimental failure speed at mean roof height of 3-ft

$$\vartheta = \vartheta_{ref} \times \left(\frac{h}{1.1596 \times h_{ref}}\right)^{1/6.1916} \quad (1-7)$$

Solving Equation 1-7 yields an experimental failure wind speed of approximately 117.5 mph. Recall that the theoretical failure wind speed estimated from structural analysis conducted on the roof was found to be approximately equal to 115.6 mph.

Equation 1-8 below shows the percentage error between the theoretical and experimental values obtained.

$$\% \text{ Error} = \left| \frac{\text{Theoretical value} - \text{Experimental value}}{\text{Theoretical value}} \right| \times 100 \quad (1-8)$$

where the theoretical and experimental values are equal to 115.6 mph and 117.5 mph respectively.

Solving Equation 1-8, the percentage error found was equal to about 1.6%. This value obtained is considered acceptable and the results obtained are deemed satisfactory. The above results show that the failure wind speed for FRP roof-to-wall connection for any given roof configuration can be accurately estimated based on component level testing of the uplift capacity of the connection and comparing that with the wind loading estimated from ASCE 7-10.

## 1.4 Conclusion

Non-intrusive FRP connections were considered as replacements or retrofitting alternatives for intrusive metal connectors for roof-to-wall connections in residential buildings. The advantages of using the FRP connection system are as follows: (1). Because the FRP connection is nonintrusive (i.e., it uses high-strength adhesive rather than nails as metal connections do), it does not weaken the wood members through nail penetration [4]. Thus the application of the FRP connection to existing structures in need of retrofitting will prevent further weakening of wood members caused by nails and screws; (2). The corrosion resistance of the FRP connection in harsh environments such as in coastal areas contributes to the durability of the housing system and the lowering of its life-cycle costs; (3). No intrusion into the wooden members reduces the risk of wind driven rain ingress.

The uplift capacity of the FRP connections were determined from uniaxial load tests conducted in the structures lab. The uniaxial load test results were used to estimate the theoretical failure wind speed for the FRP connection. The aim was to compare the theoretical value with the failure wind speed obtained experimentally.

The results of the WOW testing showed that the uplift load capacity of the FRP connection is adequate for resisting wind induced loads at high wind speeds (up to 115 mph, which represents Category 3 hurricane condition). The WOW tests were used to experimentally validate the theoretically calculated failure wind speed for the connection. The percentage difference between the theoretical and experimental failure wind speeds was equal to about 1.6%, which was deemed satisfactory. It was concluded that the failure wind speed for FRP roof-to-wall connection for any given roof configuration can be accurately estimated based on component level testing of the uplift capacity of the connection and comparing that with the wind loading estimated from ASCE 7-10. Further study is also needed to determine the effect of scaling factors.

## 1.5 References

1. NSB (National Science Board) (2007) Hurricane Warning: The Critical Need for a National Hurricane Research Initiative. NSB, Arlington, VA, NSB-06-115, pp. 1–36.
2. Kikugawa, H., Bienkiewicz, B., *Wind Damages and Prospects for Accelerated Wind Damage Reduction in Japan and in the United States*, Proceedings of 37<sup>th</sup> Joint Meeting Panel on Wind and Seismic Effects, 2005, Tsukuba, Japan

3. Arindam Gan Chowdhury, Ivan Canino, Amir Mirmiran, Nakin Suksawang and Thomas Baheru, *Wind-Loading Effects on Roof-to-Wall Connections of Timber Residential Buildings*, Journal of Engineering Mechanics, 2013.139, 386-395
4. Sheikh Saad Ahmed, Ivan Canino, Arindam Gan Chowdhury, Amir Mirmiran and Nakin Suksawang, *Study of the Capability of Multiple Mechanical Fasteners in Roof-to-Wall Connections of Timber Residential Buildings*, Practice Periodical on Structural Design and Construction, February 2011, pp. 2-9
5. Canino, I., Chowdhury, A. G., Mirmiran, A., & Suksawang, N., *Triaxial Load Testing of Metal and FRP Roof-to-Wall Connectors*, Journal of Architectural Engineering, 2001, 17(3), 112-120
6. Cetin Canbek, Amir Mirmiran, Arindam Gan Chowdhury and Nakin Suksawang, *Development of Fiber-Reinforced Polymer Roof-to-Wall Connection*, Journal of Composites for Construction, July/August 2011, pp. 644-652
7. Chowdhury, A. G., Canino, I., Mirmiran, A., Suksawang, N., & Baheru, T., *Wind-Loading Effects on Roof-to-Wall Connections of Timber Residential Buildings*. Journal of Engineering Mechanics, 2013, 139(3), 386-395
8. Canino-Vazquez, I. R., *Aerodynamic Load Characteristics Evaluation and Tri-Axial Performance Testing on Fiber Reinforced Polymer Connections and Metal Fasteners to Promote Hurricane Damage Mitigation*, 2009, Master's Thesis, Florida International University
9. A. Gan Chowdhury, I. Zisis, P. Irwin, G. Bitsuamlak, J.-P. Pinelli, B. Hajra and M. Moravej, *Large-Scale Experimentation Using the 12-Fan Wall of Wind to Assess and Mitigate Hurricane Wind and Rain Impacts on Buildings and Infrastructure Systems*, Journal of Structural Engineering, 2017, 143(7)

## 2. Assessment of Aerodynamic Loads on Elevated Homes

### Executive Summary

*Elevated homes are common in many coastal communities to minimize the impact of storm surge on the residences. Many other structures, including as mobile homes, trailers, and homes built on crawl space foundations, have an air gap between the floor level and the ground. However, the aerodynamics effects of elevating a structure above the ground are not well addressed in the building codes. To provide more information for these situations, large-scale experiments were conducted at FIU's WOW facility on a representative single-story residential gable roof house. The primary testing was conducted on a 1:5 scale model of the test building for four different elevation conditions: 1) no building elevation, 2) 2-ft equivalent full-scale elevation, 3) 7-ft equivalent full-scale elevation, and 4) 12-ft equivalent full-scale elevation.*

*Results show that the largest wind loads exerted on the building are: the lateral force in the along-wind direction, the vertical uplift force, and the overturning moment about the lateral axis. It was found that the along-wind shear force increases with increasing stilt height, the uplift force reduces with increasing stilt height, and the primary overturning moment increases with increasing stilt height. Strong suction pressures were found on the roof surface, the side and leeward walls, and the underside of the building model for all wind angles tested. The reduction in net uplift with increasing stilt height appears to be the result of offsetting suction pressures acting simultaneously on the roof and floor surfaces of the elevated building. Thus designers should consider the strong suction pressures acting beneath the floor to ensure that an adequate design of the floor's structural system is achieved for performance during high wind events. Careful design of the floor-to-stilt and the stilt-to-foundation connections must be considered to ensure that the building is able to resist strong bending moments exerted at these locations. The effect of Reynolds number needs to be investigated using a partial turbulence simulation approach.*

### 2.1 Introduction

In many communities located along the U.S. Atlantic and Gulf coastlines, low-rise residential buildings constructed near the ocean are vulnerable to threats from both extreme wind loads and hydrodynamic loads due to storm surge caused by hurricanes. The hydraulic forces caused by the currents, wave action, and floating debris associated with storm surge are difficult to resist because they can be much larger in magnitude than the accompanying wind forces. Designing structures to resist the direct action of storm surge can become cost prohibitive, far more than would be required to resist wind forces alone. Therefore, one strategy that can be – and often is – adopted is to elevate the building on piles, columns, piers, or stilts to a height that raises the structure above the Base Flood Elevations (BFEs) identified on Flood Insurance Rate Maps (FIRMs). In fact, elevation has been identified as one of the most important keys to successful coastal construction [1].

When the technique of elevating a structure above the BFE is adopted, the tasks for the structural designer are as follows:

1. To design the supporting columns, piers, or stilts and the foundation to withstand the force caused by storm surge and possible floating debris, and
2. To ensure that the now-elevated structure can withstand the wind forces that occur during hurricanes.

However, one challenge faced by designers is that building codes and standards do not explicitly address how to determine the appropriate wind forces on elevated buildings. Compared to typical residential buildings constructed on grade, the total wind forces and localized cladding loads on an elevated building can be significantly affected by the aerodynamic changes caused by wind flowing underneath the elevated building. Additionally, manufactured homes are built upon raised foundations only a few feet above ground level, and they form another subset of elevated structures for which aerodynamic data is limited.

The objective for this research was to determine the relevant aerodynamic force and moment coefficients for a representative elevated building. The building height was varied between small elevations of only a few feet, to simulate the air gap underneath manufactured homes, and larger elevations up to 12 ft, to simulate elevated coastal residences built on piles, columns, or piers. The Wall of Wind (WOW) facility was suitable for modelling an elevated building at large scale to determine the total forces and localized cladding pressures induced by wind acting on the raised structure.

## **2.2 Background**

Damage observations conducted by Mitigation Assessment Teams (MATs) during recent major hurricanes impacting the U.S. mainland have highlighted the importance of properly designing a coastal residence for both storm surge and strong wind events. Following Hurricane Ike in 2008, a MAT was deployed by the Federal Emergency Management Agency (FEMA), and the resulting observations and recommendations were reported in [1]. Findings from this damage assessment pointed out many failures in the affected regions of Texas and Louisiana were the result of the following: insufficiently sized piles and columns to resist the forces and bending moments caused by flooding and wind, weaknesses in the connection techniques between the house floor and the piles or columns elevating the home, weak or non-existent load paths between the columns and the foundation, poorly designed foundations, and homes elevated inadequately high enough to prevent structural damage caused by flooding. The Hurricane Ike MAT also found many instances depicting cladding failures such as roofing materials, wall siding, roof and soffit vents, and external equipment caused by localized peak wind loads on the buildings, despite the fact that Hurricane Ike's wind speeds in the affected regions of Texas and Louisiana were below design level. Similarly, damage observations following the flooding caused by Hurricane Ivan (2004) in Florida identified poor performance of pile foundations having shallow embedment depths, and pier foundations that were poorly reinforced or lacked the structural capacity to withstand loads from flooding and debris [2]. To the Principal Investigators' knowledge, no previous research has been published in the peer-reviewed literature that attempts to quantify aerodynamic loads on elevated coastal residential structures or manufactured homes installed on elevated foundations.



prototype house by eliminating the front porch and soffit overhang details, and by reducing the number of stilts to four – one stilt located in each corner of the model. These adjustments were made to simplify the experimental setup and to test a more generic building shape so that the results of the project would be more applicable to a larger variety of homes. The effect of elevation on aerodynamic loading was studied by positioning the wind tunnel models on stilts of various heights:

- 1) No stilts – to simulate a typical home built at ground-level, which served as a baseline for comparison with the elevated test cases.
- 2) 2-ft (full-scale) stilt height – to simulate a structure raised slightly above the ground, such as manufactured (mobile) homes.
- 3) 7-ft (full-scale) stilt height – to simulate the actual design elevation of the case study house.
- 4) 12-ft (full-scale) stilt height – to simulate a structure potentially raised to an elevation greater than the case study house.

A large-scale wind tunnel model of the prototype house was constructed using a length scale of 1:5, yielding model dimensions of 69 × 50.4 × 30-in (L × W × H) and equivalent stilt heights of 0.0-in, 4.8-in, 16.8-in, and 28.8-in for the four test cases. This choice of length scale completely engulfed the model well within the WOW flow field for all stilt heights and wind angles considered in the study. The 1:5 wind tunnel model was constructed from clear 9-mm thick polycarbonate panels installed onto a wooden frame built from standard 2×4 lumber stock. The model stilts were cut to length from 4×4 lumber stock.

Two types of instrumentation were used for the 1:5 scale model testing: load cells and pressure scanning system. Four JR3 model 45E15A4 multi-axis load cells, each capable of measuring the simultaneous forces and moments along the three principle axes (6 degrees of freedom), were located beneath the test model – one load cell placed near each corner (Fig. 2-2). The load cell measurement capacities were as follows: 200 lbs for  $F_x$  and  $F_y$ , 300 lbs for  $F_z$ , 1,500 in-lbs for  $M_x$  and  $M_y$ , and 1,000 in-lbs for  $M_z$ . During the model installation at ground level, each load cell was mounted directly between the wood framing inside the model house and the WOW turntable; care was taken during installation to ensure that the load path between the house and the turntable was only through the load cells. For the elevated test cases, the load cells were positioned on the WOW turntable beneath each of the four wooden stilts. Thus, the load path through the stilts was directly through the load cells as well, ensuring that the load cells captured the aerodynamics forces and moments that would be transferred to the building's foundation.

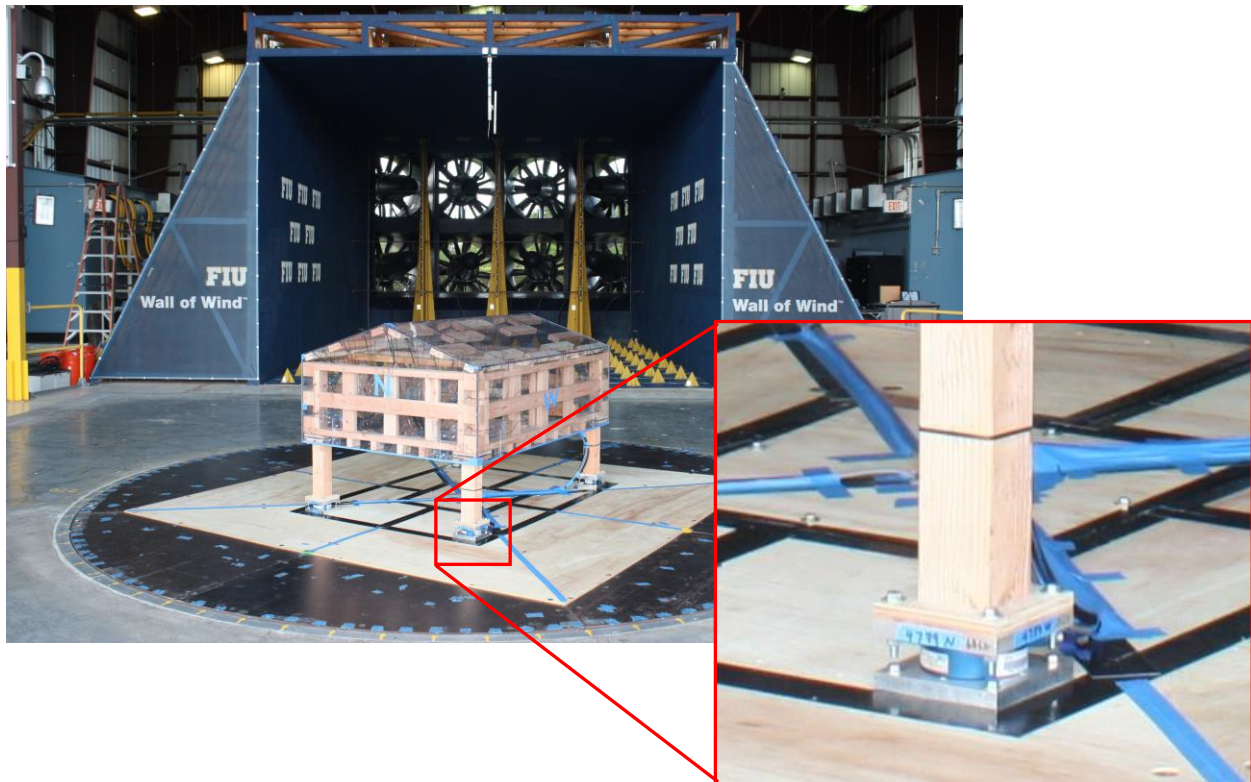


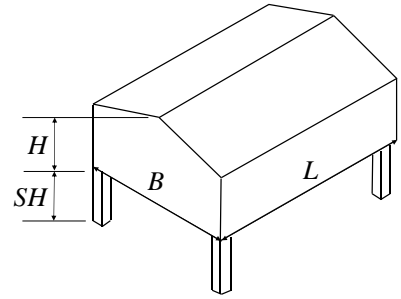
**Figure 2-2 Typical load cell installation between WOW turntable and bottom of stilt**

The 1:5 model was further instrumented with 363 pressure taps, located around the roof, walls, and floor surfaces to investigate the overall pressure distributions on the elevated houses and to determine the localized cladding loads. The pressure taps were connected to a total of six Scanivalve ZOC33 pressure scanners to acquire high-resolution pressure time histories for this study. Details of the pressure tap layout are given in Appendix A. It is also noted that the test model's floor panel was installed only during the elevated test cases, and was not in place when the model was tested at ground level since there was no air flow beneath the model during that case. Hence, floor pressure data is not reported for the 0.0-in stilt height test case.

An investigation was made to determine possible Reynold's number effects on the flow around the elevated residence by constructing a smaller model of the Key Largo case study house at a length scale of 1:60. The 1:60 model was manufactured by the researchers via a Formlabs Form 2 3D printer, which uses the stereolithography (SLA) method of production. Due to size constraints, the 1:60 model was outfitted with 80 pressure taps, each correlating to a specific pressure tap location on the larger 1:5 model. This allowed direct comparison of pressure time histories between the two models to examine Reynold's number effects. Details of the 1:60 model pressure tap layout may be found in Appendix A. The 1:60 scale Reynold's number investigation was conducted only at the 7-ft full scale stilt height (equivalent to a 1:60 model scale stilt height of 1.4-in), which represents the design elevation of the case study house. Table 2-1, below, summarizes the model dimensions used in this study. Figure 2-3 shows each of the test models installed on the WOW turntable during testing.

**Table 2-1 Summary of Stilt House Test Model Dimensions**

<b>Building, Scale</b>	<b>Length (L)</b>	<b>Width (B)</b>	<b>Height (H)</b>	<b>Stilt Heights (SH)</b>
<b>Case Study, 1:1</b>	28.75ft	21.0 ft	12.5 ft	0.0, 2.0, 7.0, 12.0 ft
<b>Test Model, 1:5</b>	69.0 in	50.4 in	30.0 in	0.0, 4.8, 16.8, 28.8 in
<b>Test Model, 1:60</b>	5.75 in	4.2 in	2.5 in	1.4 in



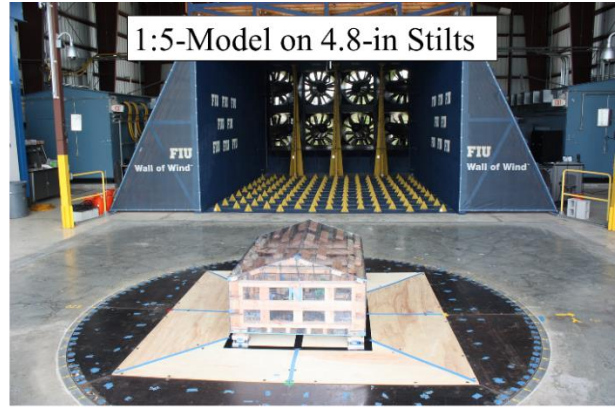
### 2.3.3 Data Acquisition

Force, moment, and pressure data were acquired on the 1:5 scale building model for wind directions ranging from 0° to 90° at 9° increments, for each of the four model elevations. Figure 2-4 shows the orientation of the test model with respect to the mean wind direction for the tests. Testing additional angles beyond 90° was unnecessary due to the symmetry of the building model surfaces, the symmetry of the load cell placement, and the symmetry of the pressure tap layout. Force and moment data were recorded at a sampling rate of 100 Hz by the WOW facility’s custom-designed LabView interface that integrates with National Instruments (NI) data acquisition modules operating on NI cRIO and cDAQ hardware. Baseline force and moment measurements were collected before and after the wind tests at each angle to isolate the aerodynamic forces and moments exerted on the model. During each wind test, pressure data were simultaneously collected at a sampling rate of 520 Hz by a Scanivalve DSM 4000 connected to the six ZOC33 pressure scanners. Wind tests were conducted for a time duration of 60 sec for each wind direction and building model elevation. Pressure data alone were acquired for the 1:60 small-scale model in a similar manner (0° to 90° at 9° increments, sampling rate 520 Hz, 60 sec test duration). Table 2-2 summarizes the test protocol. Note that test results presented in subsequent sections of this report will reference the “Test Identifier” label shown in the last column of Table 2-2, which is linked to the scaled stilt height in inches (e.g. the identifier “SH04\_8” refers to the test case of the 1:5 scale model with a stilt height of 4.8-in, corresponding to a full-scale stilt height of 2-ft).



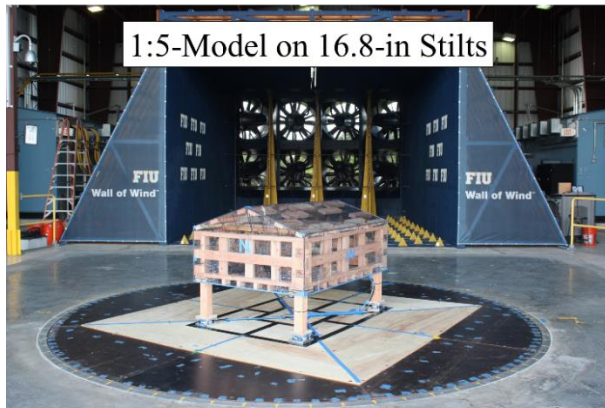
1:5-Model on ground level

(a)



1:5-Model on 4.8-in Stilts

(b)



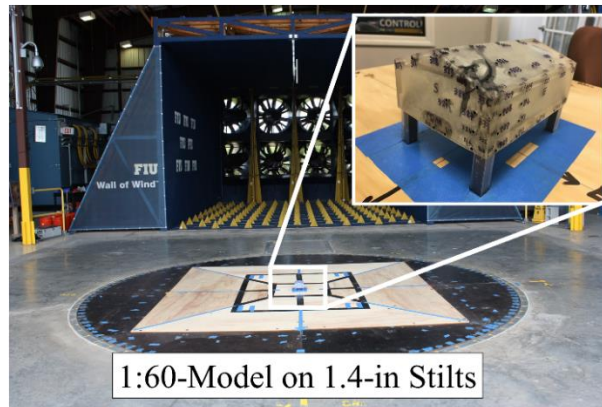
1:5-Model on 16.8-in Stilts

(c)



1:5-Model on 28.8-in Stilts

(d)



1:60-Model on 1.4-in Stilts

(e)

Figure 2-3 Test model installed on WOW turntable: (a)-(d) 1:5 scale model at various elevations, (e) 1:60 scale model

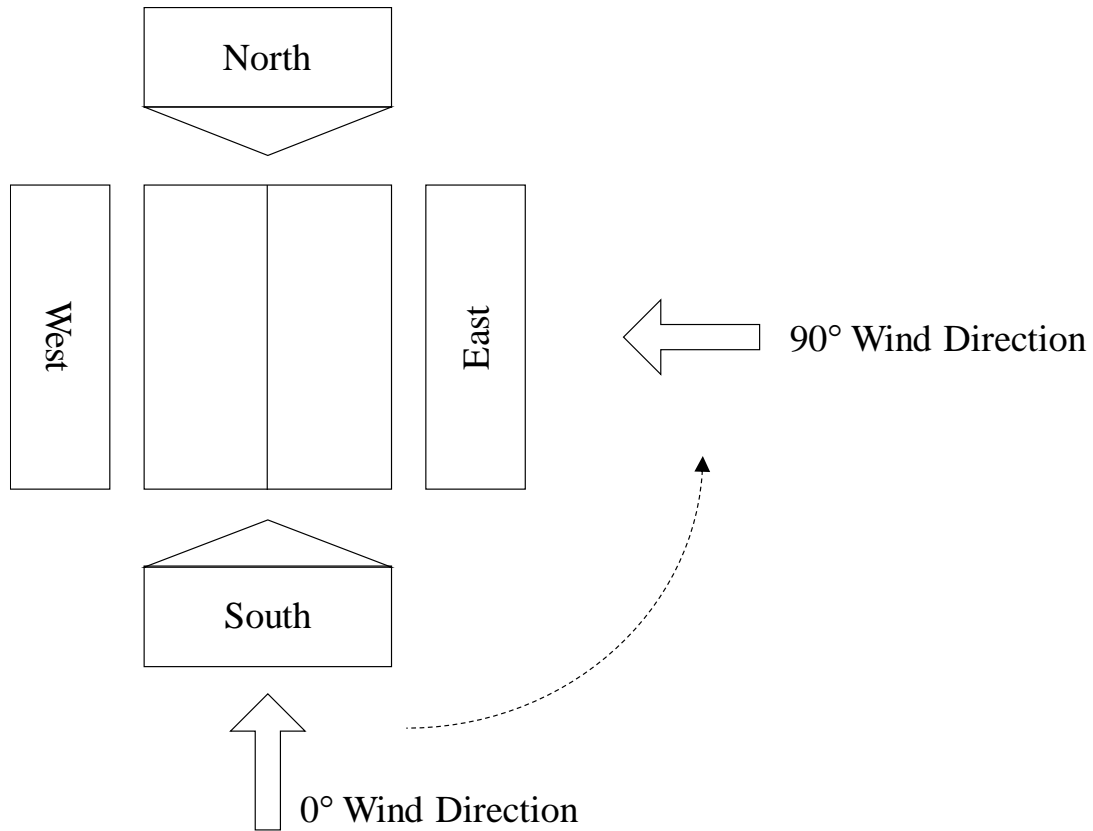


**Figure 2-4 Stilt House Model Testing Orientation**

**Table 2-2 Stilt House Test Protocol**

Test #	Model Length Scale	Stilt Height (SH) (inches)	WOW Throttle %	Instrumentation	Wind Angle	Test Identifier
1	1:5	0.0	40%	LC <sup>1</sup> , PT <sup>2</sup>	0° to 90° (9° increments)	SH00_0
2	1:5	4.8	40%	LC, PT	0° to 90° (9° increments)	SH04_8
3	1:5	16.8	40%	LC, PT	0° to 90° (9° increments)	SH16_8
4	1:5	28.8	40%	LC, PT	0° to 90° (9° increments)	SH28_8
5	1:60	1.4	40%	PT	0° to 90° (9° increments)	SH01_4

<sup>1</sup> LC denotes multi-axis load cells

<sup>2</sup> PT denotes pressure taps

### 2.3.4 Data Analysis

From the test data, global force and moment coefficients were estimated to determine the overall uplift, base shear, and base moments necessary for adequate design of elevated residences and mobile homes. Time histories of the overall global loads were found by appropriately summing the individual forces and moments measured at the base of each stilt for each test direction. Mean, maximum, and minimum global force and moment coefficients were normalized according to the following equations:

$$\begin{aligned}
 C_{F_x} &= \frac{F_x}{\frac{1}{2}\rho V^2 A} & C_{M_x} &= \frac{M_x}{\frac{1}{2}\rho V^2 A H} \\
 C_{F_y} &= \frac{F_y}{\frac{1}{2}\rho V^2 A} & C_{M_y} &= \frac{M_y}{\frac{1}{2}\rho V^2 A H} \\
 C_{F_z} &= \frac{F_z}{\frac{1}{2}\rho V^2 A_z} & C_{M_z} &= \frac{M_z}{\frac{1}{2}\rho V^2 A_z L}
 \end{aligned}
 \tag{2-1}$$

The velocity,  $V$ , in the normalization Equations (2-1) was defined as the mean wind speed in the along-wind (+  $x$ ) direction measured at the mean roof height of the building model for each stilt height tested. The areas used to normalize the force and moment coefficients are the projected areas of the house as illustrated in Figure 2-5, below. The area  $A$  was defined as the largest vertical projection of the building model and was used for normalization in the  $x$  and  $y$  directions. The area  $A_z$ , was defined as the horizontal plan of the building model and was used for normalization along the  $z$  axis.

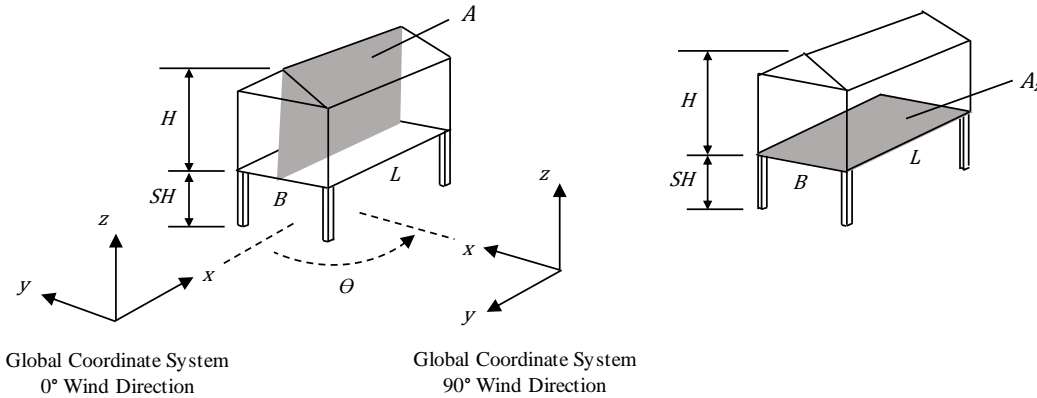


**Figure 2-5 Lengths and Areas Chosen for Normalizing the Global Force and Moment Coefficients**

Similarly, mean, maximum, and minimum pressure coefficients were derived from the experimental data to provide guidelines for adequate design of the building's outer envelope. Pressure coefficients were determined according to Equation 2-2:

$$C_P = \frac{P}{\frac{1}{2}\rho V^2} \quad (2-2)$$

where the velocity,  $V$ , in Equation (2-2) was again defined as the mean wind speed in the along-wind direction measured at mean roof height.

## 2.4 Results and Discussion

### 2.4.1 Force and Moment Measurements

Figure 2-6 shows the observed mean force and moment coefficients. From these plots, it may be seen that the mean loads with the largest overall magnitudes were observed to occur when cornering winds impacted the building model between angles of  $45^\circ$  through  $63^\circ$ . The mean plots indicate that the most significant design loads exerted by the wind on the building are the lateral force in the along wind ( $+x$ ) direction, the vertical uplift force in the  $+z$  direction, and the global bending moment about the  $y$ -axis. General trends in these three loads may be observed as the building model rises vertically on the stilts. First, the lateral force coefficient in the  $x$ -direction,  $C_{F_x}$ , tends to increase with increasing stilt height above the ground for any given wind direction. It is interesting to note that increasing the stilt height from 4.8 to 16.8 inches did not produce a significant change in the mean  $C_{F_x}$  values when compared to raising the model from 0.0 to 4.8-in, and again from 16.8 to 28.8-in.

The mean vertical uplift coefficient,  $C_{F_z}$ , follows a decreasing trend as the model was raised higher above the ground. The largest magnitude mean uplift forces were observed when the model was installed directly on the ground (0.0-in stilt height), and the smallest magnitude mean uplift forces were observed when the model was placed on the tallest stilt height tested in this study, 28.8-in. This indicates that allowing air to flow underneath the building by raising it on the stilts creates a lower pressure zone underneath the building, which causes suction pressures on the floor to counteract the uplift suction pressures on the roof. The net result of the opposing suction pressures is a reduced net uplift force. For both the 16.8 and 28.8-in stilt heights, the mean global loads in the  $+z$  direction were similar in magnitude throughout all angles tested, and the net vertical forces actually pointed downward for wind angles between  $72^\circ$  and  $90^\circ$ . This implies that the net suction forces beneath the floor surface were larger than the net uplift forces on roof surface for these wind angles.

The global bending moment coefficient about the  $y$ -axis,  $C_{M_y}$ , demonstrated a generally increasing trend as the building model was raised vertically above the ground. Since the global bending moment about the  $y$ -axis is produced by the interaction of the net lateral and uplift forces acting on the building's surfaces, it can be concluded that the lateral force  $F_x$  becomes the primary force contributing to the overturning moment on an elevated building due to the increased lever arm of this force relative to the ground. In contrast, the combined effect of the lateral and uplift forces must be considered for a building constructed on the ground or raised only slightly above ground level.

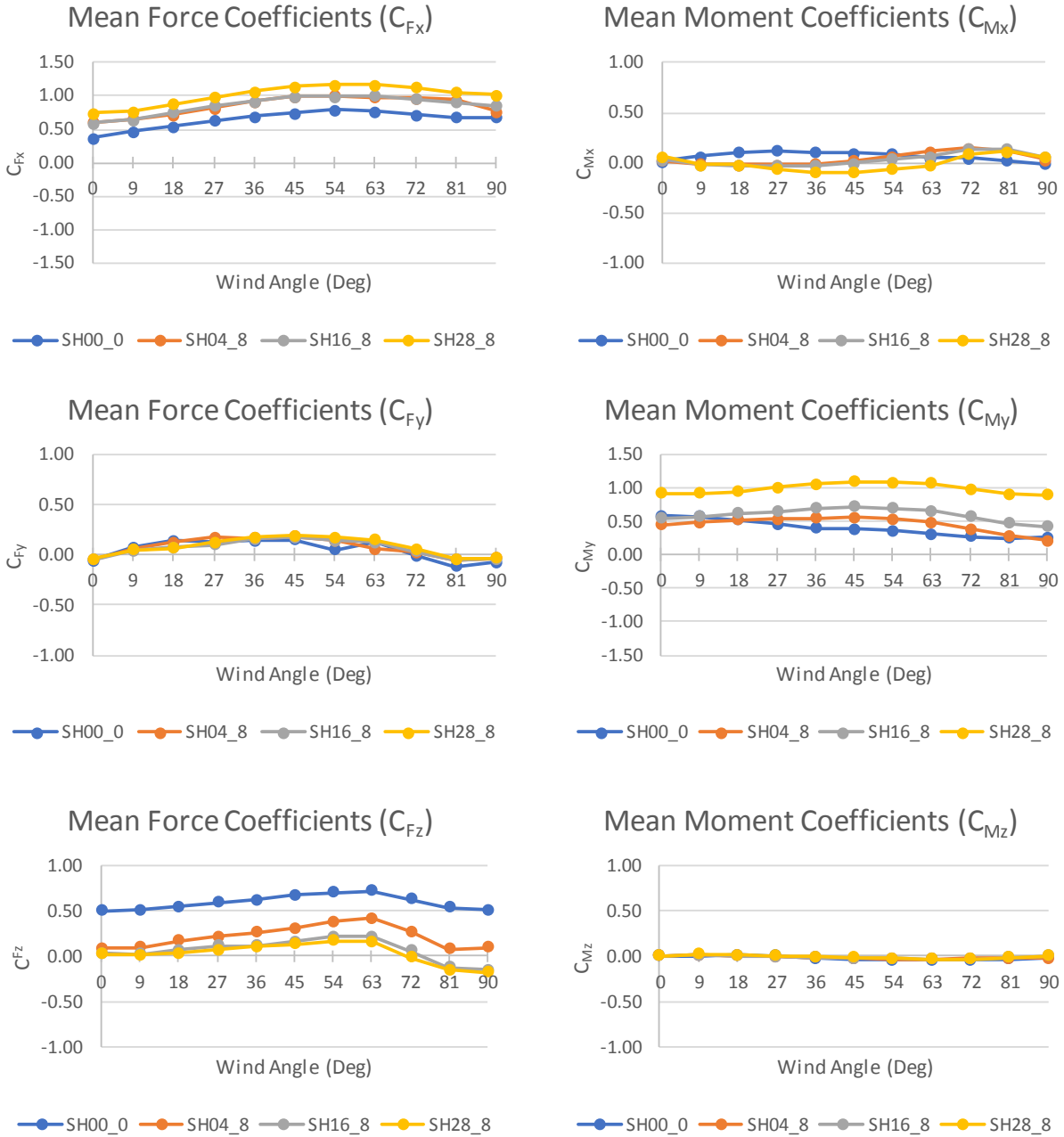


**Figure 2-6 Observed Mean Force and Moment Coefficients**

The discussion of observed peak global loads will be limited to  $C_{Fx}$ ,  $C_{Fz}$ , and  $C_{My}$  since these are the significant contributing loads on the building. Figure 2-7 shows plots of the maximum and minimum observed  $C_{Fx}$ ,  $C_{Fz}$ , and  $C_{My}$  for all angles considered in this study; similar plots for  $C_{Fy}$ ,  $C_{Mx}$ , and  $C_{Mz}$  may be found in Appendix B. The observed peak plots shown in Figure 2-7 agree with the general trends previously described for the mean loads: namely that peak  $C_{Fx}$  values tend to increase with increasing stilt height, peak  $C_{Fz}$  values tend to decrease with increasing stilt height, and peak  $C_{My}$  values tend to increase with increasing stilt height. The highest observed  $C_{Fx}$  values were: 1.08 for the 0.0-in stilt height at the 81° wind angle, 1.40 for the 4.8-in stilt height at the 72°

wind angle, 1.53 for the 16.8-in stilt height at the 90° wind angle, and 1.92 for the 28.8-in stilt height at the 72° wind angle. This represents at 78% increase in the peak lateral force coefficient between a home built on the ground versus a home raised on 12-ft tall (full-scale) stilts. The highest observed  $C_{Fz}$  values were: 0.94 for the 0.0-in stilt height at the 63° wind angle, 0.71 for the 4.8-in stilt height at the 63° wind angle, 0.44 for the 16.8-in stilt height at the 54° wind angle, and 0.44 for the 28.8-in stilt height at the 63° wind angle. This represents at 47% decrease in the peak uplift coefficient between a home built on ground level versus the tallest stilt case tested. It is also noted that the peak observed uplift coefficient did not change significantly between the 16.8-in and 28.8-in stilt height tests for all wind directions tested. The highest observed  $C_{My}$  values were: 1.01 for the 0.0-in stilt height at the 0° wind angle, 0.92 for the 4.8-in stilt height at the 9° wind angle, 1.23 for the 16.8-in stilt height at the 9° wind angle, and 2.09 for the 28.8-in stilt height at the 18° wind angle. This represents at 207% increase in the coefficient between a home built on ground level versus the tallest stilt case tested. Considering the load envelope, defined here as the range between the maximum and minimum coefficients for a given stilt height and wind angle, it may be seen that the load ranges deviate more for both  $C_{Fx}$  and  $C_{My}$  as the model is raised farther above the ground. The range between maximum and minimum  $C_{Fz}$  values remains relatively consistent throughout all test cases considered, with the greatest  $C_{Fz}$  deviations occurring during the ground level tests.

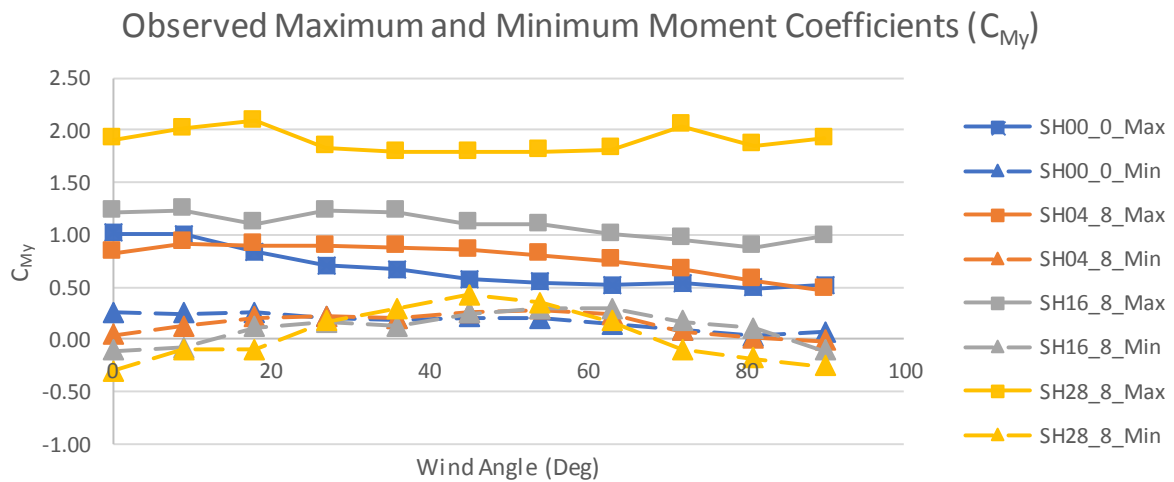
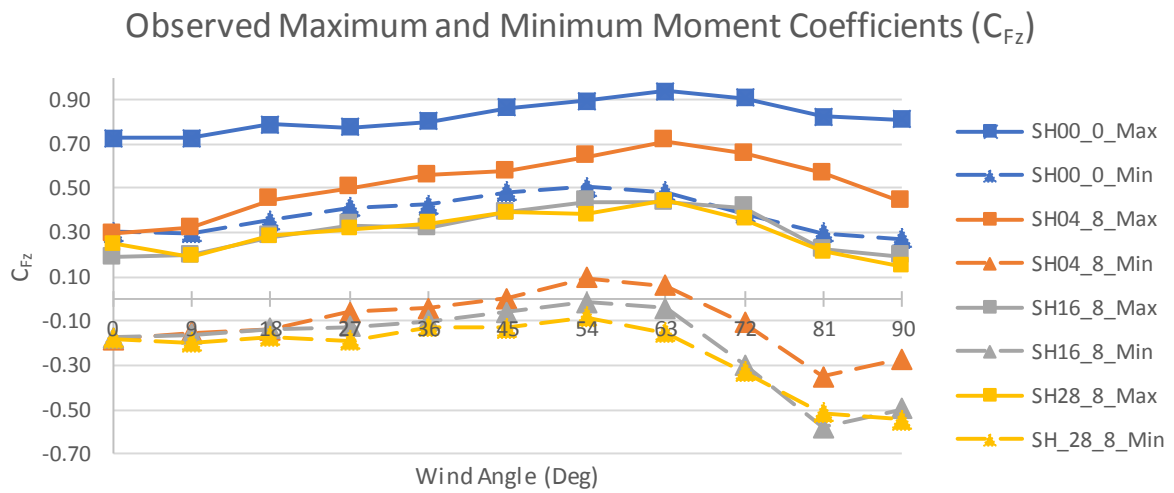
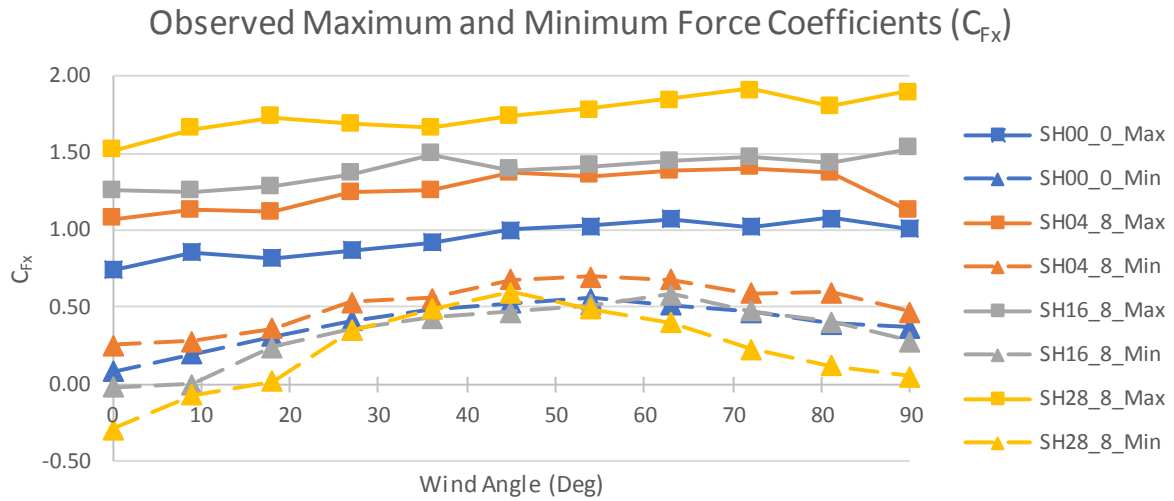


**Figure 2-7 Observed Maximum and Minimum Force and Moment Coefficients for  $C_{Fx}$ ,  $C_{Fz}$ , and  $C_{My}$**

### 2.4.2 Pressure Measurements

Contour plots of the mean pressure distributions acquired during the tests are shown in Figures 2-8, 2-9, 2-10, and 2-11, for wind directions of 0°, 45°, 63°, and 90°, respectively. The 63° wind angle was highlighted in this discussion because the force data revealed that many of the highest magnitude global loads occurred when the wind approached the test models from this oblique direction. Overall, the contour plots show that significant regions of high suction pressures exist on the leading windward edges of the roof and side walls for the 0° and 90° wind directions, as expected. The leading windward edge of the floor also experiences high suction pressures for the 0° and 90° wind directions for the cases when the model house was elevated above the ground. For the 45° and 63° wind directions, large regions of high suction pressures exist along the roof ridgeline and the leeward portion of the roof surface, due to flow separation at the roof ridge and windward eaves. Large suction pressures also exist on the floor surface around the windward stilt for the elevated test cases.

Since post-storm damage assessments have observed common cladding failures to occur in regions of high suction pressures [1, 2], Figures 2-12, 2-13, 2-14, and 2-15 show comparisons of the peak observed suction pressures ( $C_{p \text{ min}}$ ) measured during the experiments for wind angles of 0°, 45°, 63°, and 90°, respectively. Similar plots of peak positive pressures may be found in Appendix B. From the peak pressure plots, it appears that large suction pressures exist on the building model at every elevation. Comparing the relative sizes of peak pressure contours, it appears that the regions of high suction pressures near the roof edges, roof ridge, leeward wall, and beneath the floor (for elevated test cases) all appear to be more severe on the 0.0-in stilt height and 4.8-in stilt height cases than on the 16.8-in and 28.8-in test cases.

For structural designers, one implication of these findings is that the floor level of an elevated home must be designed to withstand high suction pressures. It also appears that high pressure regions are more prevalent on a slightly elevated structure in comparison to more substantial elevations. This indicates that the design of floor systems, decorative skirts and wall cladding should be carefully considered for mobile homes, modular spaces, classroom portables, and homes constructed upon crawl space foundations. Another point of consideration is that the aerodynamic behavior of an elevated structure may be altered if both storm surge and high winds impact the building simultaneously. Under these conditions, the higher water levels due to storm surge can reduce the open clearance between the floor and the water surface, potentially causing a house elevated at 7-ft or 12-ft behave more aerodynamically like a house elevated at only 2 ft.

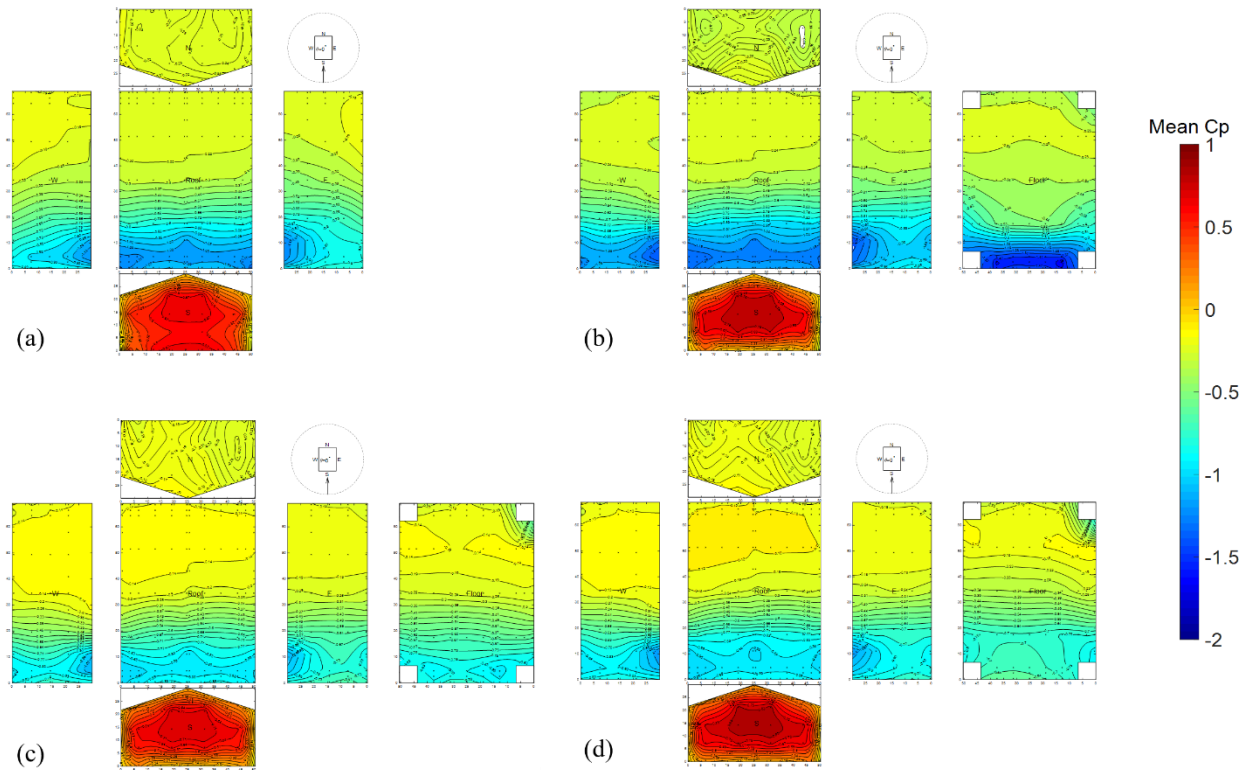


**Figure 2-8 Observed  $C_p$  mean for  $0^\circ$  wind angle: (a) 0.0-in, (b) 4.8-in, (c) 16.8-in, (d) 28.8-in**

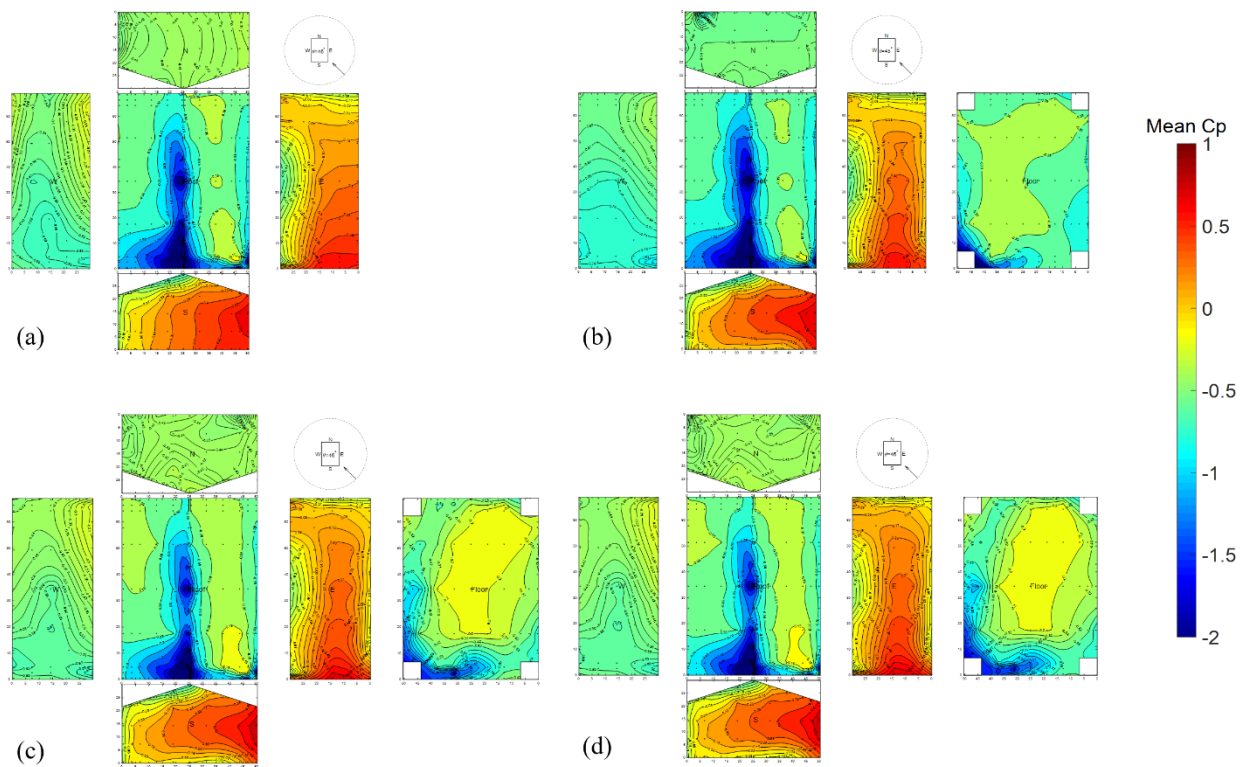


**Figure 2-9 Observed  $C_p$  mean for  $45^\circ$  wind angle: (a) 0.0-in, (b) 4.8-in, (c) 16.8-in, (d) 28.8-in**

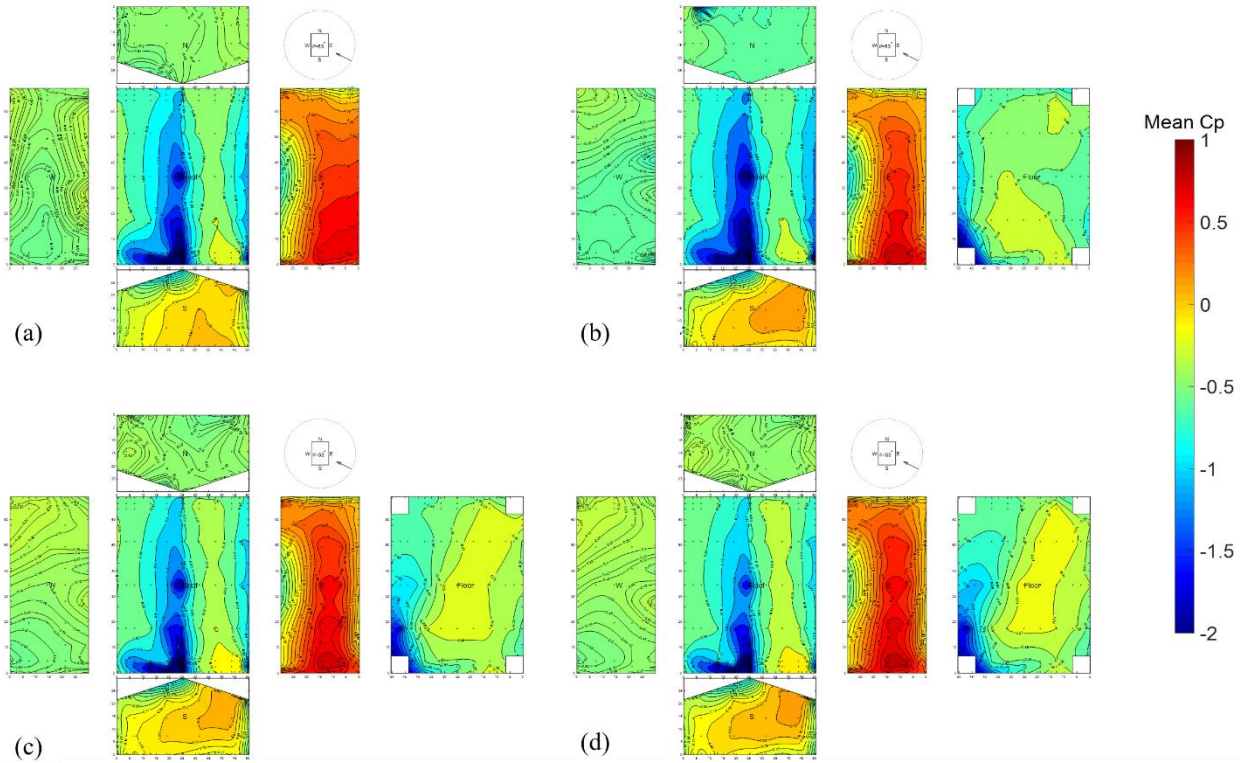


**Figure 2-10 Observed  $C_{p\ mean}$  for 63° wind angle: (a) 0.0-in, (b) 4.8-in, (c) 16.8-in, (d) 28.8-in**

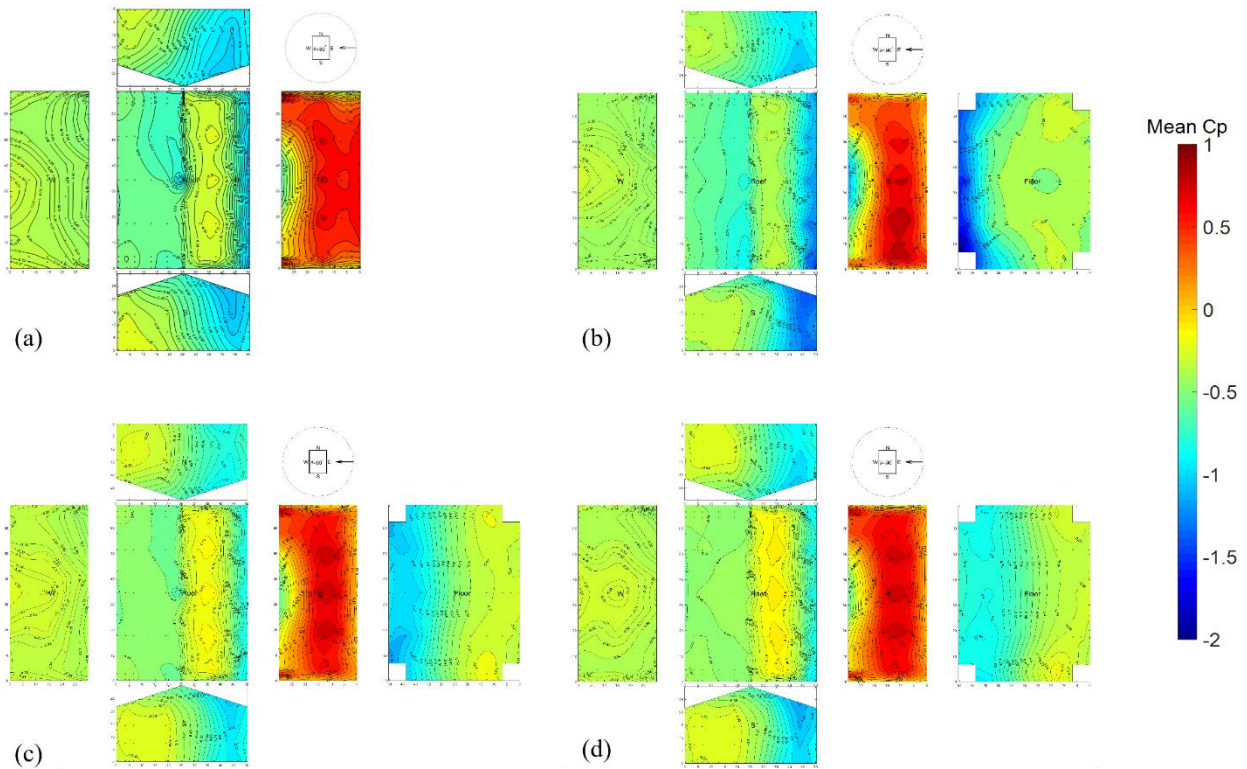


**Figure 2-11 Observed  $C_{p\ mean}$  for 90° wind angle: (a) 0.0-in, (b) 4.8-in, (c) 16.8-in, (d) 28.8-in**

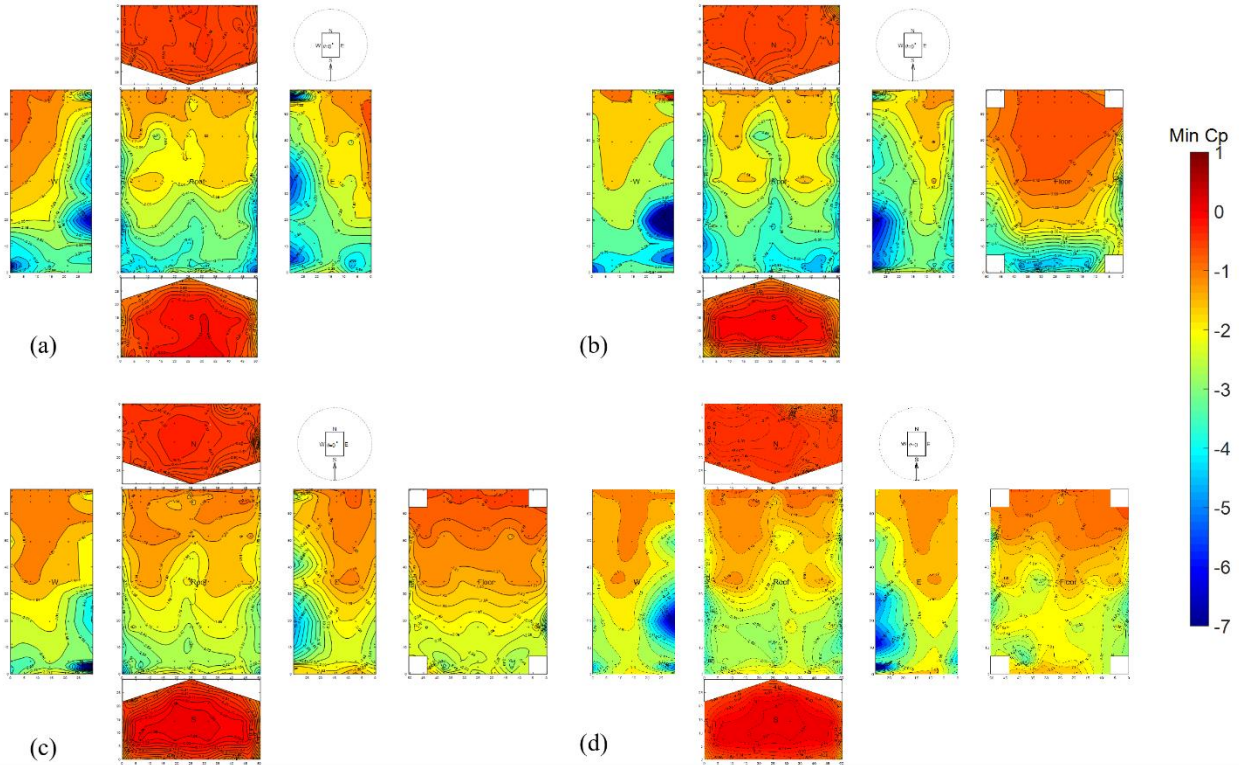


**Figure 2-12 Observed  $C_{p\ min}$  for  $0^\circ$  wind angle: (a) 0.0-in, (b) 4.8-in, (c) 16.8-in, (d) 28.8-in**

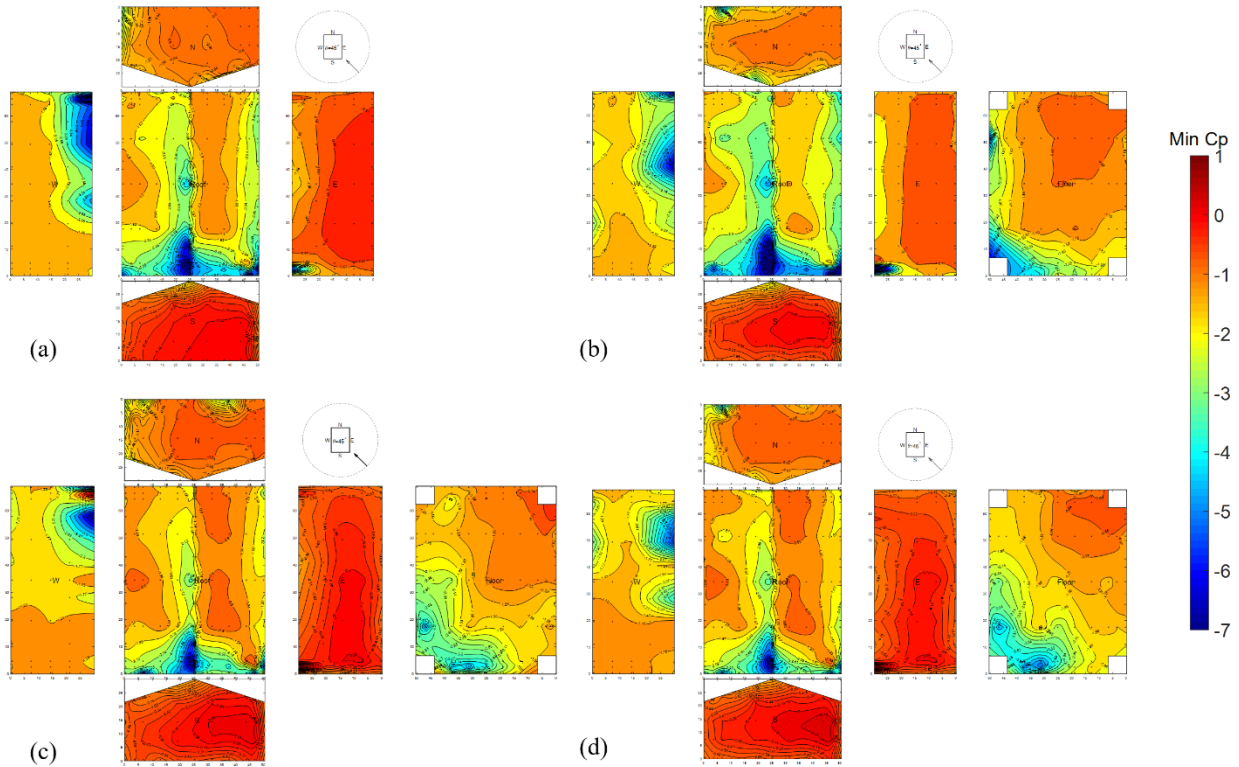


**Figure 2-13 Observed  $C_{p\ min}$  for  $45^\circ$  wind angle: (a) 0.0-in, (b) 4.8-in, (c) 16.8-in, (d) 28.8-in**

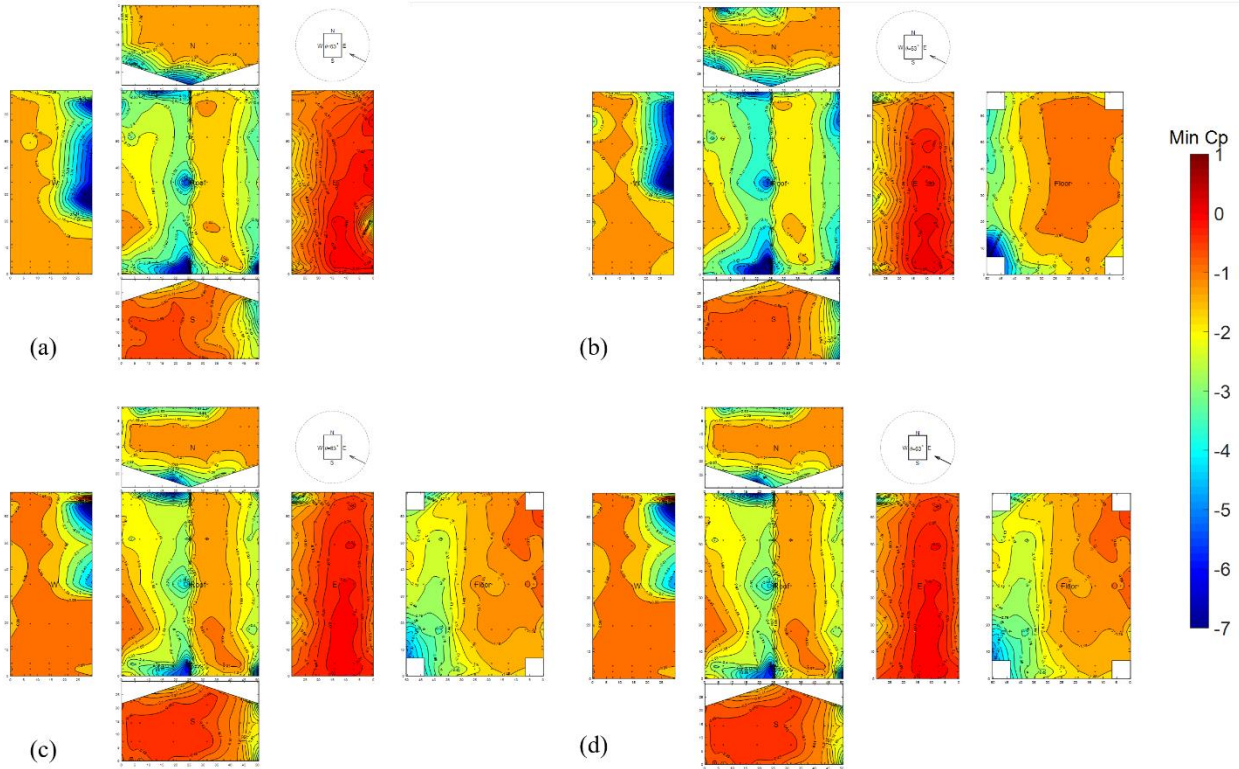


**Figure 2-14 Observed  $C_{p\ min}$  for 63° wind angle: (a) 0.0-in, (b) 4.8-in, (c) 16.8-in, (d) 28.8-in**

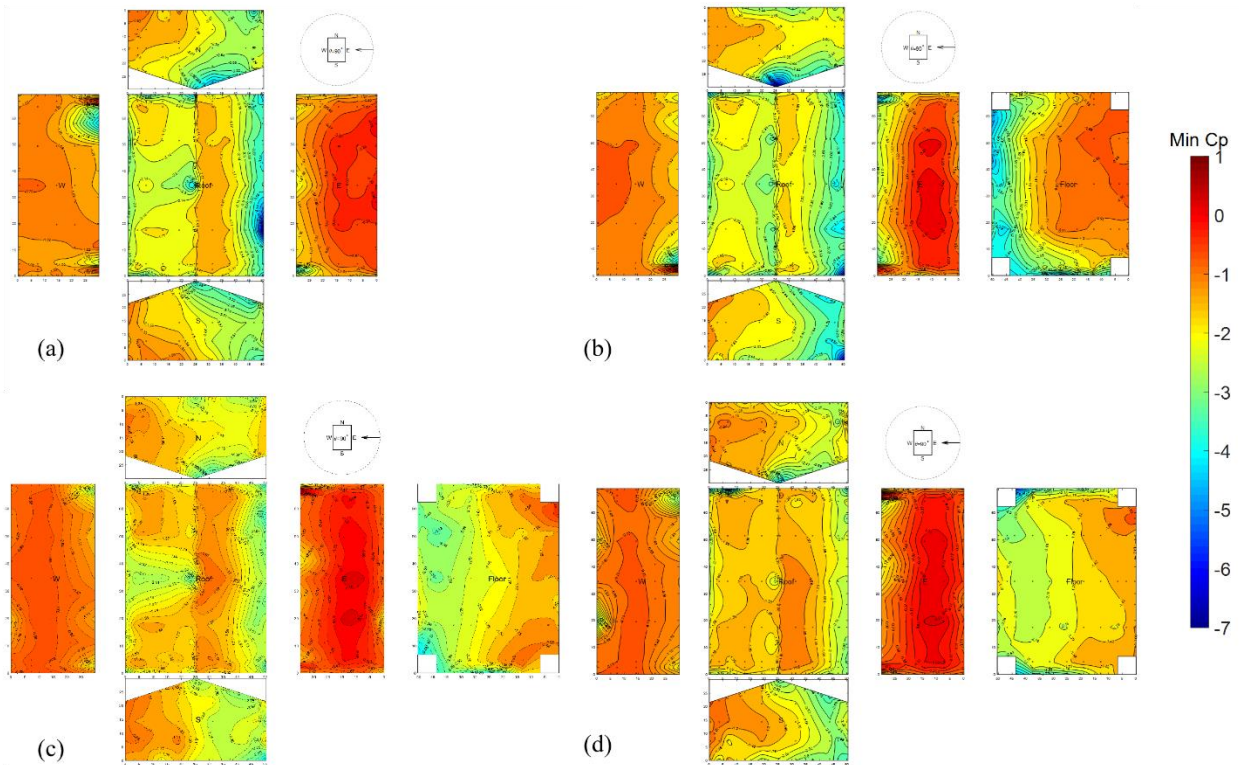


**Figure 2-15 Observed  $C_{p\ min}$  for 90° wind angle: (a) 0.0-in, (b) 4.8-in, (c) 16.8-in, (d) 28.8-in**

### 2.4.3 Reynolds Number Effects

The effect of Reynolds number on the flow was investigated by comparing measurements from the 1:5 scale model with similar measurements from the 1:60 scale model, both elevated atop equivalent full-scale stilt heights of 7 ft. Wind angles of  $45^\circ$  and  $63^\circ$  were considered for this discussion. To compare the models, two rows of pressure taps along the building's surface were isolated: a line of pressure taps on the gable wall and along the roof parallel to the length of the building (labelled the "along" case), and second line of pressure taps on the side wall and the roof parallel to the width of the building (labelled the "across" case). These lines of pressure taps are illustrated in Figure 2-16. Results of this comparison are shown in Figure 2-17 for the  $45^\circ$  wind angle and Figure 2-18 for the  $63^\circ$  wind angle. Figures 2-17 and 2-18 both show that the trends and magnitudes of the mean pressure coefficients are in general agreement for the two wind angles considered here. However, the observed peak pressure coefficients show significant differences, with the 1:60 model consistently experiencing peak pressures of considerably higher magnitude than the 1:5 scale model. These results are inconsistent with the findings of Hoxey et. al [3]. One of the possible reasons could be the effect of missing low frequency turbulence for the larger model. Further research is needed to investigate this using a partial turbulence simulation approach.

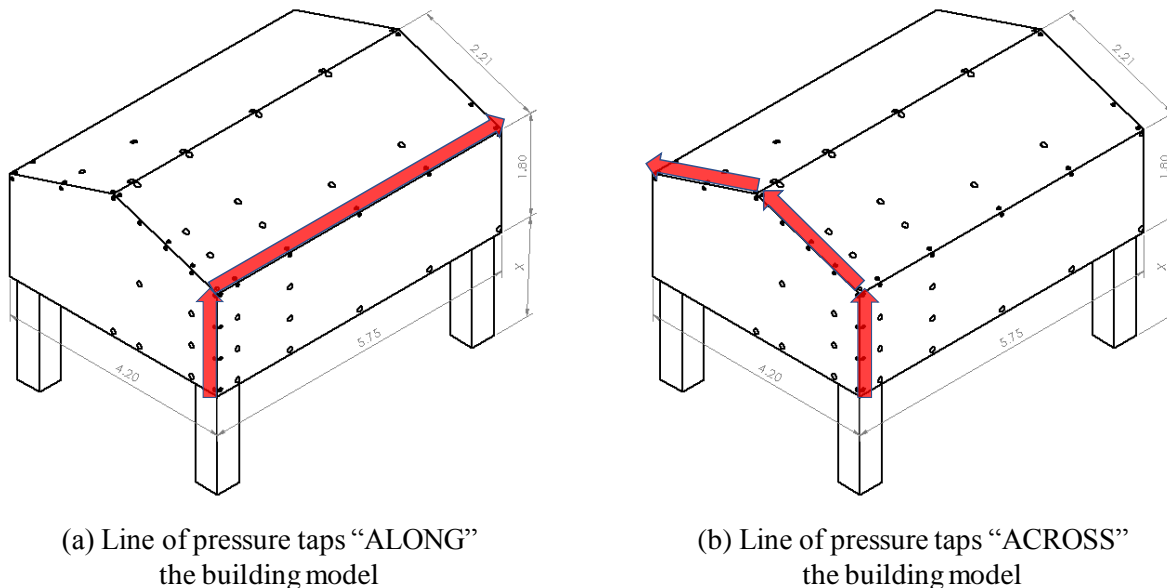


**Figure 2-16 Pressure tap lines used to compare the 1:5 and 1:60 scale models for Reynolds number effects: (a) "Along" the building, and (b) "Across" the building**

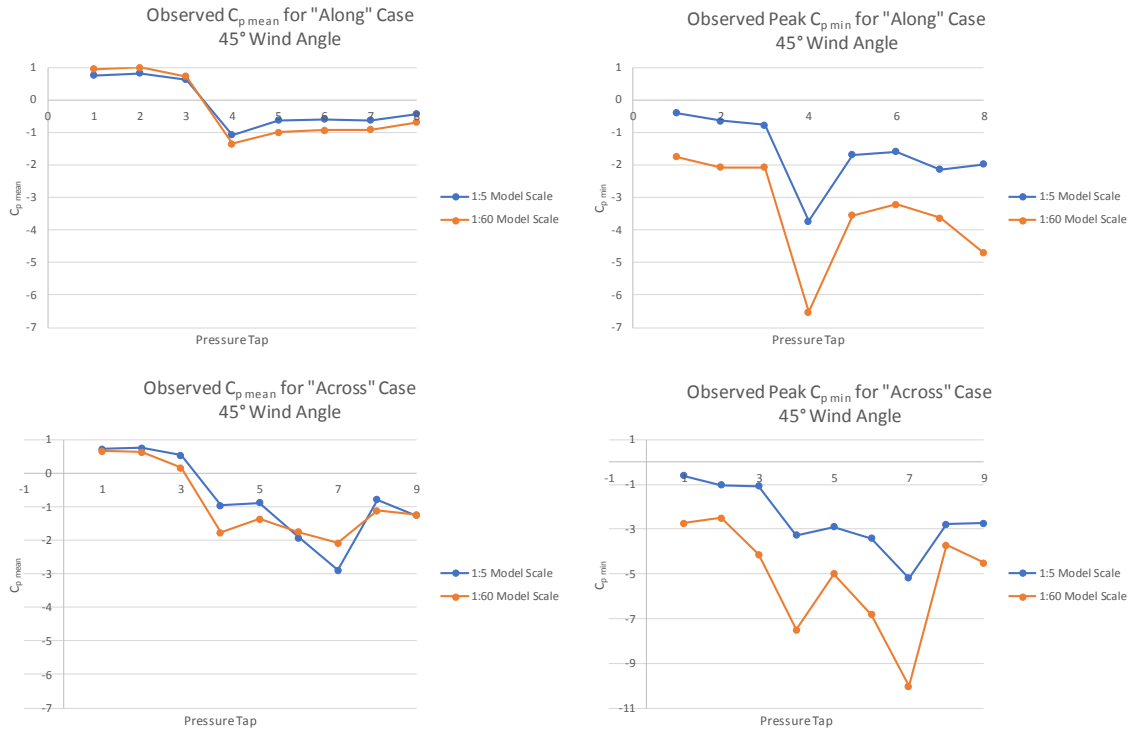


**Figure 2-17 Comparison of observed mean and peak minimum pressure coefficients for 1:5 and 1:60 scale models at the 45° wind direction**

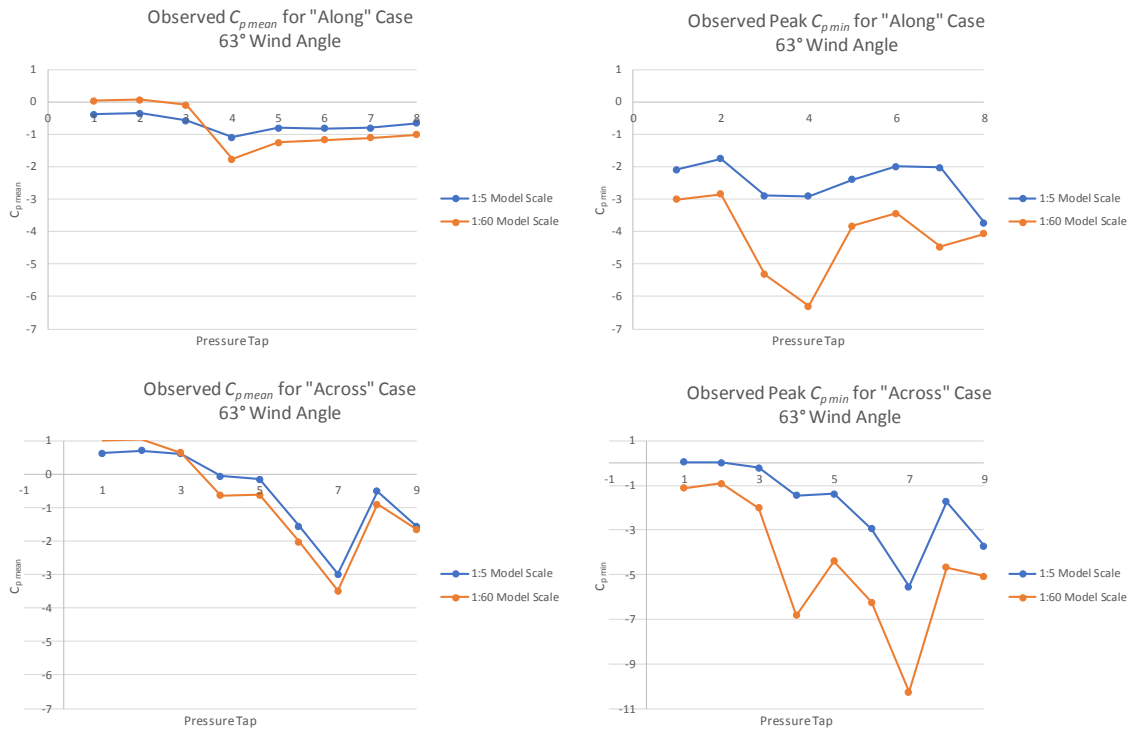


**Figure 2-18 Comparison of observed mean and peak minimum pressure coefficients for 1:5 and 1:60 scale models at the 63° wind direction**

## 2.5 Conclusions and Recommendations

Elevated homes are common in many coastal communities to minimize the impact of storm surge on the residences. Many other structures, including as mobile homes, trailers, and homes built on crawl space foundations, have an air gap between the floor level and the ground. However, the aerodynamics effects of elevating a structure above the ground are not well addressed in the building codes. To provide more information for these situations, large-scale experiments were conducted at FIU's WOW facility on a representative single-story residential gable roof house. The primary testing was conducted on a 1:5 scale model of the test building for four different elevation conditions: 1) no building elevation, 2) 2-ft equivalent full-scale elevation, 3) 7-ft equivalent full-scale elevation, and 4) 12-ft equivalent full-scale elevation. The 1:5 model was instrumented with four multi-axis load cells and 363 pressure taps to capture the aerodynamic forces and bending moments transferred to the ground and the fluctuating pressure distributions on all surfaces of the building model. Additional pressure testing was conducted on a 1:60 scale model of the structure installed at the 7-ft equivalent full-scale elevation to check for Reynold's number effects in the testing.

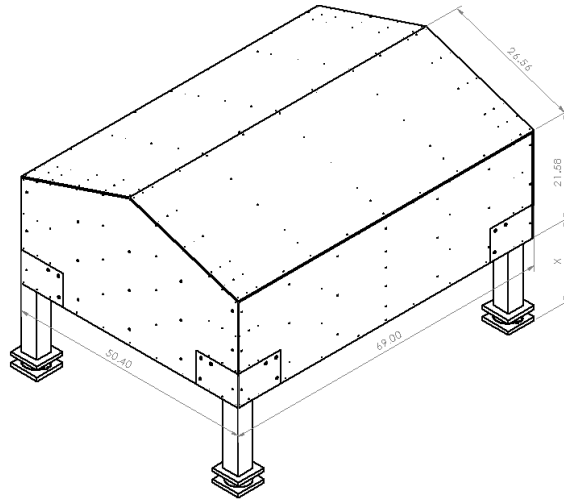
Results show that the largest wind loads exerted on the building are: the lateral force in the along-wind direction, the vertical uplift force, and the overturning moment about the lateral axis. It was found that the along-wind shear force increases with increasing stilt height, the uplift force reduces with increasing stilt height, and the primary overturning moment increases with increasing stilt height. Strong suction pressures were found on the roof surface, the side and leeward walls, and the underside of the building model for all wind angles tested. The reduction in net uplift with increasing stilt height appears to be the result of offsetting suction pressures acting simultaneously on the roof and floor surfaces of the elevated building. It is concluded that, for elevated buildings, designers should consider the strong suction pressures acting beneath the floor to ensure that an adequate design of the floor's structural system is achieved for performance during high wind events. Further, careful design of the floor-to-stilt and the stilt-to-foundation connections must be considered to ensure that the building is able to resist strong bending moments exerted at these locations. Effect of Reynolds number needs to be investigated using a partial turbulence simulation approach [4].

## 2.6 References

1. Federal Emergency Management Agency (FEMA), *FEMA P-757, Mitigation Assessment Team Report: Hurricane Ike in Texas and Louisiana. Building Performance Observations, Recommendations and Technical Guidance*, April, 2009.
2. Federal Emergency Management Agency (FEMA), *FEMA 490, Summary Report on Building Performance:2004 Hurricane Season*, March, 2005.
3. Hoxey, Roger, et al. "Reynolds number effects on wind loads on buildings." *Proceedings of the 2013 European and African conference on wind engineering, Robinson College, Cambridge, England, EACWE*. 2013.

4. Asghari Mooneghi, Maryam, "Experimental and Analytical Methodologies for Predicting Peak Loads on Building Envelopes and Roofing Systems" (2014). *FIU Electronic Theses and Dissertations*. Paper 1846. <http://digitalcommons.fiu.edu/etd/1846>

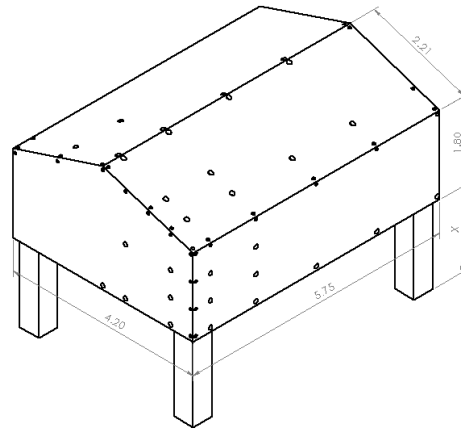
# Appendix A



ISOMETRIC VIEW

- NOTE:  
A. ELEVATION MEASURED FROM FLOOR TO BOTTOM EDGE OF STRUCTURE  
B. STILT ELEVATION PROFILES: X= 4.8", X=16.8", X=28.8"  
C. 1:5 SCALE MODEL

**Figure A- 1 Isometric View of 1:5 Stilt House Model**



ISOMETRIC VIEW

NOTE:  
 A. ELEVATION MEASURED FROM FLOOR TO BOTTOM EDGE OF STRUCTURE  
 B. STILT ELEVATION PROFILE: X= 1.4"  
 C. 1:60 SCALE MODEL

**Figure A- 2 Isometric View of 1:60 Stilt House Model**

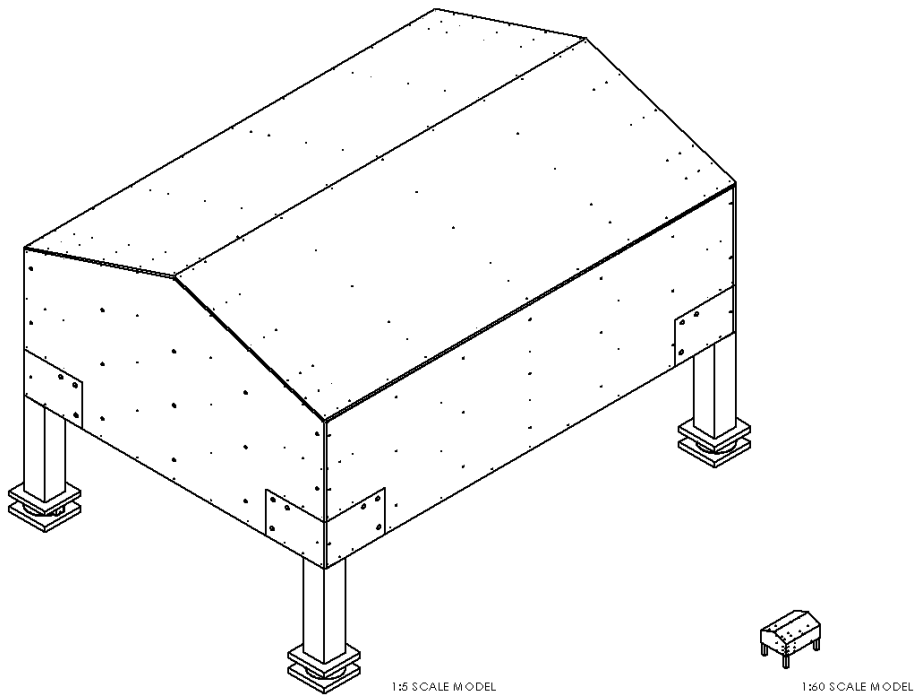


**Figure A- 3 Relative comparison of 1:5 and 1:60 scale models with 7-ft equivalent full-scale stilt height**

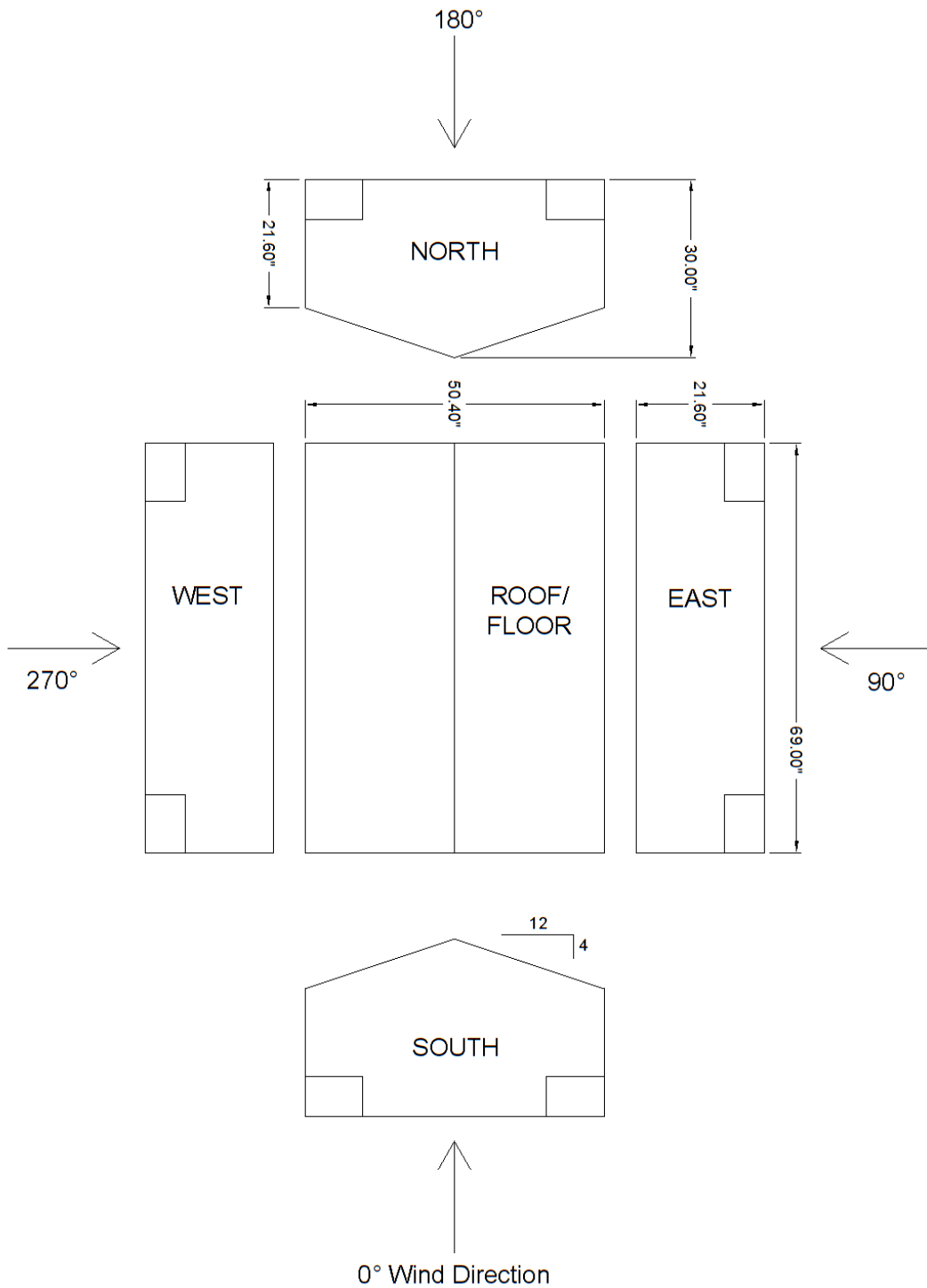


**Figure A- 4 Dimensions and Orientation of 1:5 Scale Stilt House Model**

**(Note: Rectangular regions shown in the lower corner of each wall are removable panels for instrumentation access)**

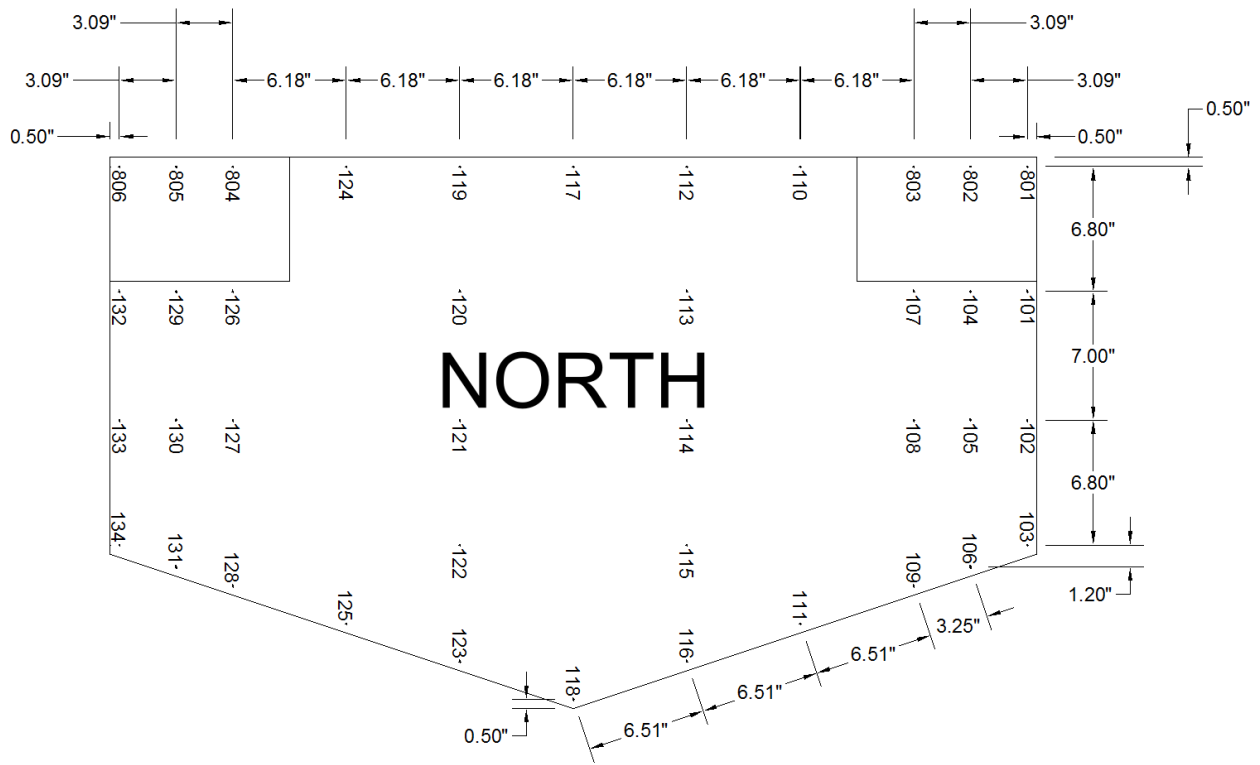


**Figure A- 5 Pressure Tap Layout on 1:5 Scale Model: North Gable Wall**



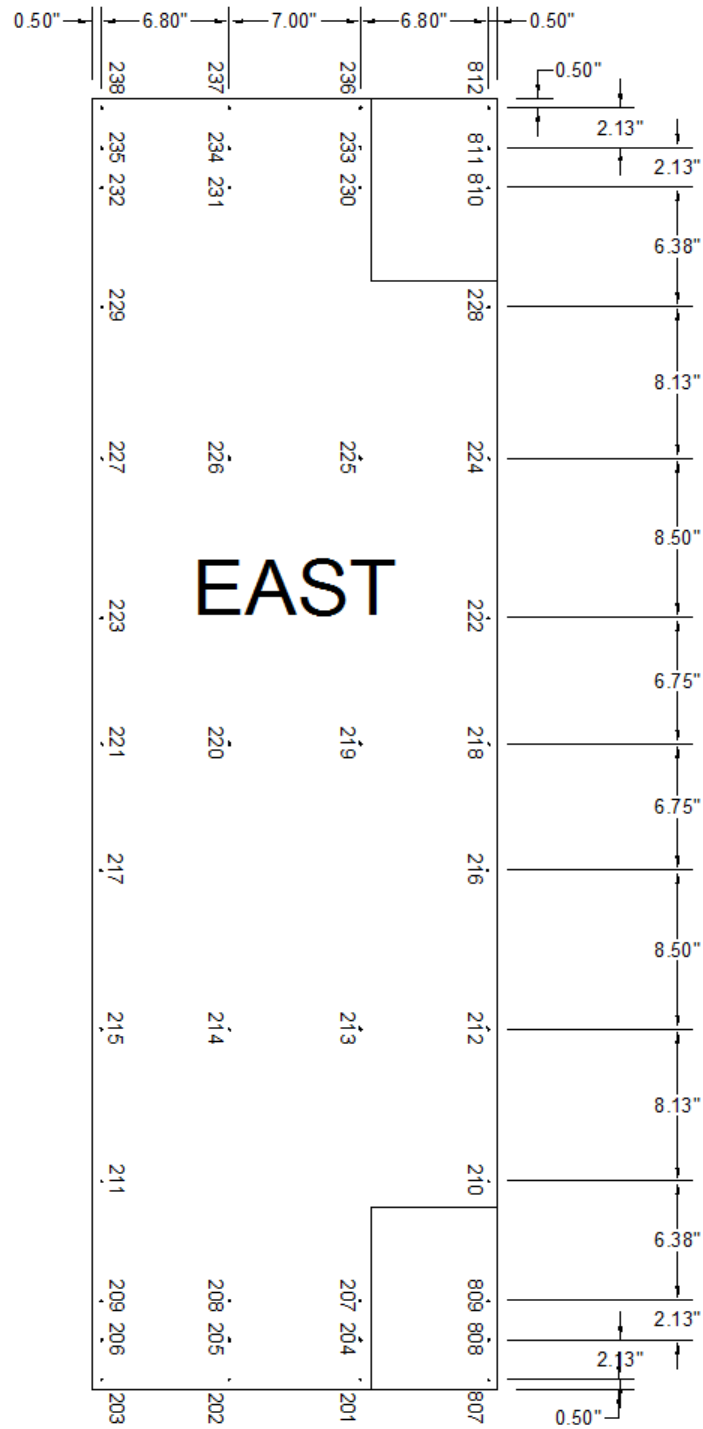


**Figure A- 7 Pressure Tap Layout on 1:5 Scale Model: East Wall**

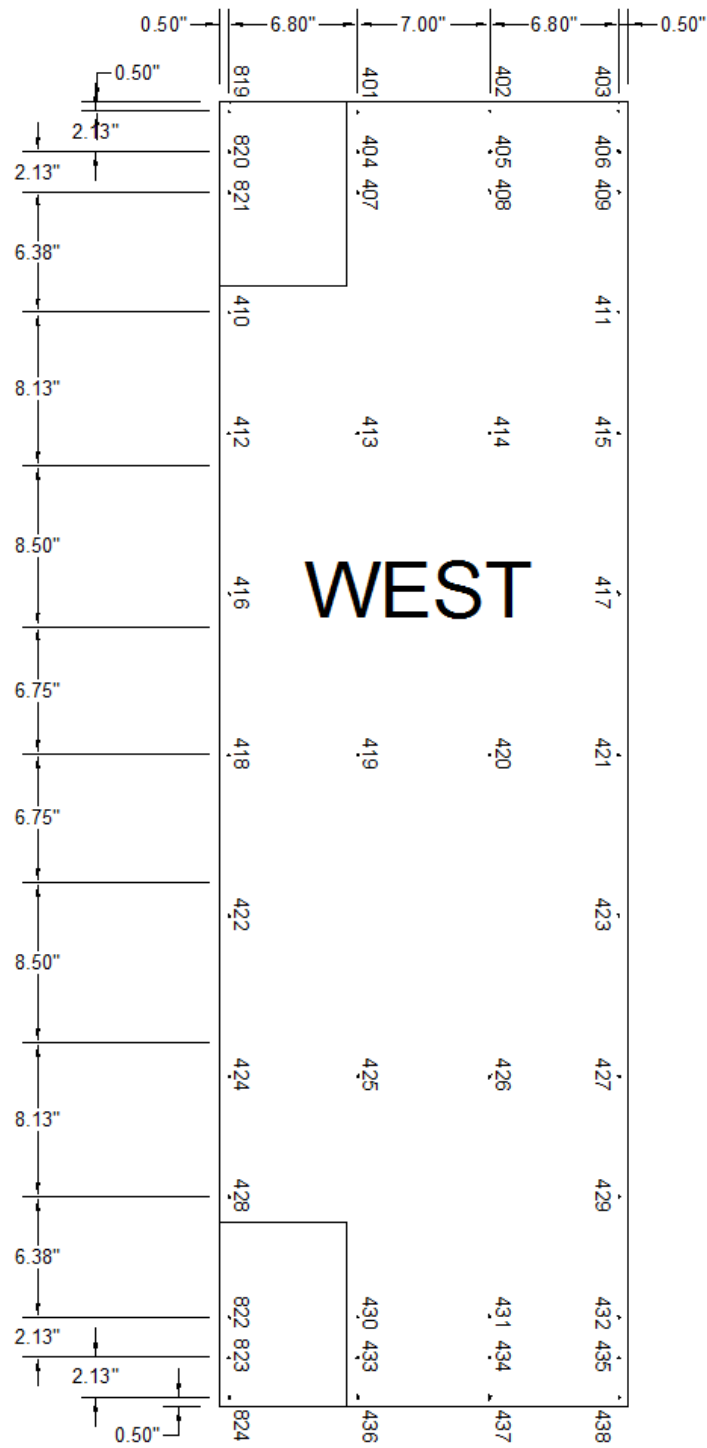


**Figure A- 8 Pressure Tap Layout on 1:5 Scale Model: West Wall**

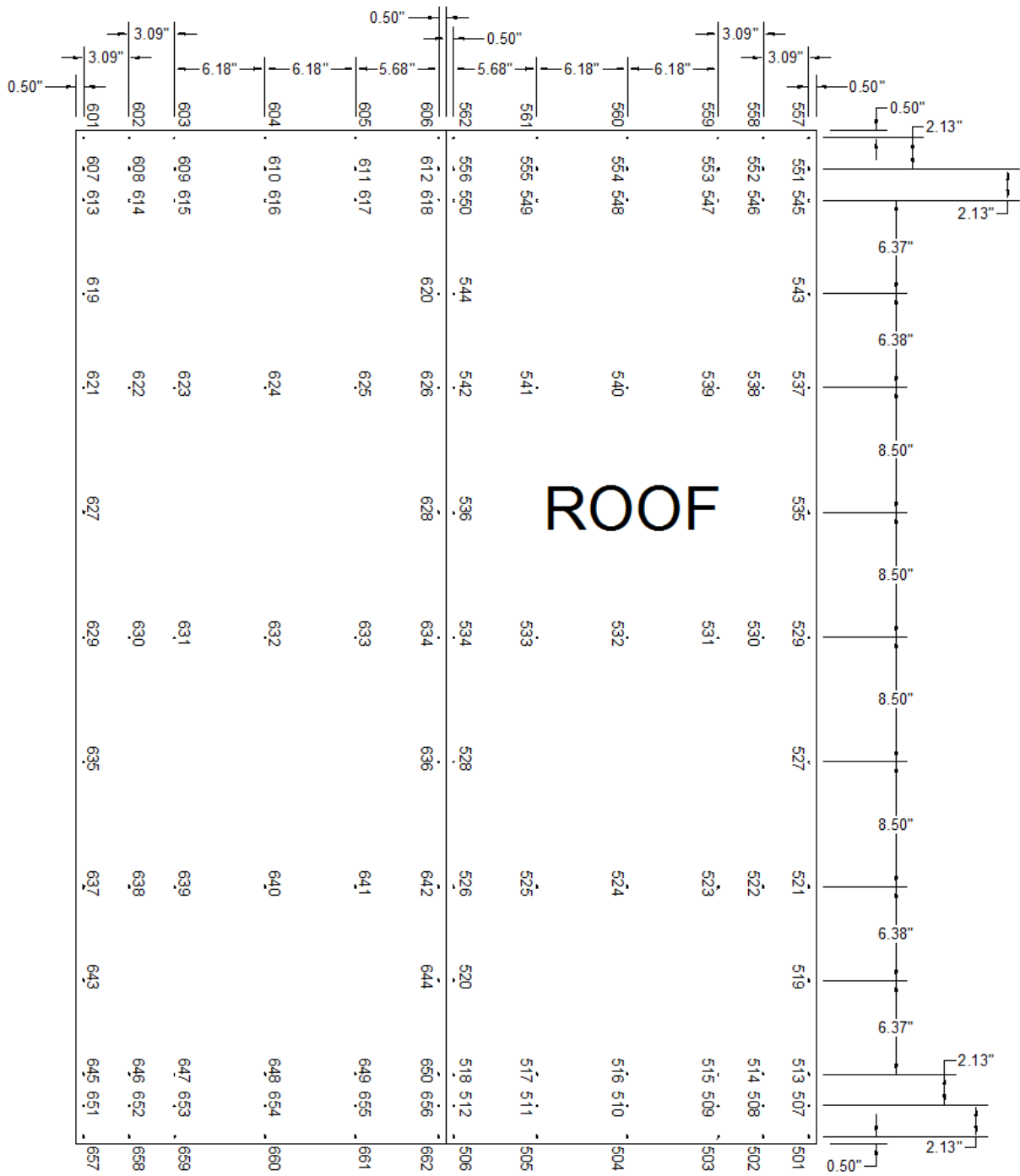


**Figure A- 9 Pressure Tap Layout on 1:5 Scale Model: Roof (Plan View looking from above)**

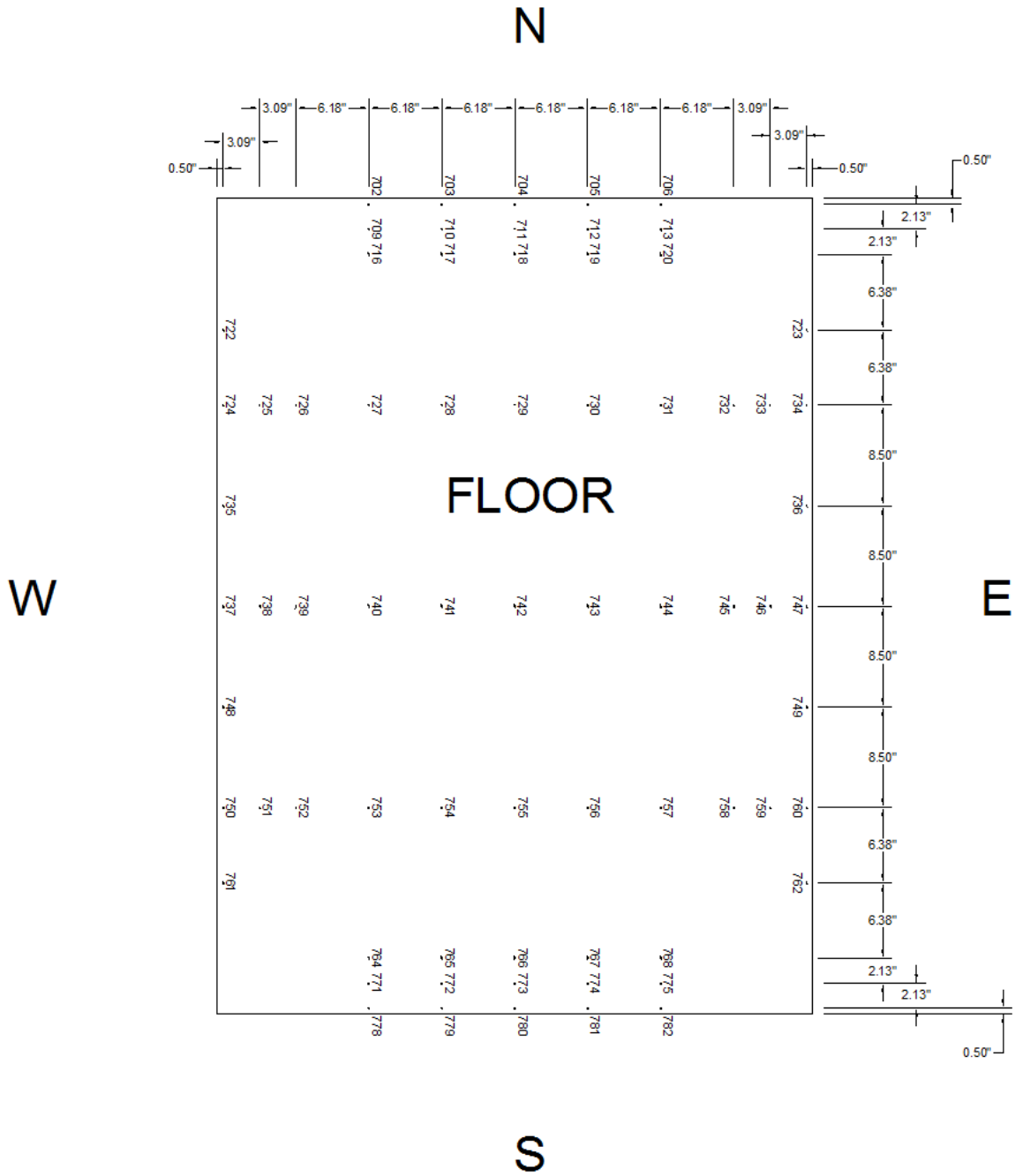


**Figure A- 10 Pressure Tap Layout on 1:5 Scale Model: Floor (Plan View looking from above)**

## Appendix B

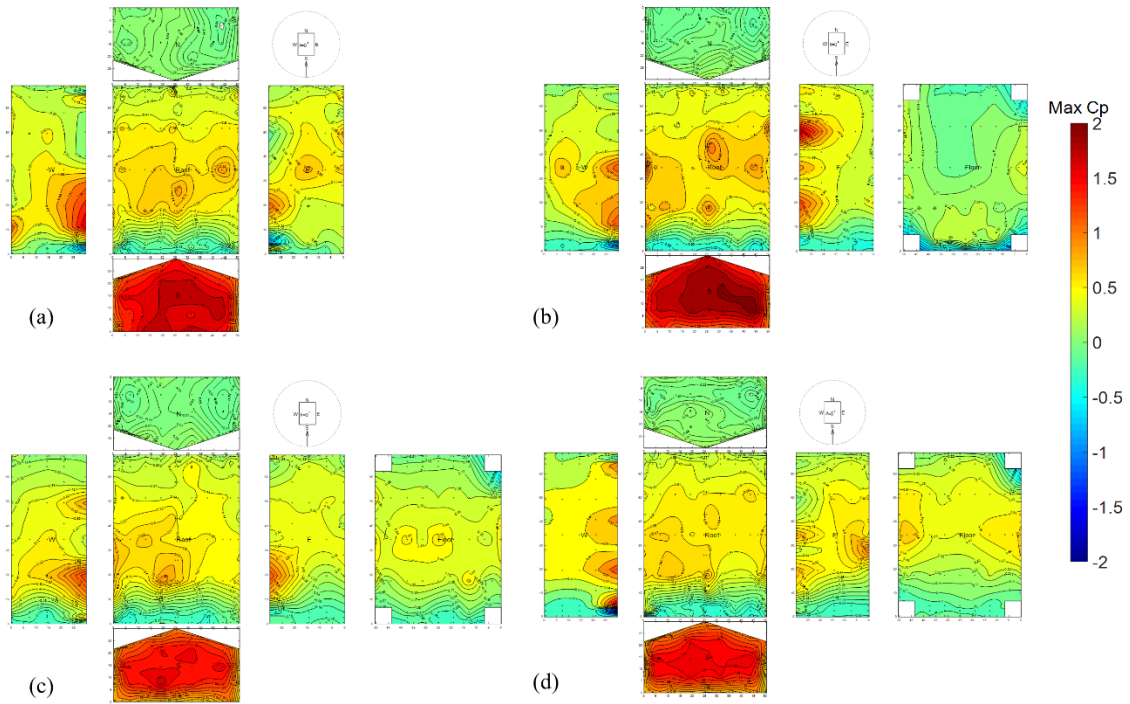


**Figure B- 1 Observed  $C_p$  max for  $0^\circ$  wind angle: (a) 0.0-in, (b) 4.8-in, (c) 16.8-in, (d) 28.8-in**

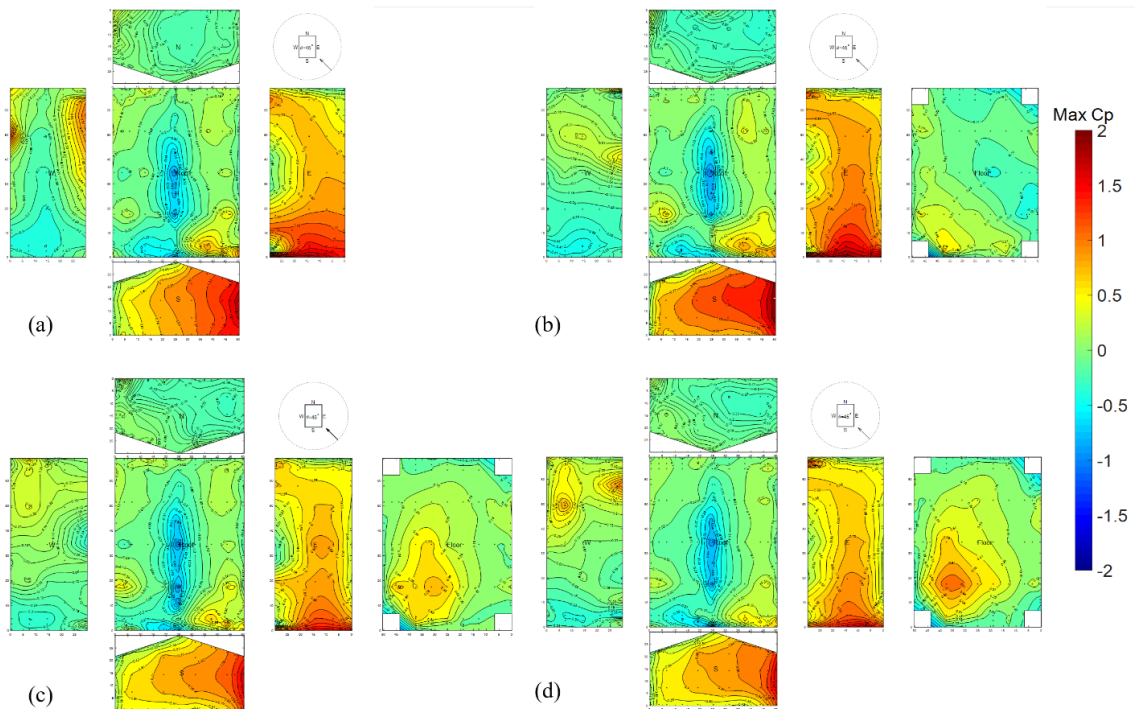


**Figure B- 2 Observed  $C_p$  max for  $45^\circ$  wind angle: (a) 0.0-in, (b) 4.8-in, (c) 16.8-in, (d) 28.8-in**

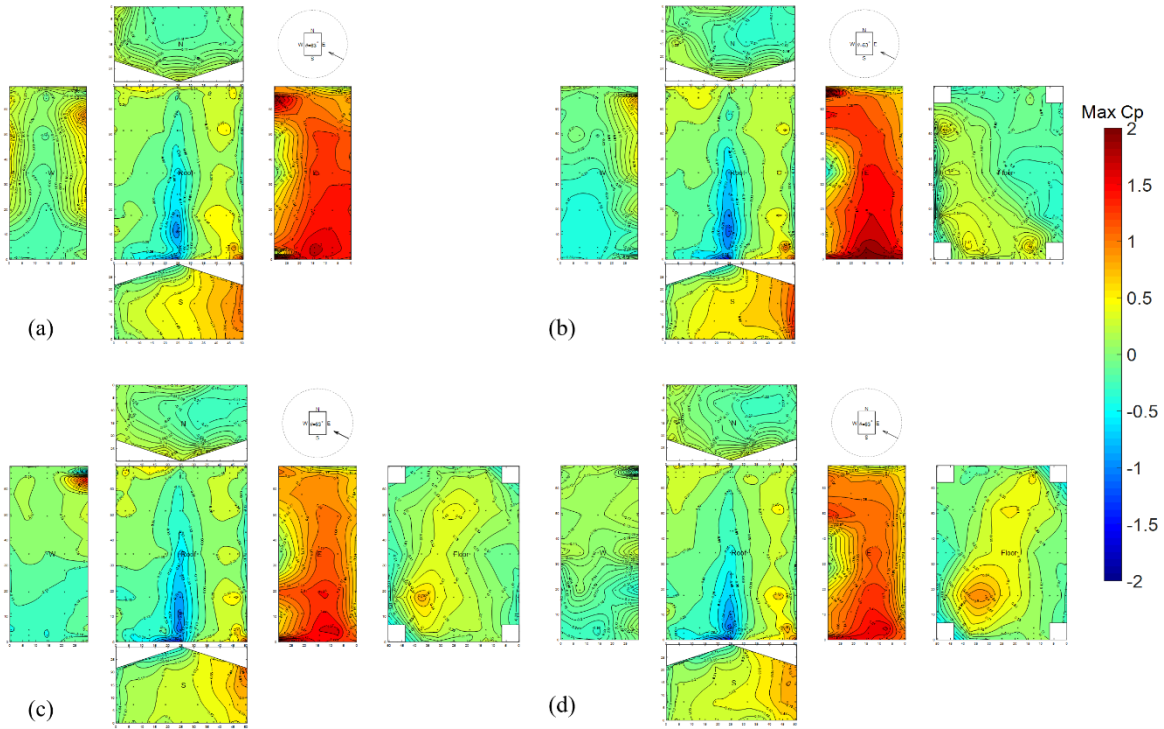


**Figure B- 3 Observed  $C_p$  max for 63° wind angle: (a) 0.0-in, (b) 4.8-in, (c) 16.8-in, (d) 28.8-in**

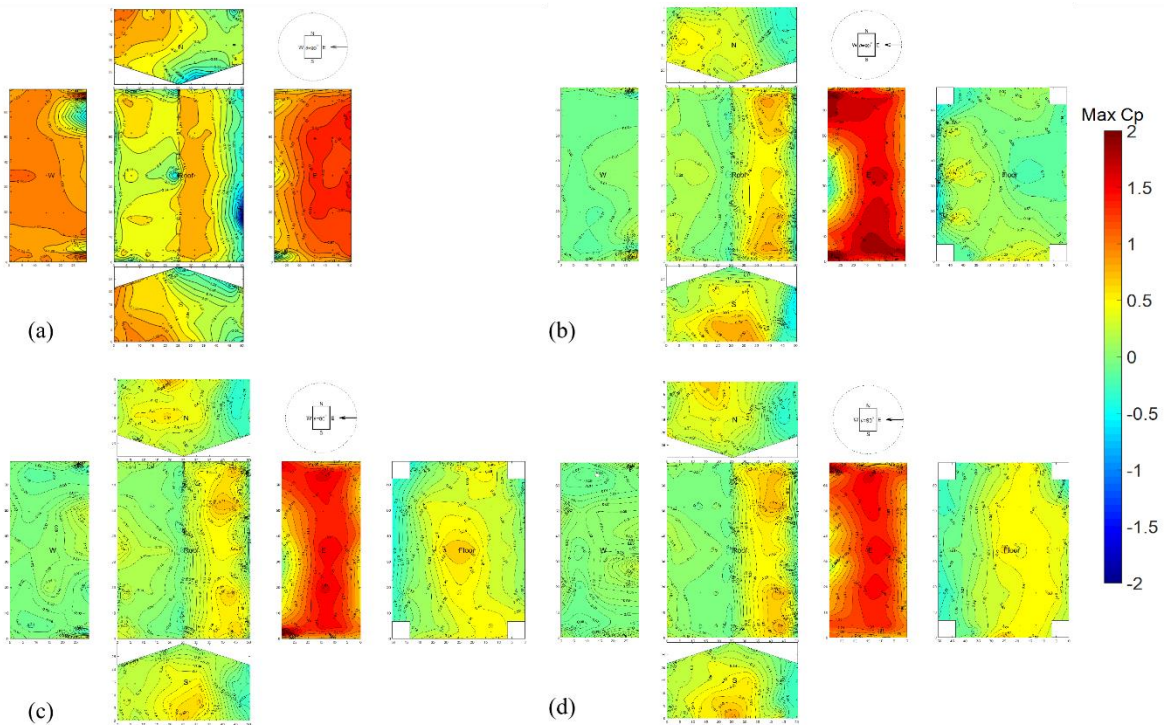


**Figure B- 4 Observed  $C_p$  max for 90° wind angle: (a) 0.0-in, (b) 4.8-in, (c) 16.8-in, (d) 28.8-in**



*A Resource for the State of Florida*

***SECTION 3***

**Investigation and Incorporation of Wall Of  
Wind testing outputs in the Florida Public  
Hurricane Loss Model**

A Report Submitted to:  
The State of Florida Division of Emergency Management

*Prepared By:*  
Kurtis Gurley, Ph. D  
Jean-Paul Pinelli, Ph.D., P.E.

University of Florida  
Florida Institute of Technology

July 31, 2017

---

# FPHLM ENGINEERING TEAM

## **Principal Investigators**

Kurtis Gurley, Ph. D.  
Associate Professor  
Civil and Coastal Engineering Department  
University of Florida

Jean-Paul Pinelli, Ph.D., P.E.  
Team leader  
Professor  
Civil Engineering Department  
Florida Institute of Technology

## **Graduate Research Assistants**

Nick Miller  
Graduate Research Assistant  
Civil Engineering Department  
Florida Institute of Technology

Karthik Yarasuri  
Graduate Research Assistant  
Civil and Coastal Engineering Department  
University of Florida

---

# **INVESTIGATION AND INCORPORATION OF WOW TESTING OUTPUTS IN THE FLORIDA PUBLIC HURRICANE LOSS MODEL**

## Introduction.

One of the key components of a better mitigated and therefore more disaster-resilient Florida involves recovery and reconstruction funding for homeowners, and a key element of that funding derives from insurance coverage, which is increasingly driven by cost considerations. The Florida Public Hurricane Loss Model (FPHLM) which has been supported by the State, provides a means of evaluating hazard insurance rate requests independently of the proprietary models used by private insurers. The model is continually refined to both satisfy the standards issued by the Florida Commission on Hurricane Loss Projection Methodology, and incorporate the current state-of-knowledge in the methodologies employed by the meteorological, engineering, actuarial, statistical, and computer science teams.

Recently completed Wall of Wind (WOW) Florida Department of Emergency Management (DEM) projects (FY 2015–2016) address elements of low-rise and high-rise building performance, in particular the wind loads on high-rise balcony glass handrail systems (GHRs) and the exterior wall adjacent to the balcony. The incorporation of these experimental results within the FPHLM is investigated in this report.

## 1. Testing of typical balcony glass hand-railing systems used in mid-high rise buildings (FIU WOW 2015-2016).

Research carried out at the WOW included the estimation of wind effects on typical balcony glass hand-railing systems (GHRs) used in mid-high rise buildings. These systems have proven to be vulnerable building components under hurricane wind and debris impacts, and represent a hazard to human life, as well as a source of insurance losses. Figure 1 shows an example of damaged GHRs during hurricane Wilma, while Fig. 2 shows a typical distribution of GHRs and the resulting distribution of damage, also from hurricane Wilma. The WOW research focused on subjecting models of buildings with balcony glass hand-railing systems to realistic hurricane conditions. Testing of large-scale models with detailed geometries facilitated knowledge advancement in hurricane-structure interaction and provided test-based data that will improve loss models such as the FPHLM. The test plans included the testing of several models of a mid-high rise building of different scales with and without balconies.



Figure 1: Damaged GHRs from hurricane Wilma



Figure 2: Typical GHRs configuration and distribution of damage

Scale models of a tall building with and without components representing glass hand railing systems (GHRs) were tested in the Wall of Wind facility (Figure 3). The model without the GHRs was the control case (no balcony modeled) and represents the units currently modeled in the mid-high rise (MHR) FPHLM. Pressure taps were installed over the surface of the models, including the walls and the balcony GHRs, and the pressures were monitored during boundary layer wind flows produced by the Wall of Wind. A primary objective was to quantify any appreciable differences in wall loading due to the presence of the balcony. That is, did the balcony hand rail system provide any shielding or accentuation of wind pressures on the building walls and associated fenestration such as sliding glass doors? Tests were conducted using model scales of 1:25, 1:67 and 1:180.

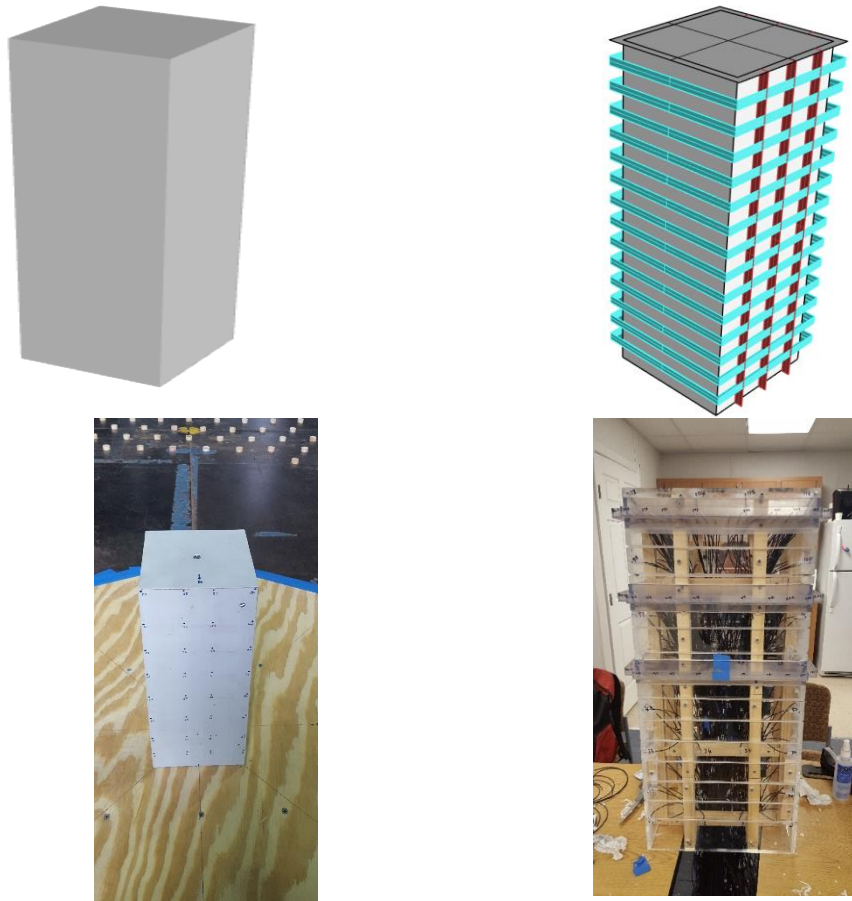


Figure 3: Illustrations and photos of MHR model without (left) and with (right) balconies with GHRS

## 2. Incorporation of the test results on balcony glass hand-railing systems in the mid-high rise buildings models of the FPHLM

### 2.1. WOW results summary

With respect to the FPHLM MHR model, the potential modification of the wall loads is significant with respect to the wind loading on the sliding glass doors that lead to the balcony. These sliding glass doors are explicitly modeled in the FPHLM and represent a primary entry point for wind driven rain if damaged. As currently modeled, the wind loading on the sliding glass doors assumes that the presence of a balcony has no influence on the wind load, nor on the vulnerability of the sliding glass doors to damage from debris.

Test results of the 1:180 scale model from the Wall of Wind testing facility were made available on June 2, 2017 to the FPHLM engineering team. The conclusions were as follows:

- For the case of positive pressure (windward walls), the presence of the GHRS made no appreciable difference on resultant wall loading
- For the case of negative pressure (side and leeward walls), the presence of the GHRS reduced pressure on the walls by a variable amount over the surface of the wall, depending on the location of the unit (along the edges of the building vs within the interior of the wall surface). The report suggested an aggregate load reduction of ~ 32%.

It appears that there may be some justification for reducing the negative loads on sliding glass doors in the current MHR FPHLM for buildings with balconies. However, the experimental datasets are still being analyzed by the Wall of Wind team to produce a more comprehensive set of results, including multiple wind directions for the 1:180 scale model and all results from the 1:67 and 1:25 scale models. If there is a convergence of findings among the three scale models and all wind directions, the FPHLM engineering team will have justification to make changes based on sound experimental results. To date, the results from the 1:180 scale model (summarized above) have been analyzed to develop and implement a strategy to incorporate changes in the FPHML MHR model. No more WOW testing is needed. However, additional data analyses from the prior WOW experiments will inform the changes in FPHLM.

## 2.2. FPHLM MHR model modification strategy

Based upon the FIU WOW document summarizing the results of experiments on scale models of MHR buildings with glass hand rail systems (BalconyReport\_6\_2\_2017\_REV), the FPHLM MHR physical damage model was modified to reflect a reduction in negative (suction) pressure on sliding glass doors that open to the balcony. The FIU report suggest a reduction of negative pressure loads on the wall behind the balcony. Negative loads on walls with balcony were found to be ~ 68% of the negative loads without balcony (~32% reduction). Positive pressure loads on the wall were found to be the same with and without balcony.

The MHR model was modified to reduce negative loads on the sliding glass doors. Only negative loads were reduced (when the wall with the sliding glass door was a side wall or leeward wall with respect to approach wind direction). This was done for each of the base MHR model types (interior and exterior entry door, corner and middle units, all with sliding door). Additionally, the debris vulnerability of the sliding glass doors was modified to reflect shielding offered by the glass handrail system. These modifications were implemented in two stages: 1) reduce negative pressure only, 2) reduce negative pressure and reduce vulnerability to debris damage.

### 2.3. FPHLM MHR model modification implementation and model configuration matrix

At this stage, the model output being investigated is the physical damage to sliding glass doors. Physical damage is determined as a result of wind pressure, debris impact, and total (either pressure or debris). The unmodified FPHLM MHR model sliding door damage provided a baseline for evaluation of the modifications. The investigation focuses on units located within the middle portion of the building face (not corner units) with an interior entry door. Corner vs middle units and interior vs exterior entry door units are all modeled identically with respect to sliding glass door vulnerability (window and entry door vulnerabilities differ, but are not the subject of this investigation).

The reduction of negative loads on sliding glass doors was implemented at 20% and 40% reduction levels, in order to envelope the experimental WOW result of ~32% reduction. The reduction of debris damage on sliding glass doors due to shielding from the GHRS was implemented as a function of the percentage of the sliding glass door projection (to the horizontal) blocked by the GHRS projection (~20% reduction).

Results (MHR physical damage model outputs) were generated with just the wind load reduction, and with the wind load reduction concurrent with debris damage reduction. These combinations were both run using two different assumptions about debris vulnerability, referred to as debris zone 1 and debris zone 3. Zone 1 applies to MHR units closer to the ground where more debris are available, and zone 3 applies to MHR units higher up the building where there are fewer debris in the wind field.

Table 1 provides a summary of the model modification configurations that were simulated using the FPHLM MHR model.

Table 1: Model configuration matrix (middle unit, interior stairway)

	Debris zone 1	Debris zone 3
Baseline unmodified MHR model	X	X
Pressure reduction only, 20%	X	X
Pressure reduction only, 40%	X	X
Pressure reduction 20% + debris reduction	X	X
Pressure reduction 40% + debris reduction	X	X

### 2.4. FPHLM MHR model modification model configuration matrix results

Results are discussed in the following order. Each discussion and associated figure includes comparisons of damage in the unmodified model with damage in the modified models.

- Figure 4: Sliding door damage due to pressure only (no debris)
- Figure 5: Sliding door total damage (pressure and debris) with pressure modification but without debris modification

- Figure 6: Sliding door damage due to impact only (residual of total and pressure-only damage) with pressure modification and debris modification
- Figure 7: Sliding door total damage (pressure and debris) with pressure modification and debris modification. This figure represents a final view of the influence of GHRS on sliding door damage

The vertical axis in each of the following plots represents the percentage of components that are physically damaged. There is only one sliding glass door in each of the model configurations being investigated. Therefore, a 30% damage value indicates a 30% probability of that single sliding glass door being damaged at the associated wind speed on the horizontal axis. All % damage results are produced by averaging over all eight approach wind directions (45 degree increments) at 500 simulations per direction.

Figure 4 presents the comparative sliding glass door pressure-only damage (debris damage neglected) in order to isolate the influence of the pressure reduction modifications. The left plot presents % damage for unmodified (baseline), and the 20% and 40% pressure reduction modifications. The right plot is the nominal difference between the baseline result and the modified results. These differential plots are observed to initially increase with wind speed and then decrease. The reason for the non-monotonic behavior is the influence of the wind direction cases that produce positive pressure on the sliding glass door. Recall that positive pressure loads are not modified (based on the results of the WOW testing). The pressure reduction modification in isolation (no debris impact reduction) begins to have an influence at ~ 110 mph, with a maximum influence at ~ 175 mph. However, the isolated pressure only damage is an incomplete view of the influence of the modifications. The upcoming discussions on total damage (pressure and debris) are more relevant to drawing conclusions.

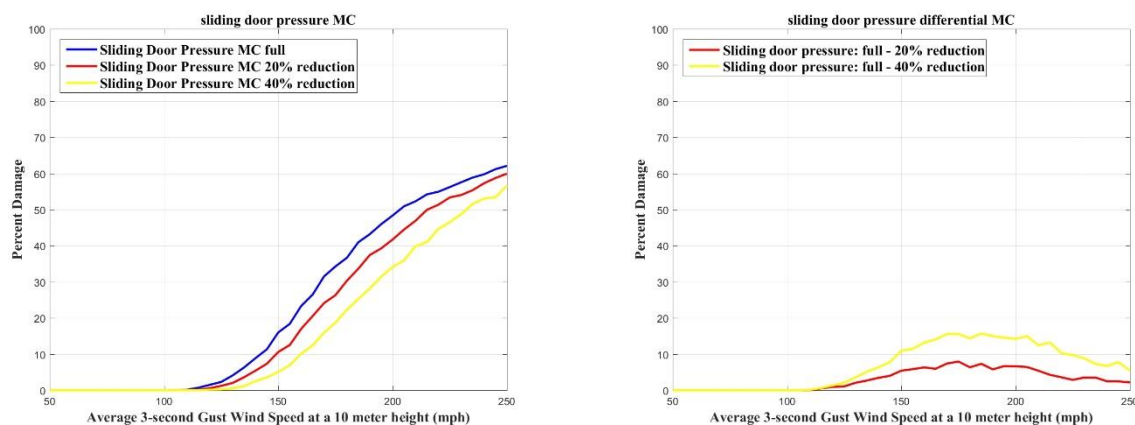
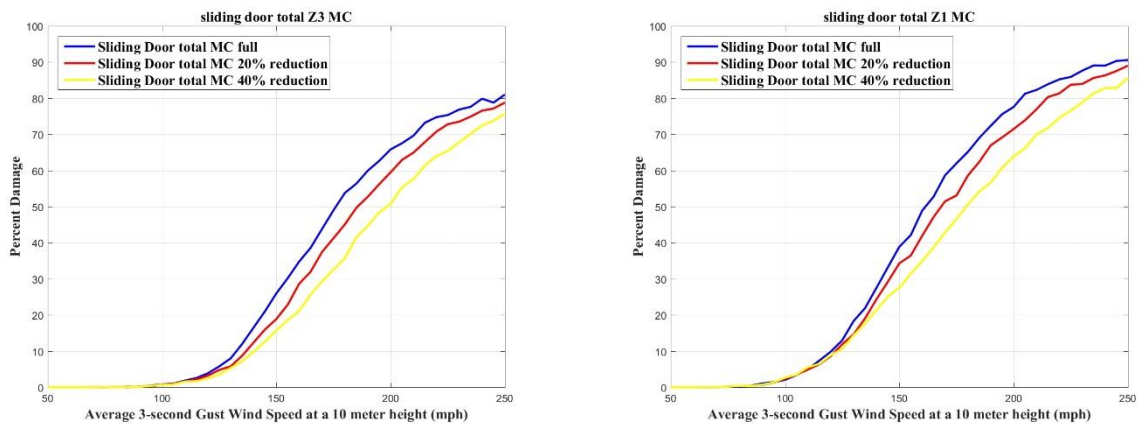


Figure 4: Sliding door pressure-only damage. Left: Unmodified (blue), 20% pressure reduction (red) and 40% pressure reduction (yellow). Debris zone and debris modification not relevant. Right: differential between: unmodified and 20% reduction (red) and 40% reduction (yellow).

Figure 5 presents the comparative sliding glass door total damage (pressure and debris), again with the pressure modification and without the debris modification. i.e., it is the same model modification configuration as in Figure 4, with impact damage now included with pressure damage. With the addition of impact damage, it is necessary to stratify results with respect to debris zones 1 (left) and 3 (right). The top plots are the physical damage for baseline and pressure reduction modifications, and the bottom plots are the nominal differences, formatted consistent with Figure 4. Comparing the differential plot in Figure 4 with the zone 3 and zone 1 differential plots in Figure 5, it is observed that the reduction in damage due to pressure modification becomes less significant as the debris damage becomes more significant relative to pressure damage. This is as expected when considering this in the limit. If the total damage is driven mostly by pressure damage, reducing pressure loads will have a strong influence on damage reduction. Conversely, if the total damage is driven mostly by debris damage, reducing pressure loads will have little influence on damage reduction. Figures 6 and 7 will now consider MHR modification configurations that include both pressure reduction and debris damage reduction due to the presence of the GHRS.



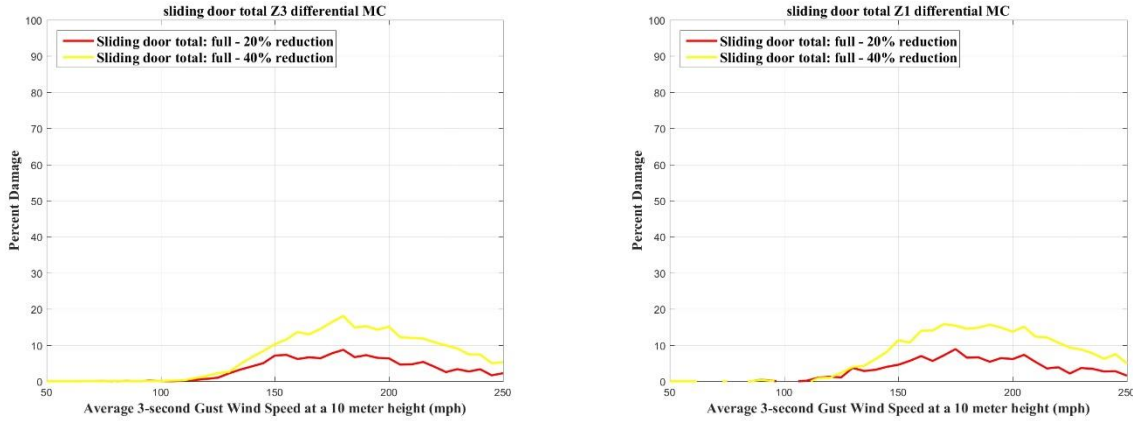


Figure 5: Sliding door total damage, debris zone 3 (left), debris zone 1 (right). Top Row: Unmodified (blue), 20% pressure reduction (red) and 40% pressure reduction (yellow). No modification for debris vulnerability. Bottom Row: differential between: unmodified and 20% reduction (red) and 40% reduction (yellow).

Figure 6 presents the comparative sliding glass door impact-only damage. The modifications include both a pressure reduction and debris reduction. It is important to know that the MHR damage assessment algorithm sequentially checks for pressure damage followed by debris damage. If the sliding glass door is already damaged by pressure, impact damage is not registered. For this reason impact damage shown in isolation may level out as wind speed increases, or even have a non-monotonic behavior with respect to wind speed. Figure 6 shows the impact only damage for the unmodified baseline model and both pressure-modified models for debris zone 1 & zone 3. Both pressure modified models use the same debris reduction factor, thus it is observed that both modified model results track together. It is also observed that zone 1 demonstrates a larger damage magnitude, as well as an obvious increase in differential damage between unmodified and modified (differentials not explicitly plotted). This is consistent with zone 1 being more debris vulnerable than zone 3. The final plot (Figure 7) now addresses the total damage considering all modifications.

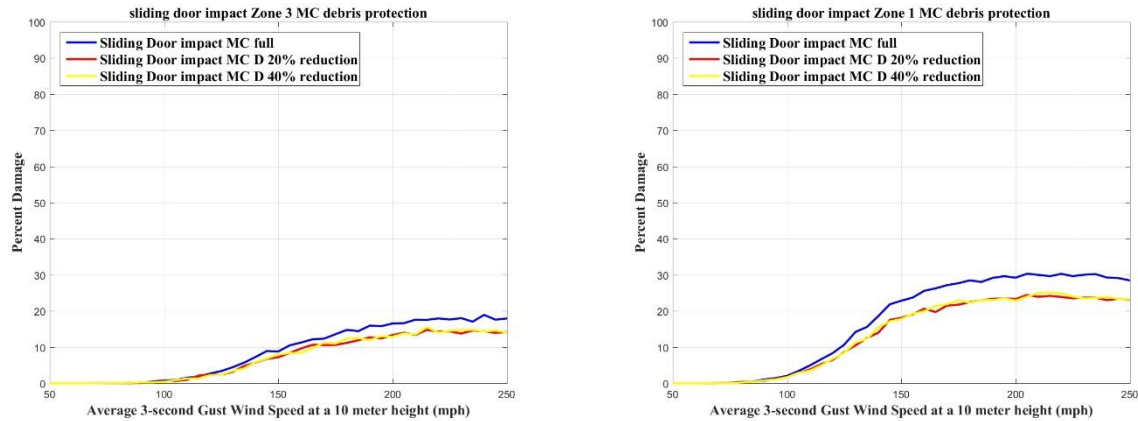


Figure 6: Sliding door impact-only damage, debris zone 3 (left), debris zone 1 (right). Unmodified (blue), 20% pressure reduction (red) and 40% pressure reduction (yellow). With modification for debris vulnerability.

Figure 7 presents the comparative sliding glass door total damage (pressure and debris), now with the pressure modification and the debris modification. i.e., it is a variant of Figure 5, but now with debris damage modification incorporated. The most important observations can be made by comparing the differential plots in Figure 7 with those in Figure 5. With both pressure and debris modifications in place, the differential between baseline and modified MHR models is most prevalent. Consider the bottom right plot in Figure 7. The MHR modifications result in the initiation of damage reduction as low as 110 mph, and increasing to a 20% reduction in likelihood of sliding glass door damage at ~ 175 mph.

## 2.5. Conclusions and future refinements for formal implementation

The results indicate that the modifications under investigation could influence FPHLM loss outputs. However, changes in loss would be very different from linearly mapping Figure 7 results from physical damage reduction to loss reduction. Sliding glass doors are not the only significant contributor to MHR losses. Windows and entry doors are also vulnerable components, and water ingress from all openings represent a significant portion of calculated losses. Additionally, the cost and vulnerability of the GHRS itself has not yet been included in this investigation (GHRS is ~ \$250/linear foot). That is, the reduced vulnerability of the sliding glass door may be offset by the increase in loss due to damage to the GHRS. With this in mind, future refinements will focus on an explicit glass hand rail vulnerability model. This will be very sensitive to the WOW experimental results currently under analysis at multiple scales. The ongoing analyses of the model scale effects on results are part of an ongoing PhD dissertation at FIU.

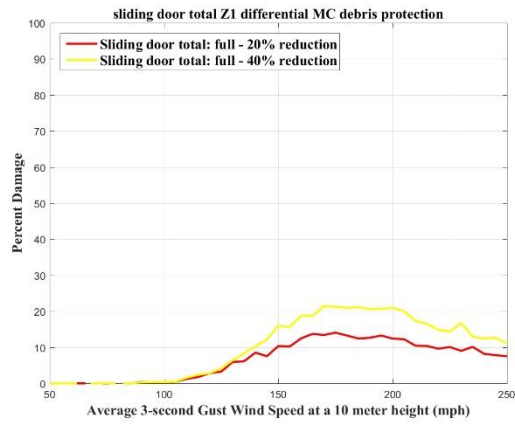
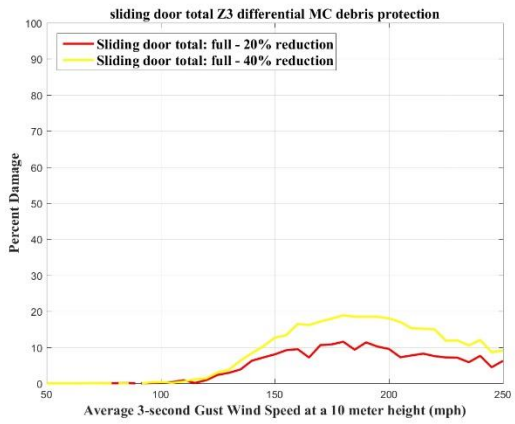
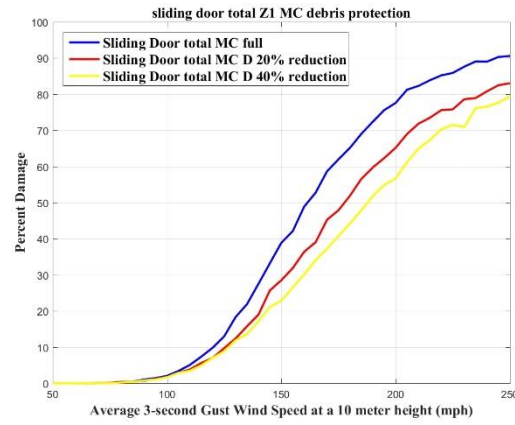
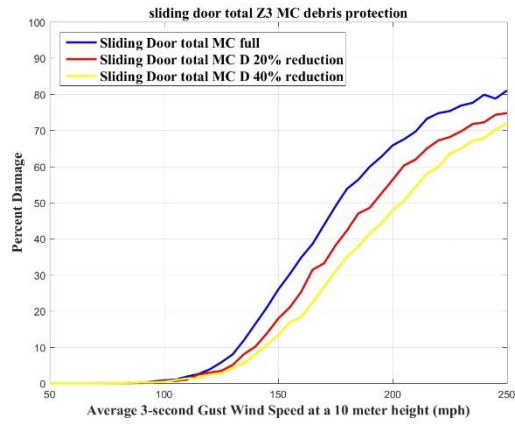


Figure 7: Sliding door total damage, debris zone 3 (left), debris zone 1 (right). Top Row: Unmodified (blue), 20% pressure reduction (red) and 40% pressure reduction (yellow). With modification for debris vulnerability. Bottom Row: unmodified and 20% reduction (red) and 40% reduction (yellow).



*A Resource for the State of Florida*

***SECTION 4***

**Hurricane Resilient Residential Building  
Construction: Wind-induced dynamic Effect on  
Photovoltaic Systems and Wind Driven Rain  
Intrusion on Interior Zones of Residential  
Construction**

A Report Submitted to:

The State of Florida Division of Emergency Management

*Prepared by:*  
Ioannis Zisis, PhD.

*Graduate Students*  
Amir Naeiji  
Farzaneh Raji  
Manuel Matus

The International Hurricane Research Center (IHRC)

Florida International University

July 2017

# Wind-induced dynamic Effect on Photovoltaic Systems

## 1 Introduction

Reduction in construction and installation costs of photovoltaic (PV) panels and inverters has led to widespread use of residential rooftop PV modules. Most recent developments even include mandatory installation of PV systems in new construction [1]. Propagation of solar energy harvesting and development of more efficient PV systems have increased the attention toward the structural design aspect of these systems and in particular the design for wind forces. Over the past decade, numerous studies have been performed and guidelines for estimating wind loads on industrial and residential structures have started to be included in some building codes and wind standards. Photovoltaic (PV) module vibrations under wind action have been found to be significant during full-scale tests while current design standards and building codes do not address this unfavorable behavior. Preliminary studies showed that the effect of PV-system vibration should be considered in the design of mounting structure. Moreover, the  $<1$  Hz fundamental natural frequency criterion used in current standards [2] to determine whether wind-induced dynamic effects should be considered or not, may not be applicable to PV systems. The goal of this study is to expand the understanding of the dynamic behavior of PV systems exposed to wind-induced loads. More specific, the study will examine vibration on the PV panels and supporting system due to turbulent action of wind.

Scaled rigid models are not suitable for investigating the dynamic effects, because such models do not simulate the dynamic properties of the systems and are unable to capture resonant response. For this study, an actual full-scale PV system (i.e. flexible panels) was mounted on a low-slope roof and instrumented using accelerometers and load cells. Then three rigid full-scale PV panels were made of wood and tested under the same conditions. In addition to the full-scale flexible and rigid models, an identical large-scale pressure-tapped model was built. All models were tested in the Wall of Wind (WOW) Experimental Facility at Florida International University (FIU). Comparison of pressure and force coefficients between the different experimental setups are reported herein. Also, the dynamic response of the flexible system was investigated in detail and an estimation of its Mechanical Admittance Function (MAF) was attempted.

## 2 Test Setup

### 2.1 Model Configuration

To investigate the dynamic response of roof mounted-PV panels it was decided to mount the PV system on a mono-slope roof building with full scale roof height of 2.13 m and roof pitch angle of  $10^\circ$ . The dynamic tests were performed using three models including two full-scale models and one 1:5 scaled down model (Figure 1). The full-scale models were tested to investigate the effect of dynamic properties of PV models, therefore for one of the specimens actual PV panels were mounted on the racking system (named flexible model throughout this report) while for the other specimen PV panels were built out of wood to represent the response of rigid system to dynamic loading. It was expected that the rigid model would not experience any dynamic effects while the flexible model would experience across the plane vibrations and dynamic amplification of the support reactions along with amplified acceleration at wind gust frequencies close to the system natural frequencies. The scaled down model provided the opportunity of investigating the scaling effects on the wind induced pressures by comparing its results to the results of full-scale rigid model.

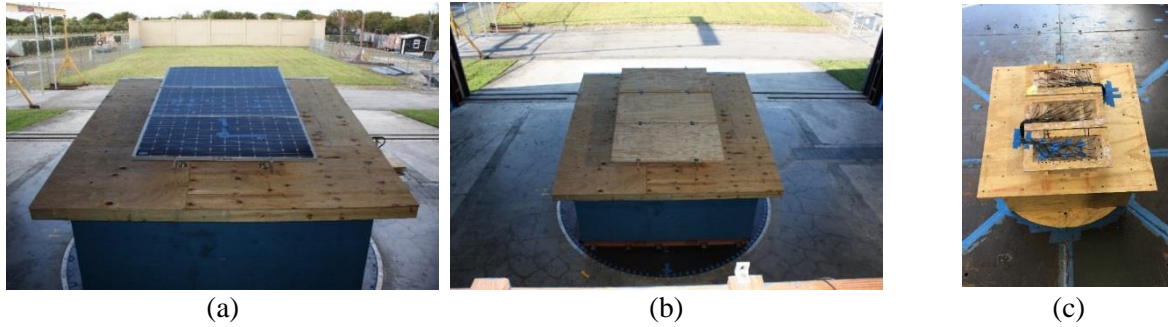


Figure 1. Three models were used in this study: (a) full-scale flexible model, (b) full-scale rigid model, and (c) 1:5 rigid model

## 2.2 Instrumentation

Load cells and accelerometers were installed on the PV panel system to monitor the dynamic response of the system during the wind loading. Dytren 3263A series accelerometers were selected for monitoring the panel acceleration due to their light weight. To decide on the location of the accelerometers the numerical model of the system was created using SAP 2000 and the critical points that were subjected to the maximum deformation in the first six modes were selected (Figure 2). Figure 3 displays the location of accelerometers installed on the PV panel modules.

The PV mounting system consisted of two aluminum rails that were supported by eight pedestals. Since it was decided to keep the 10” gap between the panels and the roof surface the load cells were mounted under the pedestals as connecting links between the pedestals and the roof trusses. The locations and the numberings of the load cells are illustrated in Figure 4.

Once the model was mounted on the racking system and got instrumented with the accelerometers, hammer tests were performed to investigate the dynamic characteristic of the PV system including the fundamental frequencies. Considering the required impact intensity for exciting the PV module, PCB Piezotronics model 086C01 impact hammer, was selected for the experimental tests (Figure 5).

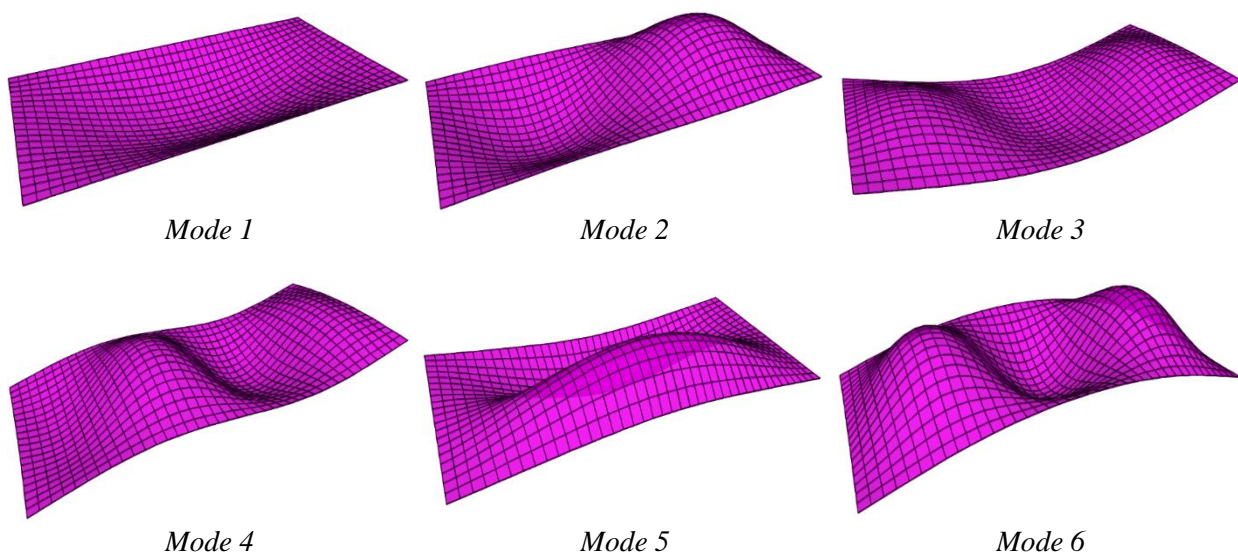


Figure 2. Mode shapes based on numerical model

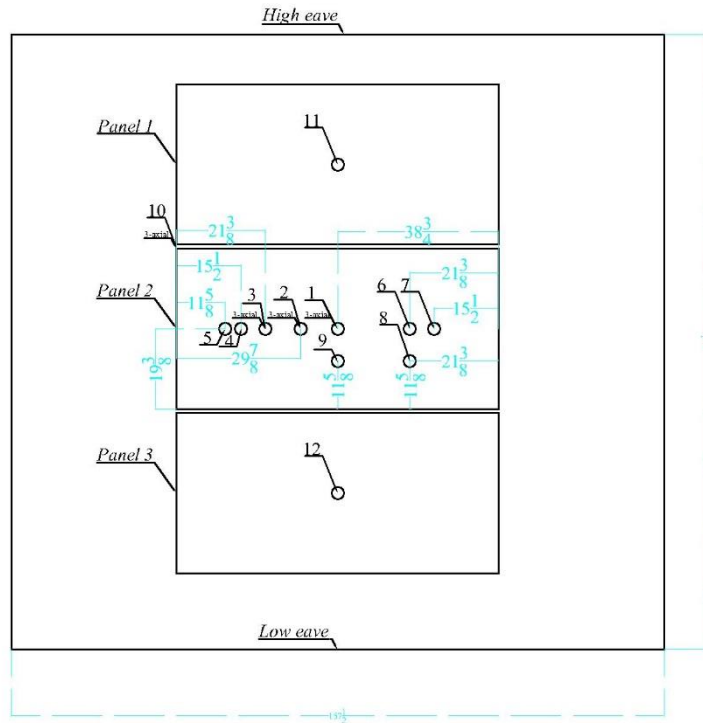


Figure 3. Location and numbering of the accelerometers on the PV modules

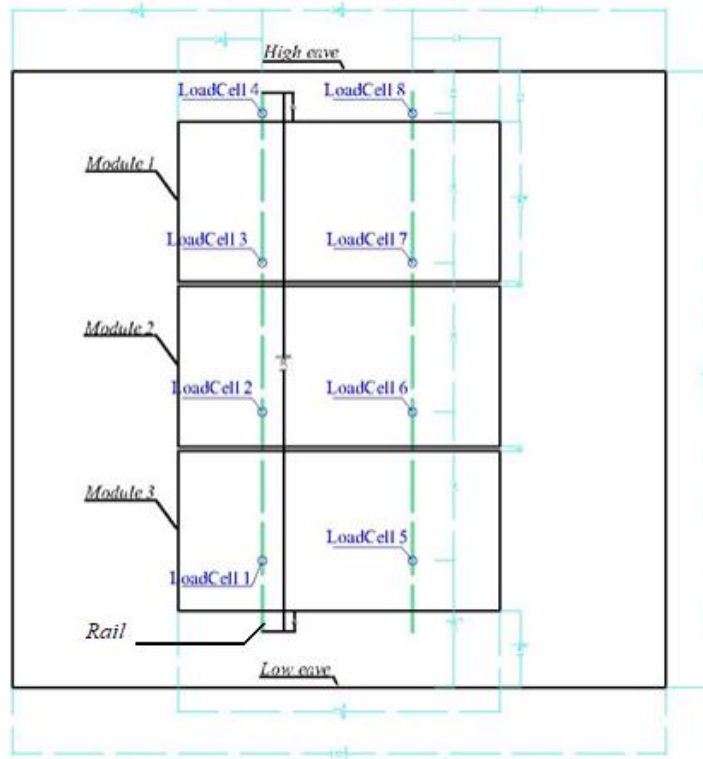


Figure 4. PV modules and load cell location and numbering on the roof



Figure 5. Impulse hammer (PCB model 086C01)

### 2.3 Flow Characteristics

All experiments were carried out at the 12-fan Wall of Wind (WOW) facility at Florida International University (FIU) (Figure 6) assuming an open terrain simulation. Details on the specification of the WOW facility and the wind flow characteristics can be found in [3]. All tests were performed at 30% fan throttle (i.e. 42 mph at roof height) except for the full-scale flexible model tests that were performed at 60% (i.e. 85 mph at roof height) and 80% fan throttle (i.e. 113.5 mph at roof height) in addition to 30% fan throttle to investigate the effect of wind speed on the dynamic response of the PV systems.

The mean wind speed and turbulence intensity profiles were calculated by using Pitot-static tubes and Cobra probes mounted at different heights at the center of the test section at the WOW facility without the model in place. The corresponding mean wind speed and longitudinal turbulence intensity profiles are shown in Figure 7 as a function of height.



Figure 6. WOW testing facility

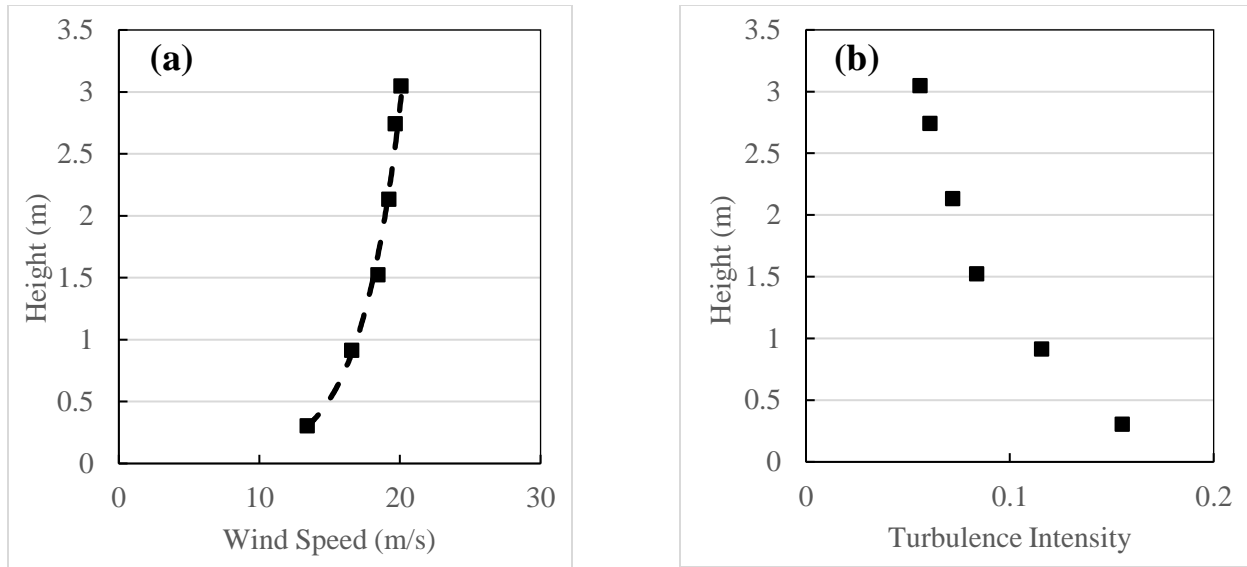


Figure 7. (a) Mean wind speed and (b) turbulence intensity profiles

The power spectra of the generated flow are presented in Figure 8. This figure also provides the comparison of the simulated spectra with the Von Karman spectrum ( $I_u = 0.2$  and  $xL_u = 20$  m). The comparison suggests the surface roughness parameter of 0.02 m, which corresponds to open terrain exposure.

Both full-scale models (flexible model and rigid model) were tested for 24 wind angles from  $0^\circ$  to  $345^\circ$  with  $15^\circ$  increments. For the large scale model the experimental tests were performed for 66 wind angles from  $0^\circ$  to  $195^\circ$  with  $3^\circ$  increments. Figure 9 shows the direction convention for the experimental tests.

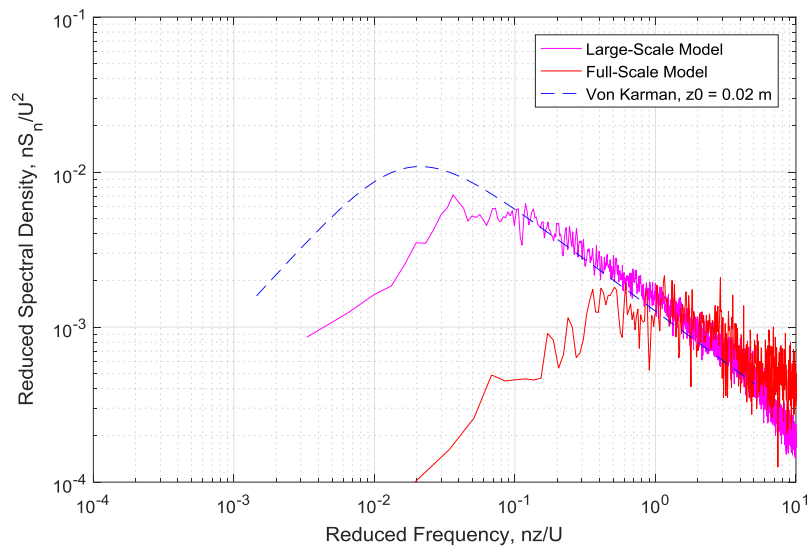


Figure 8. Wind speed spectra (at the height of full- and large- scale models) at Wall of Wind and Von Karman spectrum for  $z_0=0.02$  m

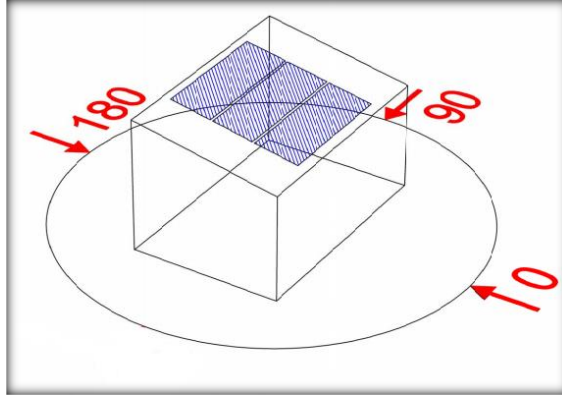


Figure 9. Reference wind directions for WOW testing

### 3 Results

#### 3.1 Hammer Test

Figure 10 shows the time history of the impact load applied by the hammer at location 1 and Figure 11 shows the corresponding accelerometer time history at location 2 (see Figure 3 for locations). The power spectra of the acceleration response at location 2 caused by the hammer impact at location 1 is presented in Figure 12. The spectrum indicates a distinct amplification of response amplitude at the natural frequencies of the model. The first noticeable peak is detected at 10.5 Hz and corresponds to the fundamental natural frequency of the system.

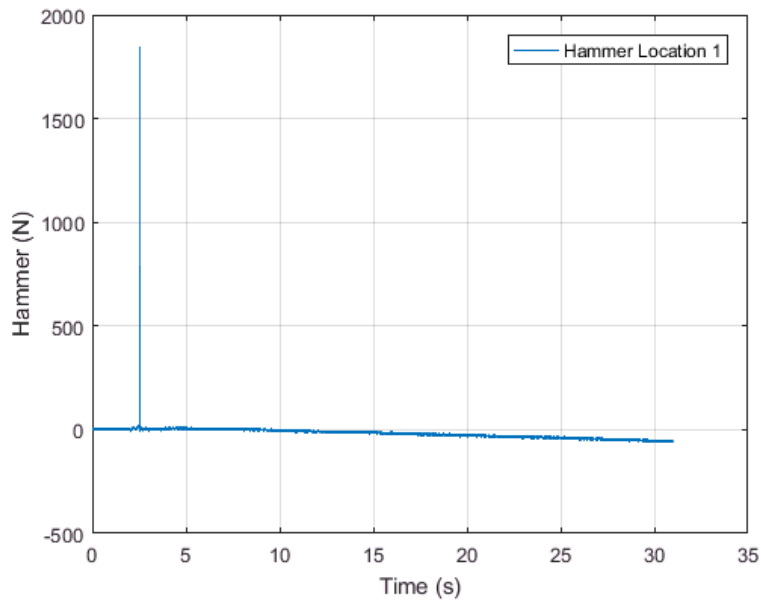


Figure 10. Time history of hammer load data

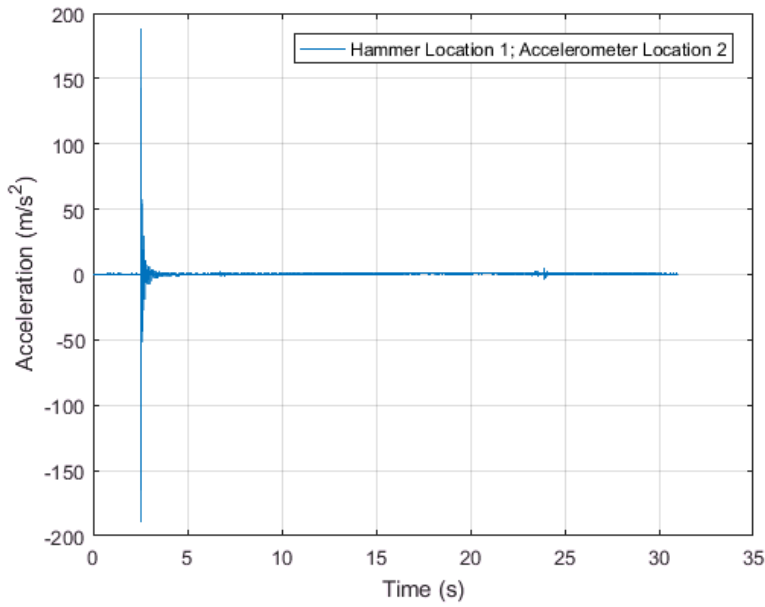


Figure 11. Time history of accelerometer 2 when location 1 was excited by the hammer

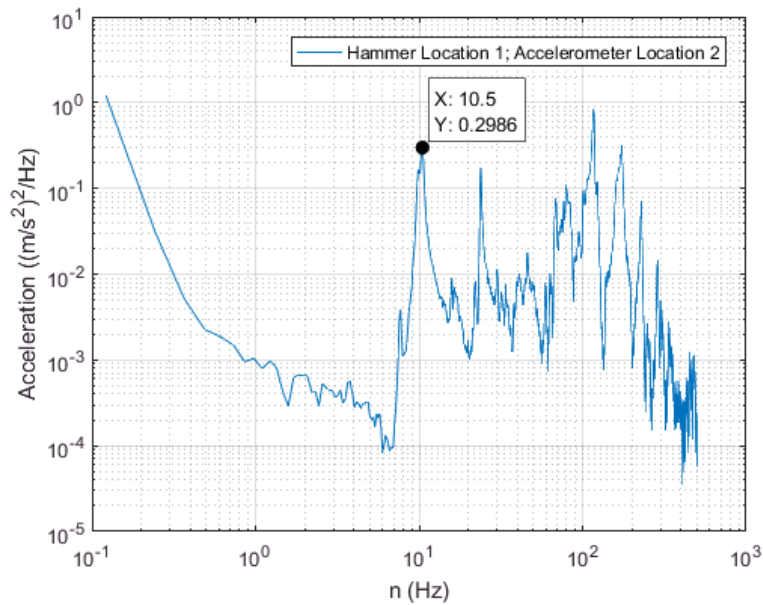


Figure 12. Spectrum of accelerations due to the hammer hit. Fundamental natural frequency of the module is 10.5 Hz

### 3.2 Dynamic Response

During the tests the load cells were recording the wind-induced reactions at the 8 racking system supports. A representative record from the flexible model tests, is presented in Figure 13 and shows the load time history for load cell 1 at 30% throttle and for 0° wind direction. To estimate the total force ( $F(t)$ ) on each module the following equations were used:

$$F_{LC}^j(t) = F_{LCRaw}^j(t) - B^j \quad (1)$$

$$F(t) = \sum_{j=1}^8 F_{LC}^j(t) \quad (2)$$

where,  $F_{LC}^j(t)$  is the net load time history of  $j$ th load cell which is calculated by removing the mean of the baseline ( $B^j$ ) from the raw load data ( $F_{LCRaw}^j(t)$ ).

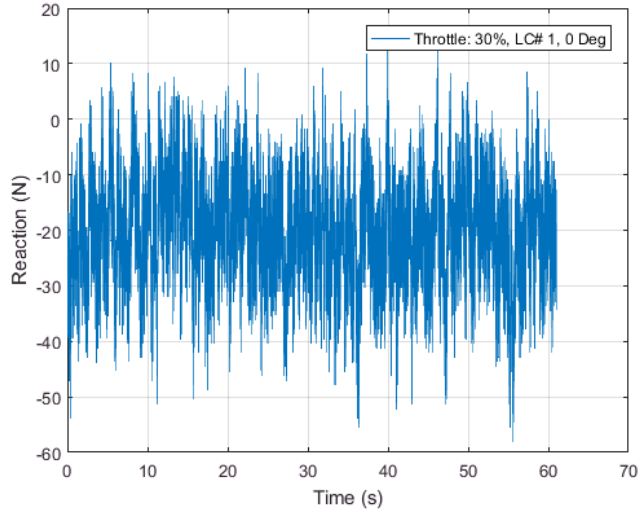


Figure 13. The time history of load cell 1 with 30% throttle, flexible model in  $0^\circ$  wind direction.

The force coefficient was calculated based on the following formula:

$$C_F(t) = \frac{F(t)}{(1/2)\rho_a V_m^2 A} \quad (3)$$

where,  $F(t)$  is total force (N),  $\rho_a$  is mass density of air ( $\text{kg/m}^3$ ),  $V_m$  is mean wind speed (m/s) at the mean roof height and  $A$  is the corresponding area ( $\text{m}^2$ ).

Figure 14 compares the mean, maximum and minimum force coefficient for 30%, 60% and 80% fan throttle at different wind angles on the full-scale flexible model. As can be observed from this figure there is not a considerable difference between the mean  $C_F$  results obtained at different percentage of the fan throttle. The peak  $C_F$  show some discrepancies for specific wind directions. For instance, the minimum  $C_F$  in the range of  $0^\circ$ - $120^\circ$  are significantly influenced by the oncoming wind speed. On the other hand, when the critical peak coefficients are observed (i.e. worst values regardless of wind direction) the discrepancies are minimal.

The comparison of the mean, maximum and minimum force coefficient values calculated based on rigid model load cell results, flexible model load cell results and rigid model pressure tap results is presented in Figure 15. The comparison, overall, doesn't show any significant difference between the force coefficient values obtained from the flexible versus the rigid model tests. When specific wind directions are considered (e.g.  $0^\circ$ - $60^\circ$ ), the flexible model experiences considerably higher  $C_F$  values when compared to the rigid model pressure tap results. These cases were considered to test for the central hypothesis of this research, regarding the dynamic amplification of the response due to panel vibrations.

When the rigid model is considered only and the  $C_F$  results obtained from the load cells and the pressure taps are compared, some discrepancies are identified. This can be partially justified by the area-averaging

approach used with the pressure tap analysis – a corresponding area is assigned to each pressure tap and it is assumed that this area experiences the same pressure time history as the point where the tap is located. Both of the above findings indicate the necessity of further investigation to justify the experimental observations.

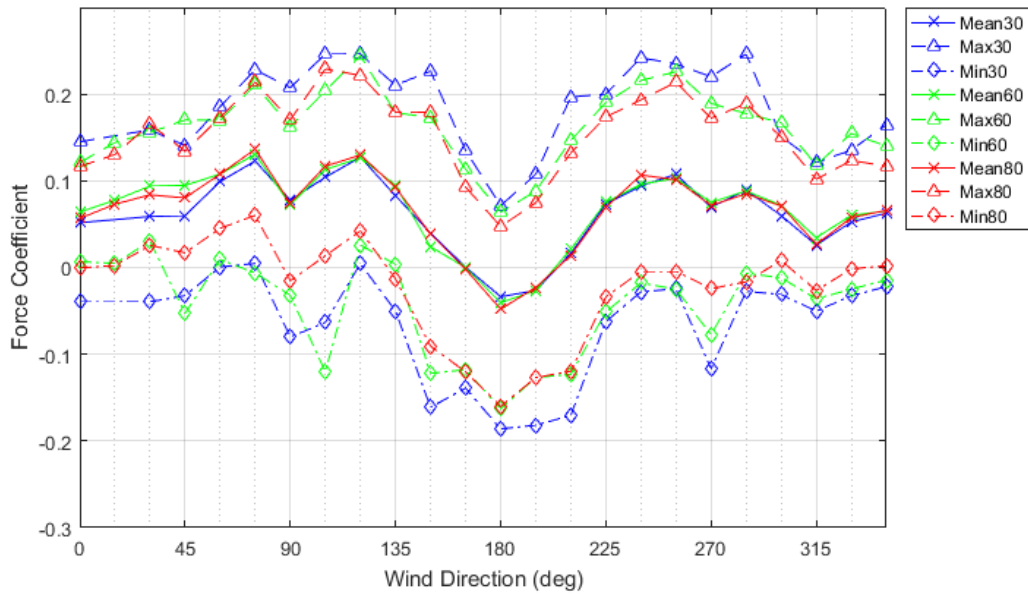


Figure 14. Mean, maximum and minimum force coefficient (at 30, 60 and 80 percent fan throttles) on the flexible model (calculated using load cell data) at different wind angles of attack

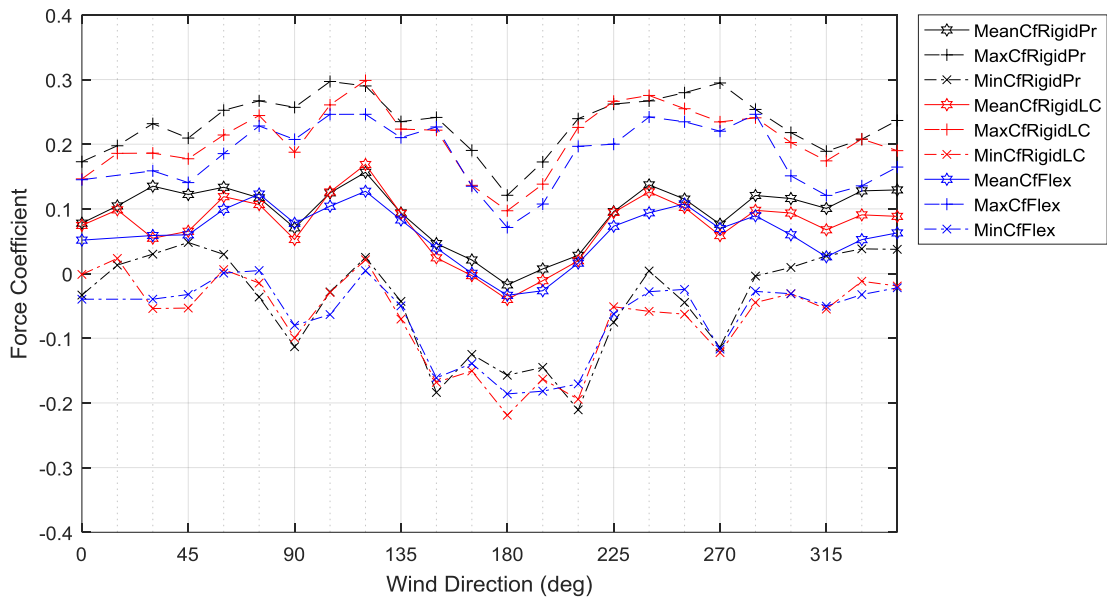


Figure 15. Mean, maximum and minimum force coefficient on the flexible model (blue), rigid model using load cells' data (red) and rigid model using pressure taps' data (black) at different wind angles of attack

Figure 16 provides the comparison of the force coefficient values between the full-scale rigid model and large-scale model. For both models the force coefficient values are calculated using the pressure tap data. The results indicate a good match between the large-scale and full-scale mean  $C_F$  values. However, for the maximum and minimum peaks the large-scale model has resulted in lower values. These discrepancies were expected since the WOW wind power spectra at different scales do not match the expected full-scale power spectrum (see Figure 8). To account for this mismatch, the Partial Turbulence Simulation (PTS) has been developed and verified by WOW researchers [4]. Figure 17 presents 3-second maximum and minimum values for the large- and full-scale rigid models when the PTS method is implemented. The results indicate a significantly improved agreement in both maximum and minimum force coefficients. However, the large-scale minimum  $C_F$  values still show a considerable deviation from the full-scale data. This requires some further investigation on the applicability of the PTS method at, or close to, full-scale pressure tests.

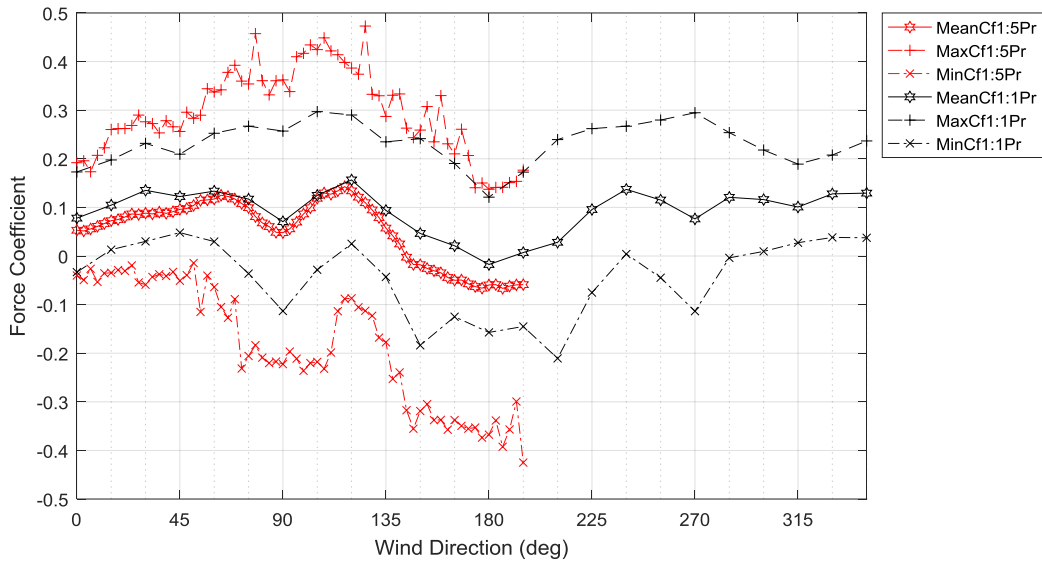


Figure 16. Mean, maximum and minimum force coefficient on the full-scale and large-scale rigid models using pressure taps' data

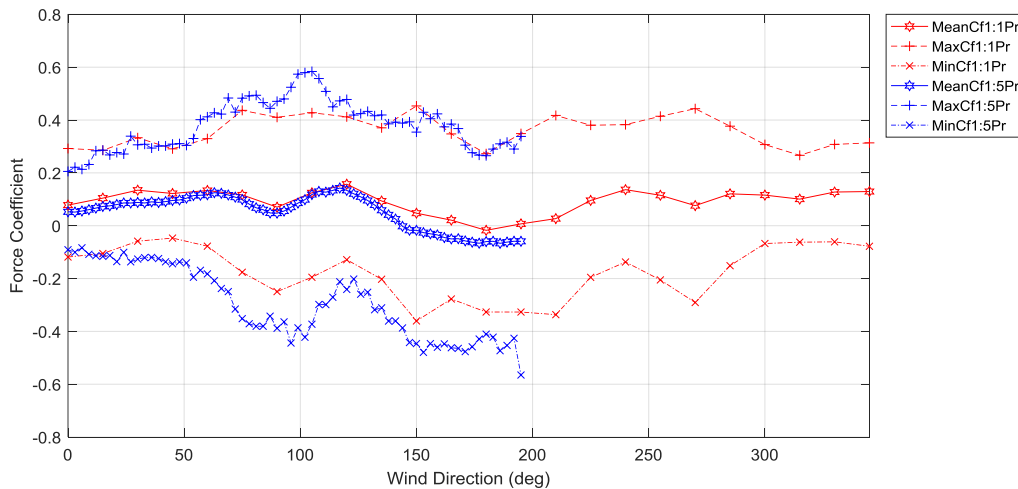


Figure 17. Mean, and PTS 3-sec peak force coefficient on the full-scale and large-scale rigid models using pressure taps' data

To further investigate the dynamic response of the PV modules and the racking system, the force power spectra were plotted. Figure 18 shows the power spectra of the reaction force at location 1 on the flexible model during the 0° wind angle test with 30% throttle. The resonant response of the system at the first natural frequency is quite notable by the illustrated peak at nb/U=1.098. Setting the wind speed (U) equal to 19.9 m/s and panel length of 2.13m, the excitation frequency was calculated by:

$$n = 1.098 * \frac{19.2}{2.13} = 10 \text{ Hz} \quad (4)$$

This value is very close to the module's fundamental natural frequency of 10.5 Hz which was established by the hammer tests. Figure 19 compares the force power spectra between the flexible model and the rigid model at 0° wind direction and at 30% fan throttle. The peak on the flexible graph indicates the resonance on the reaction force coefficient spectra which is the result of response amplification at the frequencies around the fundamental natural frequency of the structure. Except for the illustrated peak at the first natural frequency there isn't any significantly effective variation between the two graphs.

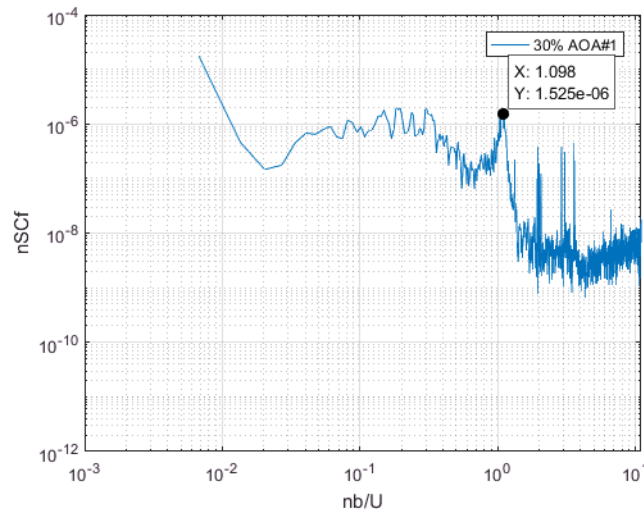


Figure 18. Force spectrum of the flexible model for 30% fan throttle and 0° wind direction

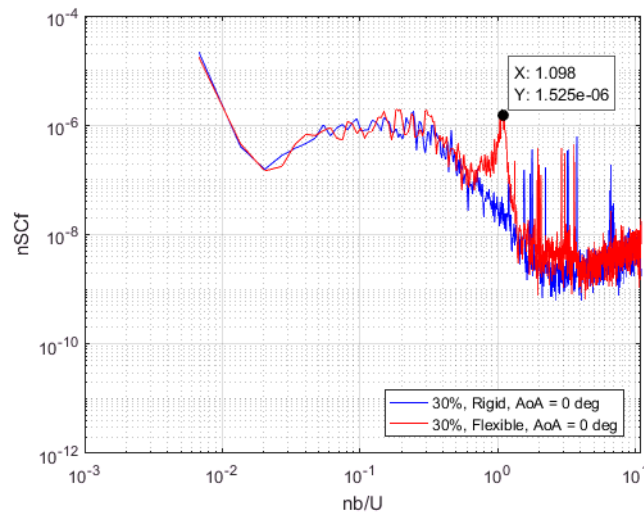


Figure 19. Comparison of force spectra of flexible and rigid models

Figure 20 shows the spectra of force coefficients calculated and averaged on all three PV panels based on the flexible model (red), load-cells on full-scale rigid model (blue), and pressure taps on full-scale rigid model (green). As can be observed from this figure for the reduced frequency ( $nb/U$ ) values greater than 0.3 the load cell spectra (both flexible and rigid models) dramatically decrease while this is not the case for the spectrum resulted from the pressure taps data. The reduced spectral density values resulted from the load cells (blue and red curves in Figure 20) in comparison to the spectral values calculated based on the pressure taps (green curve in Figure 20) implies the lower dynamic reaction forces compared to the implied wind-induced loads. This phenomenon can be resulted either from the intrinsic damping of the support structure which is composed of the timber truss and the building frame or the local damping caused by installation defects of one of the load cells. These findings call for a more thorough analysis of the obtained results using individual load cell and pressure tap time histories. Seo et al. [5] presented some equivalent viscous damping ratios in wooden frame buildings. According to this study, the damping ratios varied from 13% to 27%. Considering such a high percentage of damping, the observed dramatic decrease of spectral density may be partially justified. Figure 21 displays the spectra of all eight load cells at  $0^\circ$  wind direction at 30% fan throttle. For all the curves, the same pattern of decreased spectral density at  $nb/U$  greater than 0.3 can be observed. This observation does not indicate any defective connection in any of the load cells to the roof trusses.

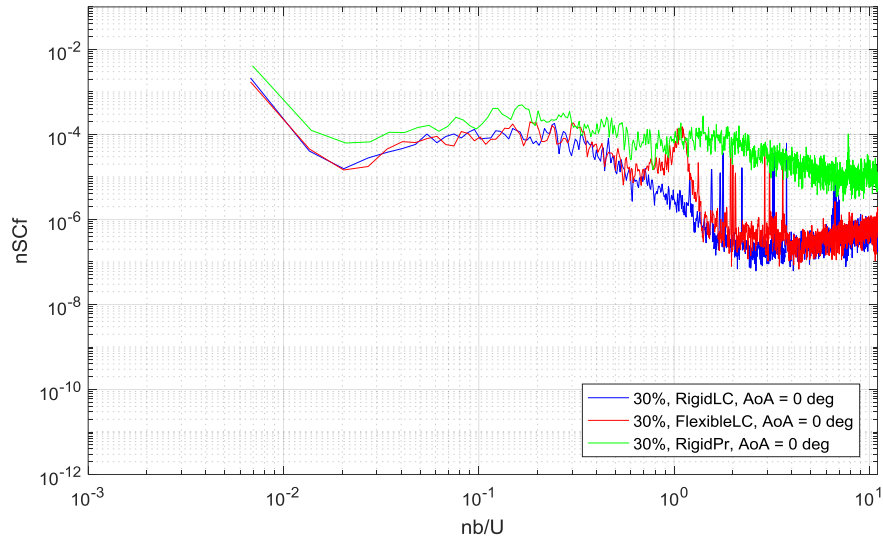


Figure 20. Comparison of spectra for the full-scale models based on the data from load cells and pressure taps

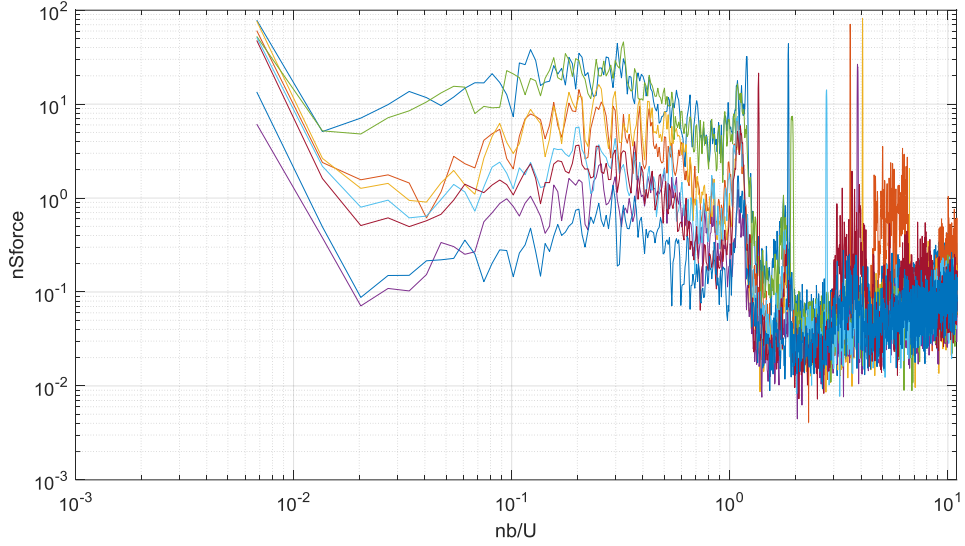


Figure 21. Spectra of all eight load cells at 0° wind direction at 30% fan throttle

### 3.3 Dynamic Amplification

In this section, the implementation of the dynamic amplification is explored by investigating the use of the Mechanical Admittance Function (MAF). The MAF is used to estimate the amplification of the flexible model response, compared to that of the equivalent rigid model (load cell data), at its fundamental natural frequency and is defined as:

$$|H(n)|^2 = \frac{1}{[1 - (n/n_1)^2]^2 - 4\eta^2(n/n_1)^2} \quad (5)$$

where  $n$  is the desired frequency,  $n_1$  is the natural frequency of the system (10.5 Hz) and  $\eta$  is the damping ratio. Figure 22 presents the MAF for the first vibration mode of the PV system. The rigid model spectrum (see Figure 23) is generated by multiplying the original spectrum to the square of Mechanical Admittance Function:

$$S_{Cf(B+R)} = |H(n)|^2 \cdot S_{Cf(B)} \quad (6)$$

where  $S_{Cf(B+R)}$  is the modified spectrum, and  $S_{Cf(B)}$  is the rigid model spectrum. The modified rigid model spectrum compares well to the flexible model which confirms the validity of using the MAF to account for the dynamic amplification.

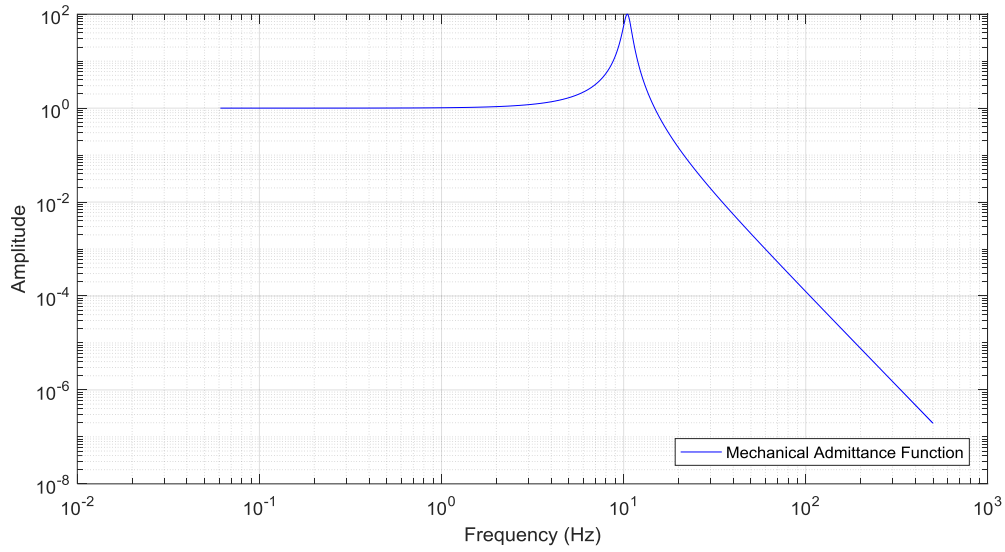


Figure 22. Mechanical Admittance Function for the first vibration mode of PV system

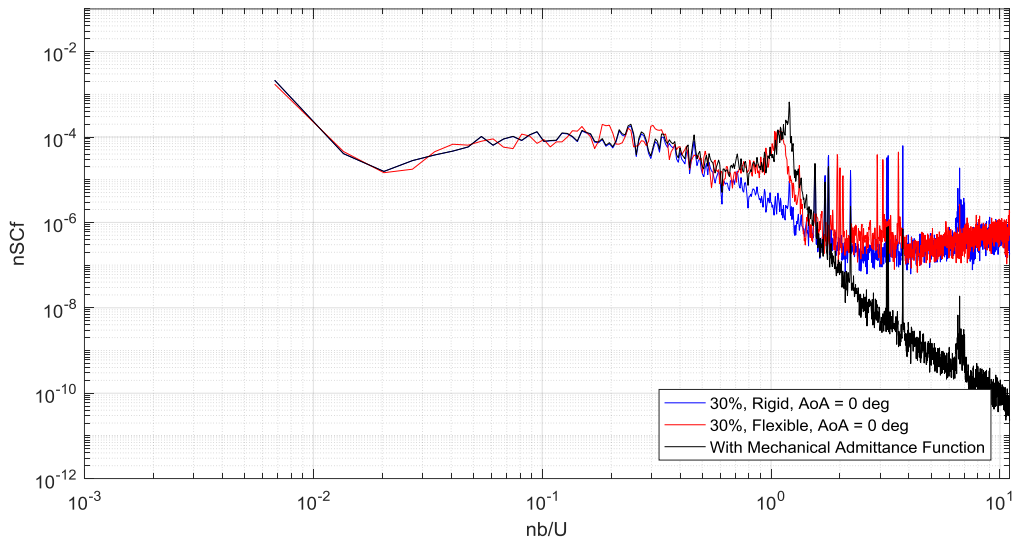


Figure 23. The modified rigid model spectrum by incorporating the Mechanical Admittance Function

To estimate the maximum and minimum force coefficient from the modified spectrum the following equations can be used:

$$\widehat{C}_f = \overline{C}_f + \sqrt{g^2_{B^*} \cdot B + g^2_{R^*} \cdot R} \quad (7)$$

$$g_R = \sqrt{2\ln(n_1 T)} + \frac{0.577}{\sqrt{2\ln(n_1 T)}} \quad (8)$$

$$g_R = \sqrt{2\ln(10.5 * 3600)} + \frac{0.577}{\sqrt{2\ln(10.5 * 3600)}} = 4.64 \quad (9)$$

In the above equation the  $g_B$  is assumed equal to 3.4, using the suggested value in ASCE 7-16 [2]. Based on the spectra of the flexible and rigid models the background and resonant components are calculated for four representative wind directions (see Table 1).

The mean, maximum and minimum force coefficients are presented in Table 2, Table 3 and Table 4 respectively. The dynamic amplification factor is applied to the rigid model force coefficients calculated based on the load-cell data. The implementation of the MAF resulted in mixed findings. Although it improved the agreement in certain wind directions, it also resulted in higher discrepancies for several cases. These findings demand for a more thorough review of the experimental data and analysis of more testing cases to confirm the validity of the hypothesis.

Table 1. Background and resonant components of force coefficient spectra

Wind Direction (deg)	B ( $\times 10^{-5}$ )	R ( $\times 10^{-5}$ )	$\sqrt{g_B^2 \cdot B + g_R^2 \cdot R}$
0	6.16	2.7	0.036
45	47	5.9	0.082
90	60.9	13.4	0.100
135	51.9	1.4	0.079

Table 2.  $C_f$ ,mean for total area (i.e. 3 PV panels on the single racking system)

Wind Direction	Flexible 1:1	Rigid 1:1
	Load Cells	Load Cells
0	0.051	0.074
45	0.060	0.065
90	0.078	0.053
135	0.083	0.093

Table 3.  $C_f$ ,max for total area (i.e. 3 PV panels on the single racking system)

Wind Direction	Flexible 1:1	Rigid 1:1	
	Load Cells	Load Cells	
		No H(f)	H(f)
0	0.145	0.146	0.182
45	0.159	0.177	0.259
90	0.207	0.188	0.288
135	0.210	0.223	0.302

Table 4.  $C_f$ ,min for total area (i.e. 3 PV panels on the single racking system)

Wind Direction	Flexible 1:1	Rigid 1:1	
	Load Cells	Load Cells	
		No H(f)	H(f)
0	-0.040	-0.001	-0.037
45	-0.032	-0.053	-0.135
90	-0.080	-0.100	-0.200
135	-0.050	-0.070	-0.149

### 3.4 Comparison to ASCE 7-16

The results from the current study are compared to the recently published ASCE 7-16 Standard [2]. It should be noted that ASCE 7-16 design values for PV arrays were predominantly based on studies of larger installations on flat roof commercial buildings whereas the focus of this study was on low-rise residential buildings.

The following equations were used based on sections 26.10.2 and 29.4.4 of the code:

$$q_h = 0.613K_zK_{zt}K_dK_eV^2 \quad (10)$$

$$p = q_h(GC_p)\gamma_E\gamma_a \quad (11)$$

where  $q_h$  velocity pressure for all surfaces evaluated at mean roof height,  $h$ , ( $GC_p$ ) is external pressure coefficient,  $\gamma_E$  is array edge factor, and  $\gamma_a$  is solar panel pressure equalization factor. The velocity pressure estimation and the corresponding results for a single PV panel and a 3 PV panel array are presented in Table 5 and

Table 6.

Table 5. Estimation of velocity pressure

Directionality Factor, $K_d$	0.85
Exposure Coefficient, $K_z$	0.85
Ground Elevation Factor, $K_e$	1.0
Topographic Factor, $K_{zt}$	1.0
Basic Wind Speed, $V$ (m/s)	40
Velocity Pressure, $q_z$ (N/m <sup>2</sup> )	708

Table 6. Design wind pressure

Case/Parameters	One panel	Three panels
Area (m <sup>2</sup> )	1.9	5.8
Array Edge Factor, $\gamma_E$	1.0	1.0
Solar Panel Pressure Equalization Factor, $\gamma_a$	0.6	0.5
External Pressure Coefficient, ( $GC_p$ )	-2.0	-0.8
Design Wind Pressure, $P$ (N/m <sup>2</sup> )	840	280

In the current study, the critical (i.e. regardless of wind direction) minimum force coefficient on the flexible model for the three-panel array is -0.2, which is lower than the proposed value (-0.8) by ASCE 7-16. When the pressure tap results are considered (PTS method on the full-scale rigid model), the values are  $\pm 0.4$  which are closer to the ASCE 7-16. Finally, the large-scale model is providing values even closer which are  $\pm 0.6$  approximately.

## 4 Summary and Conclusions

A detailed experimental study was carried out to evaluate the wind-induced response of photovoltaic (PV) arrays mounted on top of low-rise residential buildings. The focus of the study was on the dynamic response of the PV panel array and vibration issues that are induced even at lower wind speeds. Three models were tested at the Wall of Wind (WOW) facility at FIU, including a full-scale real PV panel array (i.e. flexible

model), a full-scale rigid panel array (i.e. wood model) and a large scale rigid panel array (i.e. plexiglass model). In summary, the main achievements of this study are as follows:

- The mean  $C_F$  results obtained from the flexible model tests appear to be independent of the wind speed. The peak  $C_F$  values show some discrepancies for specific wind directions.
- No significant differences were found between the  $C_F$  values obtained from the flexible versus the rigid model tests. For specific wind directions, the flexible model experiences considerably higher  $C_F$  values when compared to the rigid model pressure tap results.
- When the  $C_F$  values are calculated using the pressure tap data the results indicate a good match between the large-scale and full-scale mean values. The peak  $C_F$  values show significant discrepancies which are though reduced when the partial turbulence simulation is used.
- The resonant response of the PV array at the first natural frequency (approx. 10 Hz) is very close to the module's fundamental natural frequency of 10.5 Hz which was established by the hammer tests.
- The implementation of the MAF resulted in mixed findings. Although it improved the agreement in certain wind directions, it also resulted in higher discrepancies for several cases.
- The findings compare well with the current wind standard recommendations. The best agreement is established when the  $C_F$  values are estimated using the pressure data.

Overall, this study is expected to provide valuable information for the development of wind design guidelines for residential scale PV panel arrays. The majority of the current building codes and wind standards that include design guidelines for PV systems are based predominantly on tests that considered scaled models of large commercial PV array systems on flat industrial size buildings. These configurations are significantly different than a typical low-rise building therefore the current study is expected to add knowledge and assist in the development of more accurate design recommendation for residential scale PV installations. The State of Florida is in particular need for such guidelines as it is often impacted by strong wind events. Recent initiatives, such as the mandatory installation of PV panels in new residential construction in South Miami [1], demand for development of safe and efficient design tools for rooftop solar arrays. Furthermore, the findings related to the wind-induced vibration on the PV panels provide important insight on the dynamic response of the system. This type of information would not be possible to be extracted from small-scale rigid model tests and such knowledge will further improve our understanding of the wind-induced performance of solar arrays and assist in the development of more comprehensive building code guidelines.

## References

- [1] Alvarado, F. (2017/07/13). *South Miami set to become first city in Florida to mandate solar panels on new homes*. Retrieved from <https://therealdeal.com/miami/2017/07/13/south-miami-becomes-first-city-in-florida-to-mandate-solar-panels-on-new-homes/>
- [2] ASCE, Minimum design loads and associated criteria for buildings and other structures (ASCE/SEI 7-16), Reston, VA: American Society of Civil Engineers, 2016.
- [3] M. Aly, A. G. Chowdhury and G. Bitsuamlak, "Wind profile management and blockage assessment for a new 12-fan Wall of Wind facility at FIU," *Wind & Structures*, vol. 14, no. 4, p. 285–300, 2011.
- [4] M. A. Mooneghi, P. Irwin and A. G. Chowdhury, "Partial turbulence simulation method for predicting peak wind loads on small structures and building appurtenances," *Journal of Wind Engineering and Industrial Aerodynamics*, vol. 157, pp. 47-62, 2016.
- [5] J.-M. Seo, I.-K. Choi and J.-R. Lee, "Static and cyclic behavior of wooden frames with tenon joints under lateral load," *Journal of Structural Engineering*, vol. 125, no. 3, pp. 344-349, 1999.



# Wind Driven Rain Intrusion on Interior Zones of Residential Construction

## 1. Introduction

Considering the significant increase in the amount of economic losses caused by hurricanes during past few decades, there is a crucial need to accurately estimate vulnerability of buildings to hurricanes in coastal states like Florida [1].

Although probabilistic simulation models can be used to predict the hurricane risk, their loss projection is not accurate enough due to simplifying assumption related to interior damage prediction [2]. It has been shown that interior damages can make up 50% to 100 % of the total damage costs, so incorrect estimation of them can result in significant inaccuracy in the loss estimation models.

Post hurricane surveys have shown that interior damages are mainly caused by rain water intrusion into the building through defects or breaches [3], [4]. Evaluation of the buildings performance during water intrusion caused by wind driven rain (WDR) requires performing experimental tests. One of the main objectives of this project is to develop a framework for large-scale testing of low-rise building under WDR. For this purpose, experimental tests were performed at Wall of Wind (WOW) facility at Florida International University (FIU).

Experimental investigation of the wind driven rain effects on buildings requires research on several aspects associated with the rain field simulation ([5], [6], [7], [8], [9]), rain deposition on building façade ( [10], [11], [12], [13]), building envelope performance ( [14], [15]) and hydrothermal behavior of building components ( [16], [17] , [18]). One of the novel aspect of this project is that it incorporates multiple aspects required for investigating the WDR effects, starting from actual WDR simulation and rain deposition on building envelope to evaluation of building interior performance.

## 2. Methodology

### 2.1. Testing facility

The rain field calibration was performed for suburban terrain with the scale of 1:4 at the 12-fan WOW facility at FIU (*Figure 24*). Details on the specification of the WOW facility and the wind flow characteristics can be found in [19].



*Figure 24. 12-fan Wall of Wind (WOW)*

The mean wind speed and turbulence intensity profiles were calculated from the speed measurements by using Pitot-static tubes and Cobra probes mounted at different heights at the center of the test section at the

WOW facility without the model in place. The corresponding average wind speed and longitudinal turbulence intensity are shown in *Figure 25* as a function of height.

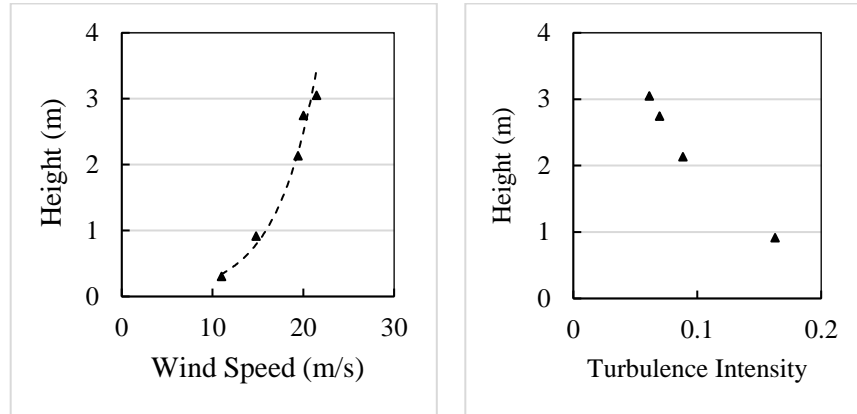


*Figure 25. Mean velocity (left) and turbulence intensity profiles (right)*

## 2.2. Rain Field Simulation

To simulate the rain field characteristics in the WOW laboratory the target rain size distribution must be determined (*Figure 26*). The target rain size distribution was obtained by fitting a Gamma distribution to the normalized rain size distribution observed during three past hurricanes by Baheru, 2014 [20]. Since damage estimation experiments were designed for 1:4 scaled residential building model, the target rain size distribution was also transferred to the scale of 1:4 (*Figure 27*).

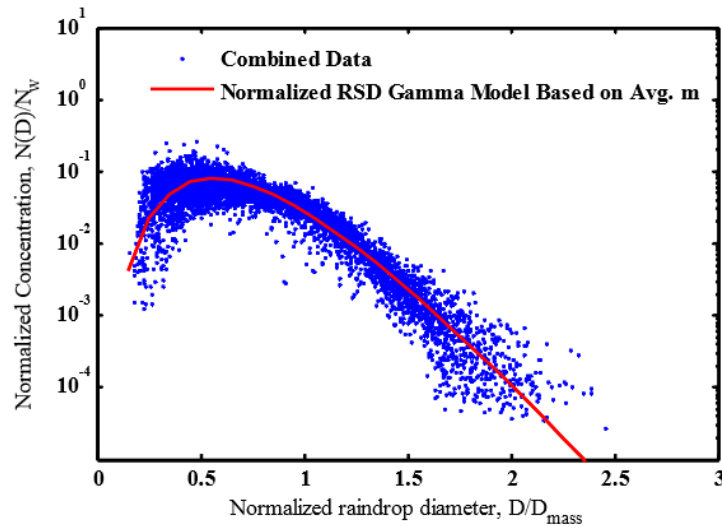


*Figure 26. Target Rain size distribution, [20]*

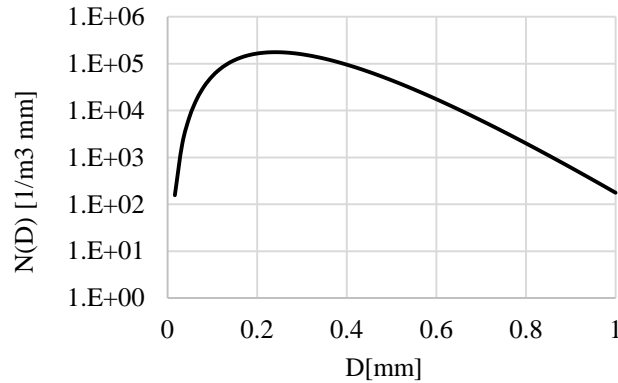


Figure 27. Scaled Rain Size Distribution

### 2.3. Droplet Measurement Devices

Parsivel<sup>2</sup> from OTT Hydromet and Precipitation Imaging Probe (PIP) were the two droplet measurement devices used in this study. While PIP is famous for its high precision for measuring the wind driven rain, there are several studies confirming the inadequacy of Parsivel performance when the wind is introduced into the measurements.

Lopez, 2011 [21] showed that the inaccuracy of Parsivel for the wind driven rain measurement is mainly associated with the oblique trajectory angle of the rain drops caused by the wind. He concluded that when the wind angle is perpendicular to the laser plane of the Parsivel, the droplet measurements are in a good agreement with the results of the PIP. However, the results showed that Parsivel underestimates the number of small drop sizes (less than 0.68 mm) even when the wind angle is perpendicular to the laser field. Tokay, 2014 [22] compared the droplet measurement accuracy of Parsivel<sup>2</sup>, Parsivel and Joss–Waldvogel (JW) disdrometer. It was shown that the accuracy of the Parsivel<sup>2</sup> is increased for small drop sizes in the range of 0.34 – 0.58 mm and it was concluded that Parsivel<sup>2</sup> is certainly an improved version of the Parsivel for the raindrop size and rainfall measurements.

In the current study, it was decided to use both Parsivel<sup>2</sup> and PIP for droplet measurements. According to Lopez 2011 [21], when droplet measurements are performed for wind driven rain situations (i.e. the wind angle perpendicular to the laser field of the sensors) the accuracy of Parsivel is intact for larger sizes (larger than 0.68mm) while a higher accuracy of Parsivel<sup>2</sup> is expected for smaller droplets (smaller than 0.5mm).

### 2.4. Measurement of Rain Size Distribution at Stagnant Air

For deciding on the type and number of nozzles several preliminary tests were performed at stagnate air condition. The main advantage of these tests was that it did not require to turn on the WOW fans which can be quite expensive. These experiments allowed for testing different nozzle types and different water pressures. To perform these tests a single nozzle was mounted above the sensors and the sprayed droplets moved in vertical direction through the stagnant air (see Figure 28). The rain size measurement was performed using both Parsivel<sup>2</sup> and PIP and the resulted RSD were compared to investigate the accuracy of Parsivel<sup>2</sup>. Based on the measured RSDs, the most proper nozzle type is selected. The effect of water pressure on the RSD of the selected nozzle is investigated in the next step.



*Figure 28. Droplet measurement using Parsivel and PIP for single nozzle spray in stagnant air*

#### 2.4.1. Nozzle types

Six different nozzle types were selected for the preliminary testing. The selection of these nozzles was based on the previous experiment performed by Baheru, 2014 [20]. In that study, Teejet extended range flat 8008-E was selected for the rain simulation. A water pressure of 52 psi was reported at the nozzle's tip during the experiment. According to the nozzle manual, TEEJET 8008 – E nozzle generates medium size droplets (See

Table 7 for details on drop sizes) at 40 - 60 psi pressures. Since the resulted RSD using the TEEJET 8008 – E showed a higher number concentration than target RSD for drop sizes larger than 0.6 mm, in this study it was tried to test the nozzles which generated finer droplets.

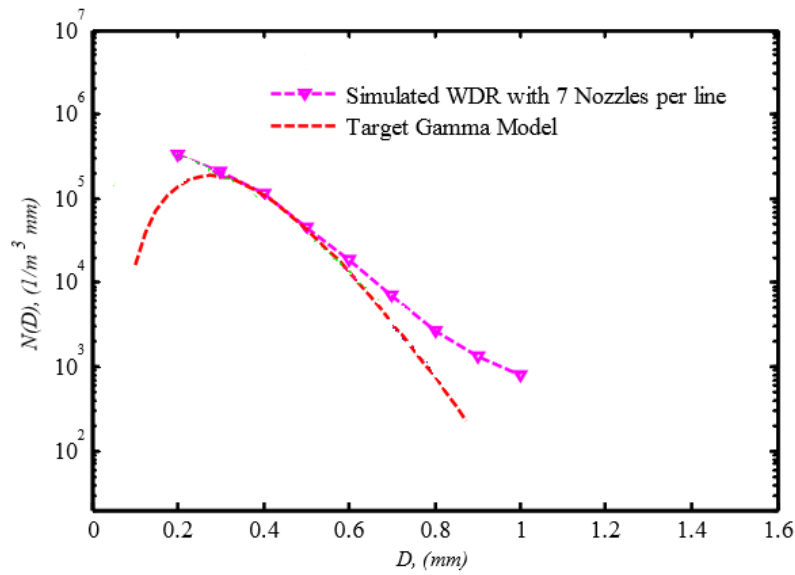


Figure 29. Target and achieved RSD, Baheru, 2014 [20]

Table 8 displays the tested nozzles along with their nozzle sizes at different water pressures. The water pressure for a single nozzle test was expected to vary between 40 to 50 psi. The same water pressure range was observed during the experiments.

Table 7. Droplet Size Classification based on ASABE S572.1

Size Classification	VMD* Range (Microns)
Extremely Fine	<60
Very Fine	61-105
Fine	106-235
Medium	236-340
Coarse	341-403
Very Coarse	404-502
Extremely Coarse	503-665
Ultra-Coarse	>665

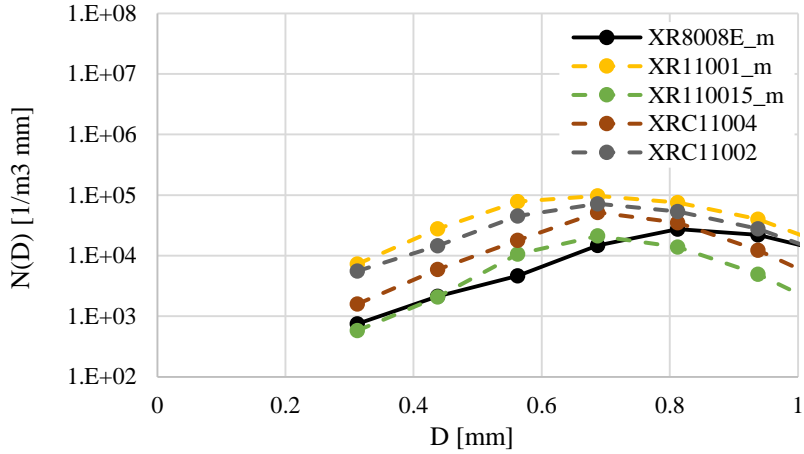
\* Volume Median Diameter

Table 8. Tested nozzles

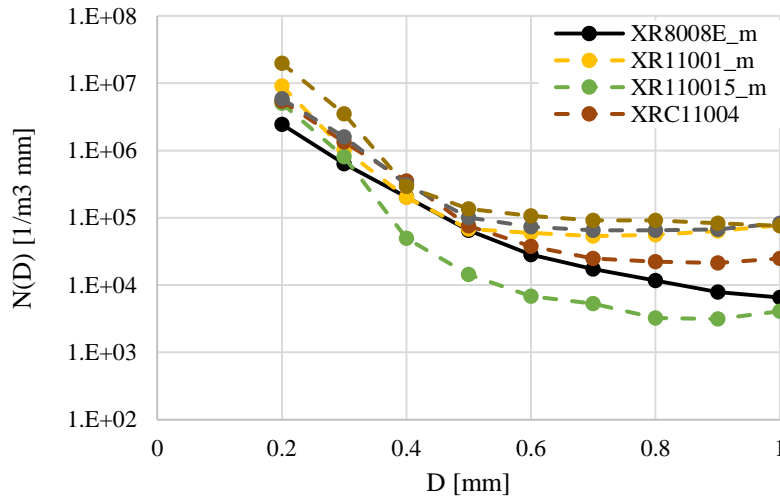
type	Water Pressure PSI						
	15	20	25	30	40	50	60
XR8008	VC	VC	C	C	M	M	M
XR11001	F	F	F	F	F	F	VF
XR110015	F	F	F	F	F	F	F
XRC11002	M	F	F	F	F	F	F
XRC11004	M	F	F	F	F	F	F
XRC80015	M	M	M	M	M	F	F

\*VC: Very Coarse, C: Coarse, M: Medium, F: fine, VF: Very fine

Figure 30 compares the droplet size distribution for different nozzles, measured using Parsivel (Figure 30a) and PIP (Figure 30b). As can be observed from Figure 30a, the Parsivel measurement showed that all the tested nozzles except for XR110015 lead to higher number concentration than XR8008E nozzle for drop sizes larger than 0.73 mm. PIP data resulted in almost similar trend except that 0.33 mm was the limit where the number concentration of nozzles (except for XR110015 nozzle) exceeded the number concentration of XR8008E nozzle. While the similar trend confirms the fact that XR110015 can be a potential substitute for XR8008E nozzle to modify the rain size distribution (decrease the number concentration for drop sizes larger than 0.6 mm to obtain a better match with target RSD), the difference between the results of Parsivel and PIP needs to be further investigated.



(a)



(b)

Figure 30. Droplet size distribution for different nozzles measured by (a) Parsivel and (b) PIP

Figure 31 compares the results of Parsivel and PIP for XR8008E nozzle. The results indicate that Parsivel data lays below the PIP curve for drop sizes less than 0.7 mm. This observation can be attributed to underestimation of number concentration for fine droplets by Parsivel. The same observation can be made when comparing the RSD of other nozzle types using Parsivel and PIP. So, it can be concluded that even in the stagnant air situation where there is no obliqueness in the trajectory angle of the droplets, the measurement of Parsivel is not accurate enough for the drop sizes less than 0.6 mm. Although this level of inaccuracy can be important for this study where the droplets are simulated with the scale of 1:4, in reality the performance of Parsivel can be accurate enough since the concentration of the rain drops lays between 1 to 3 mm.

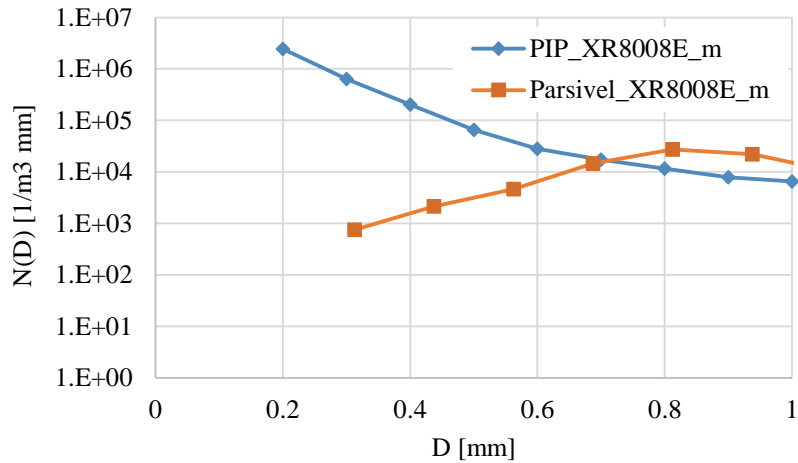


Figure 31 Comparing the RSD obtained from Parsivel and PIP, for XR8008E nozzle

#### 2.4.2. Water pressure

The water pressure is a parameter that affects the generated size distribution of the nozzle as well as its flow rate. Since the pressure head of the supplying pipeline is constant, increasing the number of nozzles that feed from the pipeline can lead to a decrease in water pressure at the tips of the nozzles. In this section, the RSD generated by XR8008E nozzle at different water pressures was investigated to assess the effect of water pressure on the generated drop sizes. The XR8008E nozzle was selected since according to the manual the size range of this nozzle was highly dependent on the water pressure. To alter the water pressure at the tips of the nozzle, the tests performed with different number of nozzles installed on the pipeline. Figure 32 displays the pressure gauge used for pressure measurement. For each test, only one of the nozzles sprayed water above the droplet measurement device, while the water from the rest of the nozzles were sprayed out of the measurement field and could not participate in the measured RSD.

*Table 9* shows the water pressure as a function of number of installed nozzles.



*Figure 32. Pressure gauge installed on the hose*

Table 9. Water pressure at tips of nozzles as a function of number of nozzles

Number of nozzles	Pressure [psi]
2	42
4	28
6	16

Figure 33 displays the RSD obtained for RX8008E nozzle at different water pressure by PIP. As can be observed from this figure increasing the water pressure from 16 to 42 psi can lead to a slight increase in the number concentration of the droplets and this increase becomes more significant by increasing the droplet sizes.

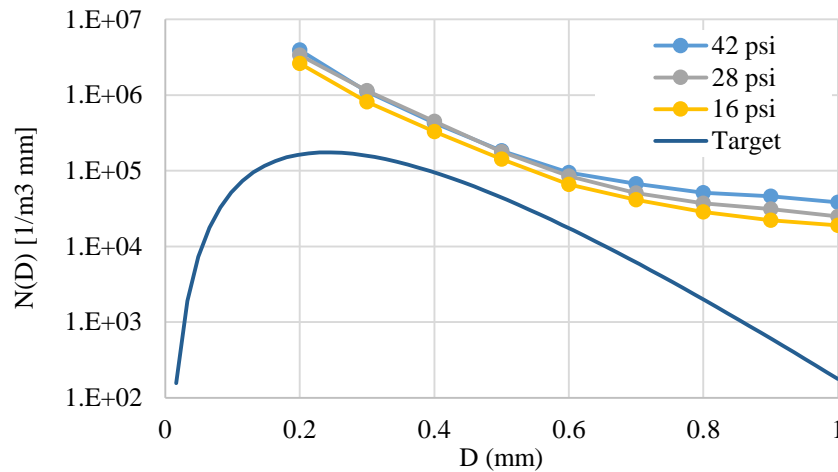


Figure 33. Effect of water pressure on RSD of droplets generated by XR8008E nozzle

### 2.5. Calibration of WOW Rain Field

The calibration of rain field at WOW test section was done by first selecting the most appropriate spraying nozzle. The results of the first phase of the testing that was designed to investigate the size distribution generated by a single nozzle at stagnant air were used for initial selection of the nozzle type. Two nozzle types were selected to be installed on the spires in front of the WOW fans (Figure 34) including XR8008E and XR110015, initially it was decided to test the nozzle types at three different arrangements on the vertical spires including:

- Case 1: Nine XR8008E nozzles on each side spire and ten XR8008E nozzles on the center spire
- Case 2: Combination of five XR8008E in between four XR110015 on each side spire and five XR8008E nozzles in between five XR110015 nozzle on the center spire.
- Case 3: Nine XR110015 nozzles on each side spire and ten XR110015 nozzles on the center spire



Figure 34. Vertical spires in front of the WOW where the nozzles will be installed on the hoses

It was decided to test each case for 5 minutes of simultaneous wind and rain. Figure 35 compares the results for case 1 and case 2. In both cases the measurement of the RSD was performed at the centerline of the WOW test section. Considering the fact that the number concentration of droplets decreases by replacing half of the XR8008E nozzles by XR110015 nozzles, it was decided that the third case would worsen the RSD results and so it was not tested. Since case 1 resulted in an acceptable match with the target RSD it was decided to select this nozzle configuration for the final test setup.

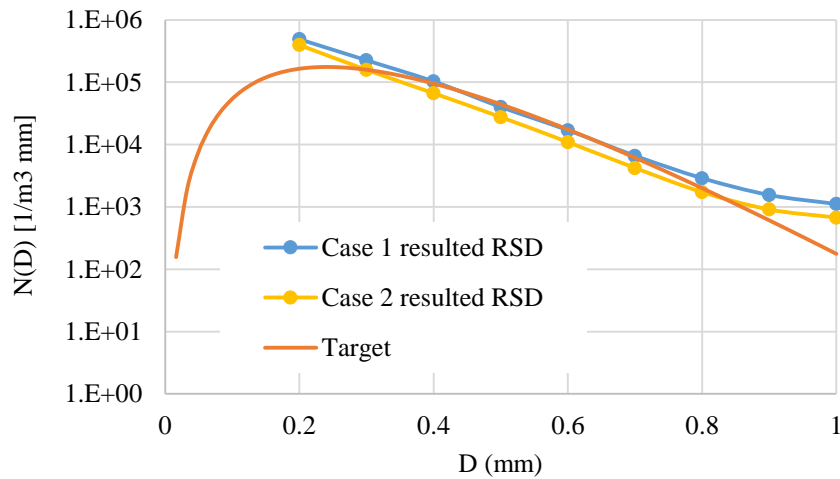


Figure 35. Resulted RSD at WOW test section

In addition to RSD measurement at the center location at P1 (6.10, 0, 0.76) the measurement was performed at five more locations in order to investigate the uniformity of the simulated rain field across the WOW test section. These locations included P2 (6.10, 0.81, 0.76), P3 (6.10, -0.81, 0.76), P4 (6.10, 1.62, 0.76), P5 (6.10, -1.62, 0.76) and P6 (6.10, 0, 1.52), where the coordinate axes are specified base on Figure 36 and the length unit is meter.

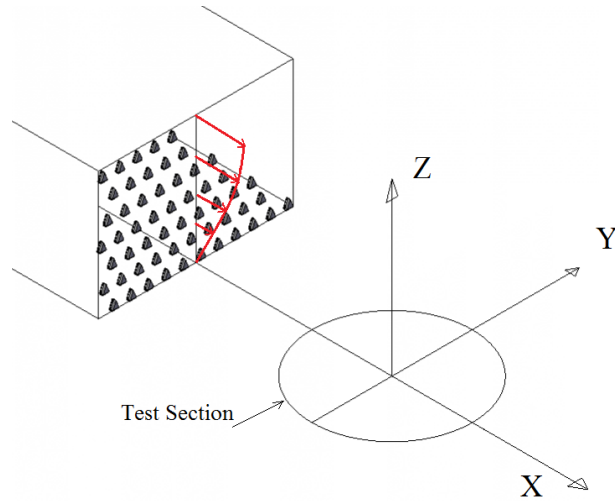


Figure 36. Coordinate system

The resulted RSDs are presented in Figure 37. As can be observed from this figure there is a good consistency between the resulted RSDs and we can consider the rain field to be uniformly simulated.

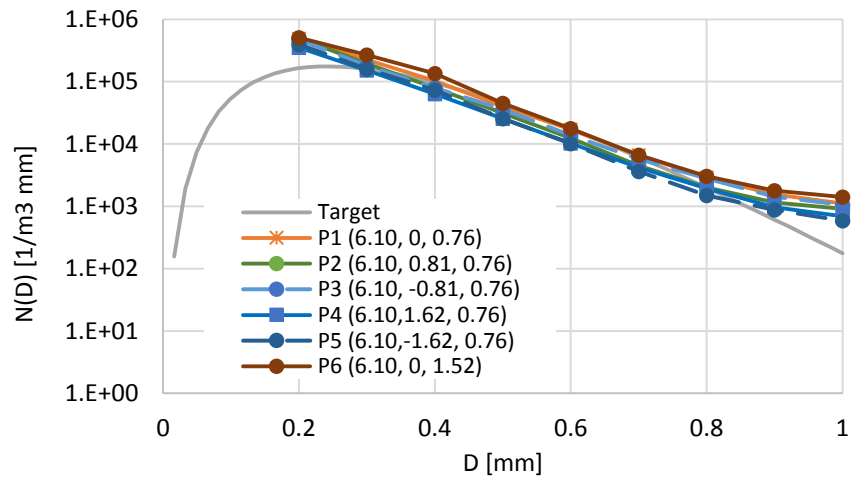


Figure 37. Comparison of RSD at different location across the test section

Once the rain field was calibrated to achieve close enough RSD to the target, the vertical rain rate was measured at P1 to P5 in order to compare the uniformity of the vertical rain rate ( $RR_v$ ) at the scaled model eave roof height. The rain rate measurement was performed by using TB3 rain gauge (Figure 38). The WDR collecting gauge had dimensions of 21.5 cm (8.5 in) x 26 cm (10.25 in) x 12 cm (4.75 in) (width x height x depth). There was a vertical opening on the front face of the rain gauge bucket with the area of 217.5 cm<sup>2</sup> (33.7 in<sup>2</sup>). The top openings of the TB3 rain gauges were covered so it didn't allow direct rain entering into the tipping buckets. The TB3 rain gauge registered a pulse for every 0.254 mm (0.01 in) rainfall received through vertical openings of rain collecting buckets and recorded the time history data to ML1-FL data logger housed within the gauge's cover.



Figure 38. TB3 rain gauge connected to vertical rain collecting bucket

The resulted rain rate with time is compared for different locations in Figure 39. As can be observed for all the locations the rain rate is almost in the same range and it can be concluded that the rain has been uniformly simulated across the test section. The vertical rain rate that is the mean value of the time averaged rain rate among all of the five locations equals 180 mm/hr.

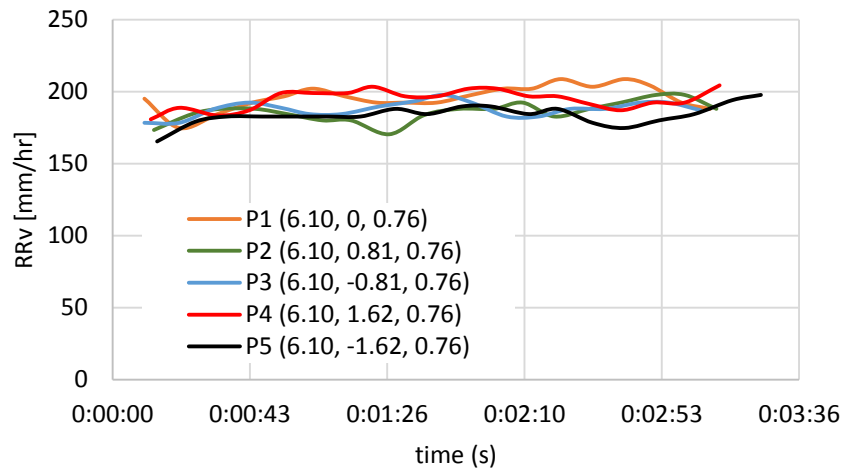
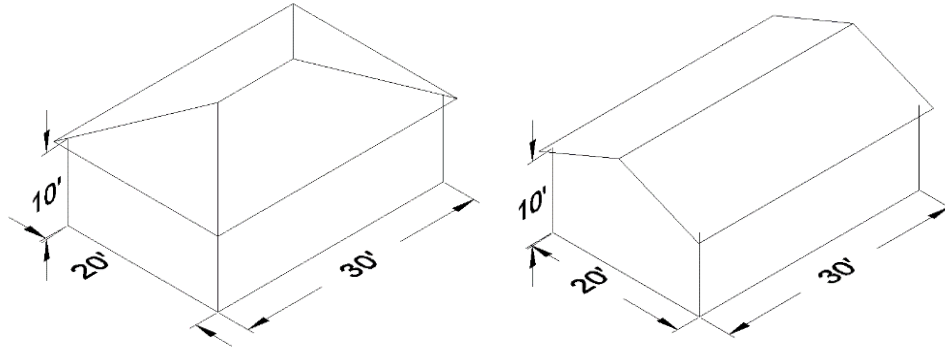


Figure 39. Vertical Rain Rate (RRv) at different locations across the test section

### 3. Large-Scale Experimental Water Propagation Tests

To experimentally investigate the water propagation path into the building interior, building models with the scale of 1:4 were tested at WOW laboratory. Two roof types of gable and hip were considered for the

large-scale models. A 5:12 roof pitch was selected for both gable and hip roof models with scaled overhang length of 7.62 cm (*Figure 40*).



*Figure 40. Building models (full-scale dimensions)*

For the building interior layout, it was decided to divide the building plan into 6 similar square compartments, as displayed in *Figure 41*. The 4' x 4' (dimensions in full-scale) windows were located at 2' 8" height from the floor (*Figure 42*).

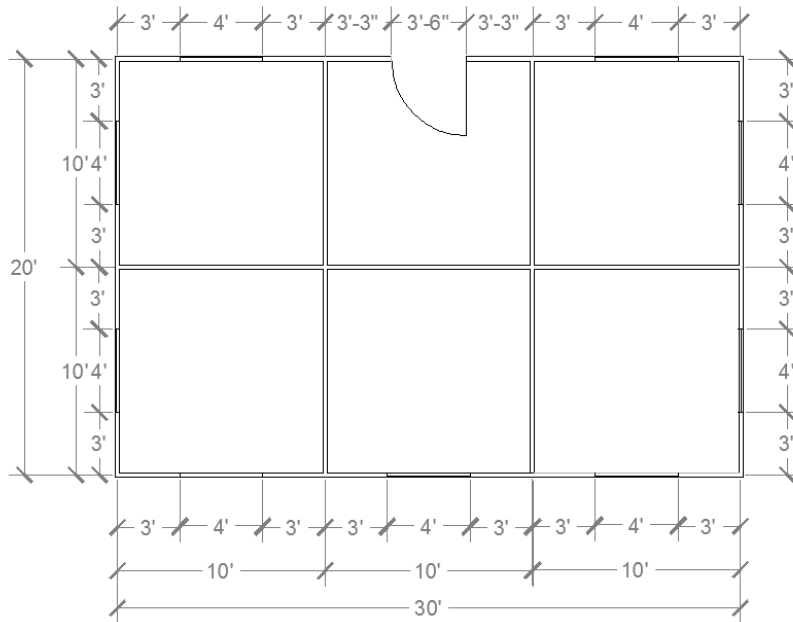


*Figure 41. Building plan layout (full-scale dimensions)*



Table 11 and Table 12 show the mean damages at each damage state, for gable and hip roof models, respectively.

Table 10. Mean damages of medium building construction type, for gable and hip roof models at different damage states

Gable Roof				Hip Roof			
	Sheathing Damage (%)	Roof Cover Removal (%)	Failed Window #		Sheathing Damage (%)	Roof Cover Removal (%)	Failed Window #
DS0	2.2	3.7	0	DS0	1.7	2.5	0
DS1	13.4	16.8	2	DS1	11.0	12.9	2

Table 11. Damage condition of gable roof model for each damage state

Damage State	Damage Ratio	Damaged Roof Sheathing	Removed Roof Cover	Broken Windows
No Damage (DS0)	up to 6%	0%	5%	0
Minor (DS1)	10%	15%	20%	2

Table 12. Damage condition of hip roof model for each damage state

Damage State	Damage Ratio	Damaged Roof Sheathing	Removed Roof Cover	Broken Windows
No Damage	up to 6%	0%	5%	0
Minor	10%	10%	15%	2

### 3.2. Evaluation of Pre-existing Building Defects

Two types of defects were considered:

1. Window sill cracks below the window;
2. Sealant missing between the electrical outlet/ventilation ducts. This opening was located above the outlet at 1.78 m height from the floor.

The decision on the size and location of these water entry points was made based on the following two studies:

- Baheru (2014), “Development of Test-Based Wind-Driven Rain Intrusion Model for Hurricane-Induced Building Interior and Contents Damage”, Florida International University [20].
- Lacasse, M. A., et al. (2003), Report from Task 6 of MEWS Project: Experimental Assessment of Water Penetration and Entry into Wood-Frame Wall Specimens - Final Report, Institute for Research in Construction [23].

### 3.3. Test plan

The large-scale tests were performed at 30 mph wind speed at the roof eave height of the models. The wind driven rain field is calibrated for WDR rate of 86 mm/hr. Two building models, one with gable and one with hip roof, was tested at two different damage state of No Damage (DS0) and Minor Damage (DS1). Each damage state was tested at three different wind angles (*Figure 43*). Each wind angle was tested for 5 minutes of simultaneous wind and rain. These resulted in 12 different cases; i.e. two roof types tested at two damage states subjected to three different wind angles of attack.

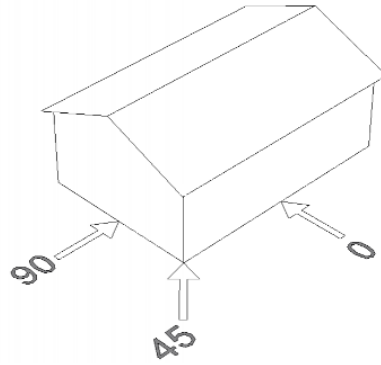


Figure 43. Wind Directions

### 3.1. Model preparation

The building models were built out of wood including details of openings, defects and internal compartments (Figure 44). Two removable roof types of hip and gable were prepared to get mounted on the same building model. Both interior and exterior surfaces were covered with waterproofing wood stain in order to reduce water absorption by the wooded material.

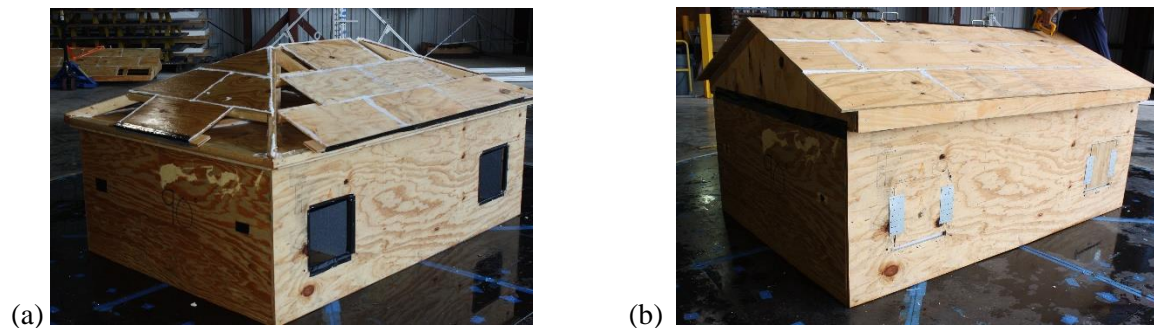
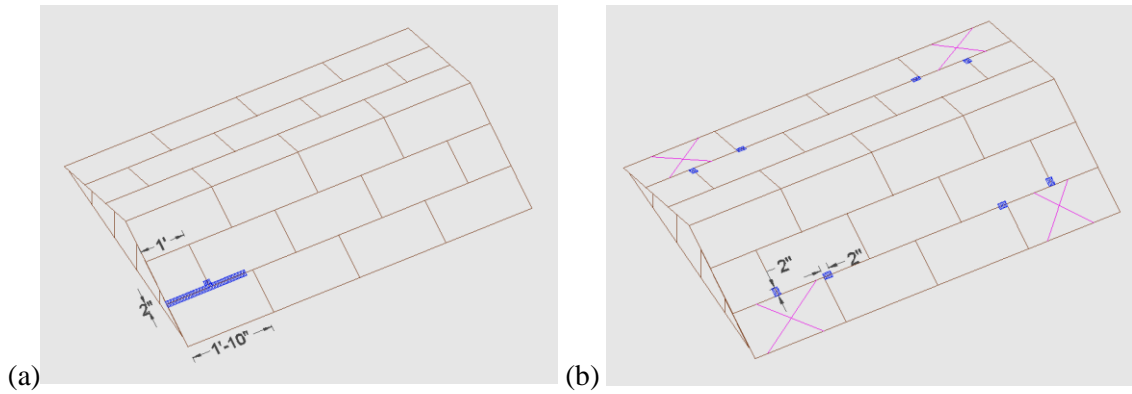


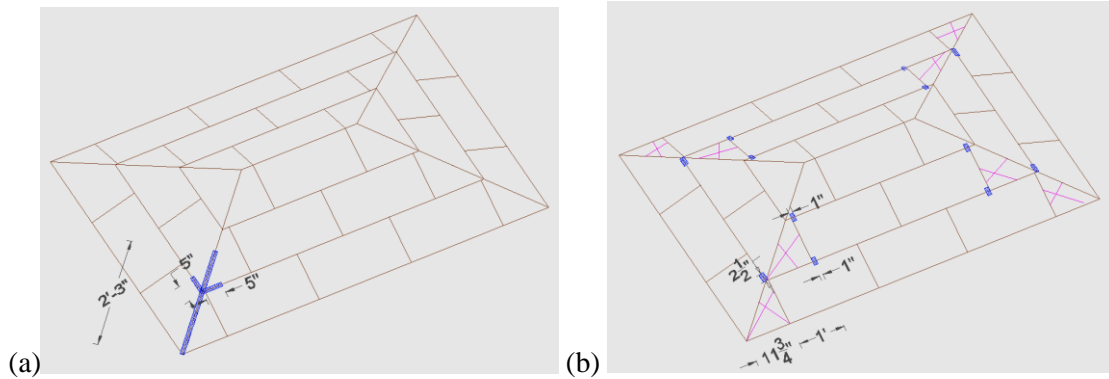
Figure 44. 1:4 scaled models out of wood

In order to prepare the model for the Minor damage state it was required to decide on the location of the wind induced envelope breaches. The locations of the breaches were selected based on expert opinion and previous post hurricane observations. Figure 45 displays the geometry and location of the wind induced breaches on roof at No-damage and Minor damage states for gable roof type. The same type of information for hip roof can be found in Figure 46. In both gable and hip roof models the roof sheathing was modeled with scaled down 4' x 8' wood panels. In order to model the roof covering the gap between the panels was sealed with caulk, so the roof cover removal was captured in the model by removing the caulk and leaving the gap unsealed (Figure 47). Figure 48 displays the wall breaches at No-Damage and Minor damage states for both gable and hip roof models.



✕ Removed sheathing, 
 ▨ Removed Roof Cover Removed

Figure 45. Gable roof breaches at (a) No damage and (b) minor damage states (scaled model dimensions)



✕ Removed sheathing, 
 ▨ Removed Roof Cover Removed

Figure 46. Hip roof breaches at (a) No damage and (b) minor damage



Figure 47. Unsealed gap between sheathing

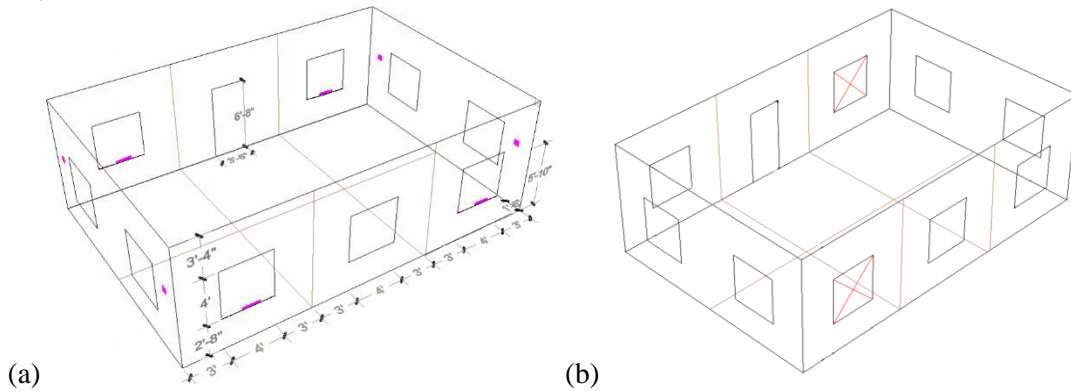


Figure 48. Wall breaches at (a) No damage and (b) minor damage (full scale dimensions)

In order to measure the amount of water within each interior wall surface, the interior surface of the walls was covered with high-absorbent pads. The pads were weighted before and after the tests and the increase in weight was used to obtain the amount of absorbed water (Figure 49).



Figure 49. Interior walls covered with water absorbent pads

The water intruded through the roof breaches was drained from six compartments (each compartment covering one room ceiling) and accumulated in the buckets that were hung below the turn table and connected to the ceiling by clear vinyl tubes. The same method was used for obtaining the amount of poured water on the floors (Figure 50).



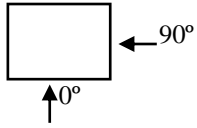
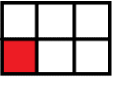
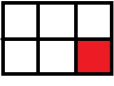
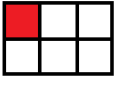
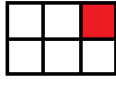
Figure 50. Water collection buckets

## 4. Results

### 4.1. Quantitative water propagation results

The volume of water intruded from the envelope breaches into each internal compartment is presented in *Table 13*. In this table the total amount of water intruded from all roof breaches is presented by a single number. This number is obtained by summing up the volume of water intruded into all of the six compartments covering the rooms' ceilings. The water volume presented for each room is the total amount of water intruded into the room from all types of breaches existing on its exterior walls. This value is obtained by adding up the volume of water absorbed by the pads covering the four interior walls and poured water on the floor.

Table 13. Total volume of intruded water into interior compartments (ml)

	Ceiling	Room1 	Room2 	Room3 	Room4 
Hip_No Damage_0°	157	491	503	0	0
Hip_No Damage_45°	36	284	604	0	206
Hip_No Damage_90°	95	0	325	0	238
Hip_Minor Damage_90°	1547	1340	0	0	0
Hip_Minor Damage_90°	2314	1045	0	0	0
Hip_Minor Damage_90°	988	0	0	0	0
Gable_No Damage_0°	172	449	495	0	0
Gable_No Damage_45°	58	297	581	0	190
Gable_No Damage_90°	0	0	263	0	257

Gable_Minor Damage_90°	1161	1197	0	0	0
Gable_Minor Damage_90°	1065	1101	0	0	0
Gable_Minor Damage_90°	172	0	0	0	0

Figure 51 to Figure 62 display the water propagation into different ceiling compartments as well as interior walls and floors. The percentage of water propagation into each interior wall is obtained by dividing the volume of the water absorbed by the pad covering that wall to the total volume of water intruded into the room (as presented in Table 13). Likewise, the percentage of water propagation into the floor represents the ration of the poured water on the floor to the total volume of water intruded into the room (as presented in Table 13).

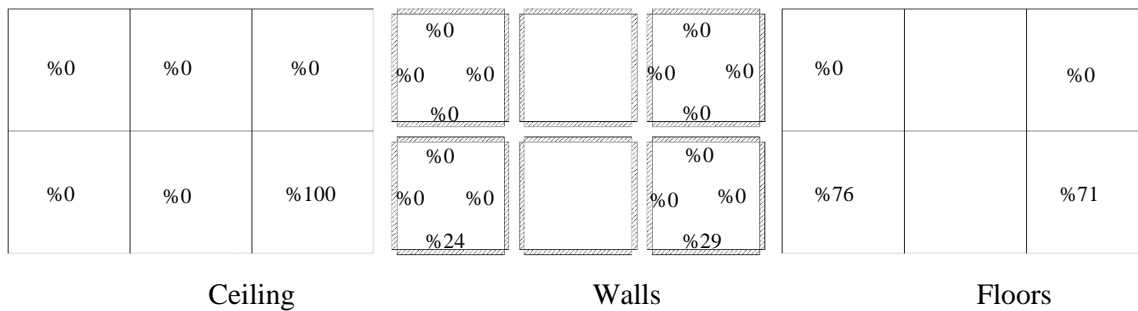


Figure 51. Water propagation hip roof model at No-damage state at 0° wind angle (percentage values)

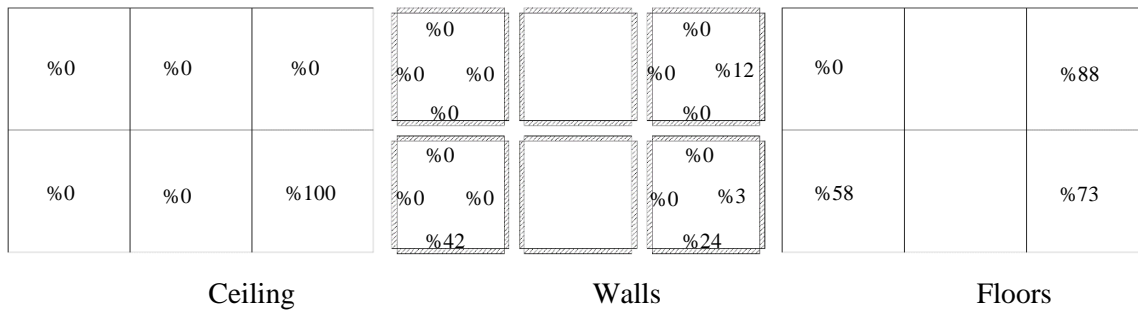


Figure 52. Water propagation hip roof model at No-damage state at 45° wind angle

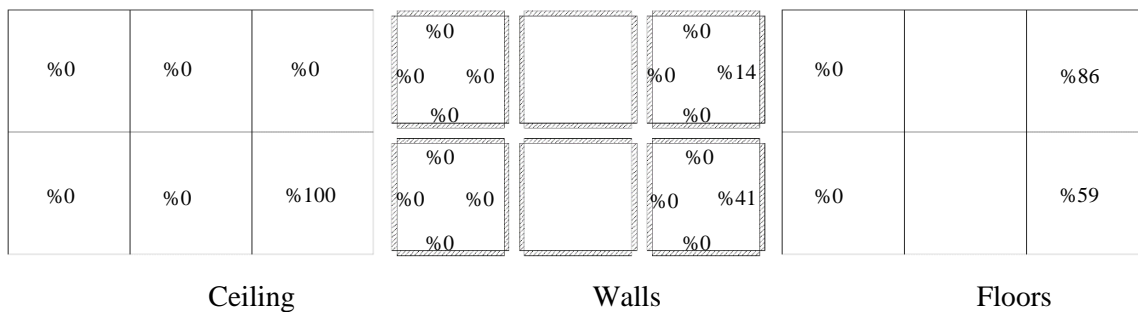


Figure 53. Water propagation hip roof model at No-damage state at 90° wind angle

%0	%0	%0	%0 %0 %0 %0		%0 %0 %0 %0	%0		%0
%0	%0	%100	%0 %0 %0 %24		%0 %0 %0 %26	%76		%74
Ceiling			Walls			Floors		

Figure 54. Water propagation gable roof model at No-damage state at 0° wind angle

%0	%0	%0	%0 %0 %0 %0		%0 %0 %16 %0	%0		%84
%0	%0	%100	%0 %0 %0 %56		%0 %0 %2 %28	%44		%70
Ceiling			Walls			Floors		

Figure 55. Water propagation gable roof model at No-damage state at 45° wind angle

%0	%0	%0	%0 %0 %0 %0		%0 %0 %14 %0	%0		%86
%0	%0	%100	%0 %0 %0 %0		%0 %0 %11 %0	%0		%89
Ceiling			Walls			Floors		

Figure 56. Water propagation gable roof model at No-damage state at 90° wind angle

%0	%0	%1	%0 %0 %0 %0		%0 %0 %0 %0	%0		%0
%55	%4	%45	%0 %0 %0 %0		%19 %1 %16 %10	%0		%55

Ceiling

Walls

Floors

Figure 57. Water propagation hip roof model at Minor damage state at 0° wind angle

%17	%2	%18	%0 %0 %0 %0		%0 %0 %0 %0	%0		%0
%39	%7	%19	%0 %0 %0 %0		%9 %30 %1 %23	%0		%38

Ceiling

Walls

Floors

Figure 58. Water propagation hip roof model at Minor damage state at 45° wind angle

%6	%0	%42	%0 %0 %0 %0		%0 %0 %0 %0	%0		%0
%6	%5	%40	%0 %0 %0 %0		%0 %0 %0 %0	%0		%0

Ceiling

Walls

Floors

Figure 59. Water propagation hip roof model at Minor damage state at 90° wind angle

%7	%2	%8	%0 %0 %0 %0		%0 %0 %0 %0	%0		%0
%36	%9	%37	%0 %0 %0 %0		%16 %0 %15 %11	%0		%58

Ceiling

Walls

Floors

Figure 60. Water propagation gable roof model at Minor damage state at 0° wind angle



Figure 63. Water propagation path into the gable roof model with broken window at 0° wind direction

Similar results for gable roof model with minor damage state at 45° wind direction are presented in Figure 64. This type of thermographic pictures can help us estimate the damages to the building interior as well as the building contents. For instance, when rain water reached a certain height of the wall, inspectors can assume a corresponding damage on the electrical system associated with the specific wall.

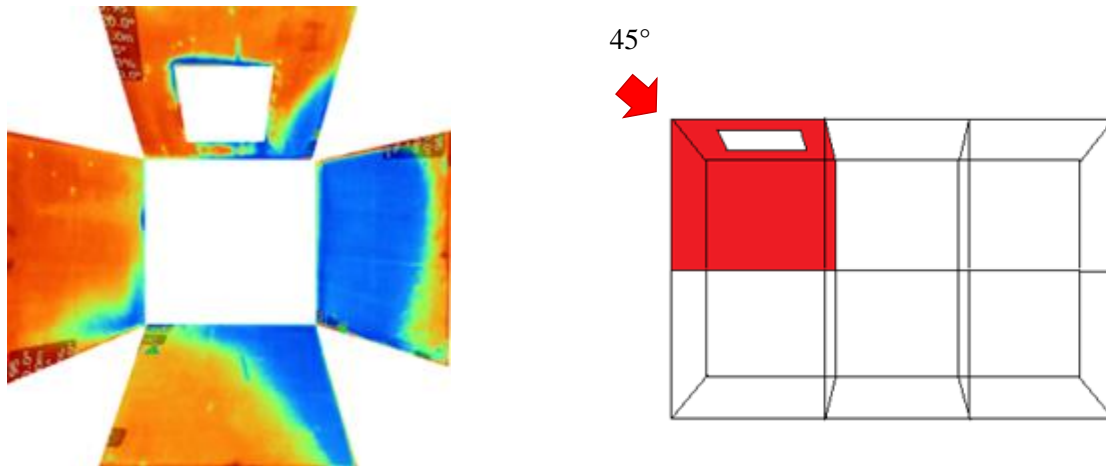


Figure 64. Water propagation path into the gable roof model with broken window at 45° wind direction

#### 4.3. Interior vulnerability model

This section introduces the suggested procedure to develop an interior vulnerability model based on the experimental tests. This is an ongoing task that requires thorough review of the existing results as well as additional testing of more building configurations. The steps required to evaluate the damage sustained by the building interior from the full-scale tests are as follows:

1. Provide an inventory of all the interior items as well as building content that a typical building includes similar to Table 14 presented by [24].
2. Define failure modes for these items and decide on performance state (damage limit) based on water propagation:
  - 2.1. Affected by direct water impinging on surface (i.e. drywalls, painting, closet, cabinet, furniture, electrical and mechanical components)
  - 2.2. Affected by accumulated water on the floors (i.e. carpet, floor)
  - 2.3. Affected by accumulated water on ceiling
3. Apply fundamental physical principles along with the results obtained from large-scale and full-scale tests to determine if the predetermined damage limits have passed for the considered items at different Exterior Damage State (ds) and wind direction (dir) and duration of rain (t) or total intruded rain (t).

Table 14. Dimensional and quantitative information required, [24]

General information for each story	General information for entire building
Total floor area	Total floor area
Finished floor area	Value of home
Total floor area covered with carpet	Number of stories
Total floor area covered with tile	Any basement
Total floor area covered with decorative wood flooring	<b>Floor on which appliances are located</b>
Total floor area covered with vinyl	Furnace location
Total length of lower cabinets	Air conditioning compressor location
Total length of upper cabinets	Water heater location
Total length of baseboard trim	Washer and dryer location
Total length of trim not including baseboards	Range location
Total length of interior walls	Refrigerator location
Total length of exterior walls which are covered on the interior surface	Garbage disposal location
Total length of exterior walls which are covered on the exterior surface	Dishwasher location
Number of windows	Vented hood location
Number of interior doors	Electrical panel box location
Number of exterior doors	<b>Heights for each story</b>
Number of closet doors	Height from floor to ceiling
Number of garage doors	Height from floor of current story to floor of story above
Number of staircases	Height of electrical outlets
Number of electrical outlets	Height of electrical switches
Number of electrical switches	
Number of light fixtures	

An example that demonstrates the above procedure is discussed here. The estimation of the sustained building loss due to interior wall damages assumes a typical one-story residential building with plan layout of *Figure 41* and total area of interior walls equal to 1800sf. The following performance states (PS) were assumed for interior walls:

- PS1: Drywalls are wet but their mechanical properties are not deteriorated;
- PS2: Drywalls are saturated and their mechanical properties are deteriorated.

The experimental tests result (section 4.1 and 4.2) need to be further analyzed in order to generate the corresponding vulnerability curves for different damage states. In *Figure 65* sample charts are presented for DS0, DS1 and DS2. These chart indicate the relation between the volume of water intruded and the corresponding PS. These relations can be used to estimate the sustained damage by the interior walls for any specific volume of water intrusion at 0° wind direction for a building with specific exterior damage state.

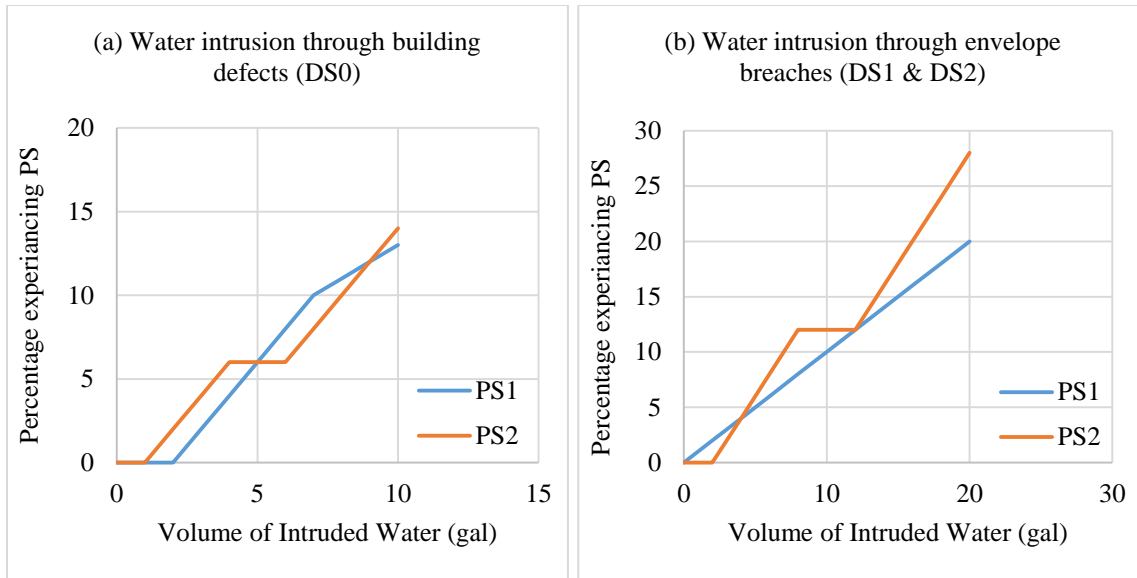


Figure 65. Percentage of one room interior wall area experiencing each performance state at 0° wind direction for (a) water intrusion through building defects and (b) through envelope breaches (hypothetical graphs)

For example, in this case if we know that the wind is blowing at 0° wind direction during the rain event, the building has exterior damage state of DS0 (i.e. two of the windward rooms are exposed to water intrusion through the window sill crack) and we estimate that the total volume of intruded water to each room through its window sill crack is 3 gal we can calculate the total damage sustained by the interior walls as follows:

$$\text{Area of interior walls experiencing PS1} = \frac{2}{6} * 1800 * 2\%$$

$$\text{Area of interior walls experiencing PS2} = \frac{2}{6} * 1800 * 4\%$$

In the case that the building would experiences DS1 (i.e. one of the windward rooms is exposed to water intrusion through the broken window) during the hurricane and the total volume of intruded water through the window is 10 gal the total damage sustained by the interior walls would be:

$$\text{Area of interior walls experiencing PS1} = \frac{1}{6} * 1800 * 10\%$$

$$\text{Area of interior walls experiencing PS2} = \frac{1}{6} * 1800 * 12\%$$

Knowing the damage condition of the building with this detail can help us to evaluate the monetary losses sustained by the building based on the corresponding repair costs.

## 5. Summary and Conclusions

In the current study the experimental large-scale tests have shown that the water propagation path follows the anticipated internal air flow. The tests were successful in capturing this propagation into the ceiling and the interior compartments. In addition, the use of absorbing pads and thermal cameras provided reliable information on the water distribution on each wall of individual compartments. These findings are extremely important and will be utilized to develop the necessary vulnerability curves that determine the performance state of different interior components in the building. In summary, the main achievements of this study are as follows:

- The rain field of WOW was calibrated in order to simulate rain characteristics during a hurricane event;
- A procedural method of simulating water propagation into building interior was presented;
- Quantitative and qualitative results were obtained that provide a better understanding of the interior damages of the building due to wind driven rain intrusion;
- The findings are expected to be implemented in Florida Public Hurricane Loss Model (FPHLM) and improve its accuracy related to the interior loss estimation.

Overall, the current study tested and modeled the interior and content damage mechanisms related to water ingress for the very first time. The acquired data will be further analyzed to develop benchmark test-based vulnerability models of hurricane induced interior and contents damage (and associated time related expenses) for typical low-rise residential coastal structures. The State of Florida will greatly benefit by the availability of such knowledge, as the information will be disseminated to the FIU, UF and FIT groups that are responsible for the Florida Public Hurricane Loss Model (FPHLM). The inclusion of the new interior, contents, and time related expenses models will enhance the existing FPHLM and increase its accuracy.

## 1. References

- [1] Munchener Ruck. Topics Geo - Natural catastrophes 2013: Analyses, assessments, positions, 302-08121, Germany: Munich Re Group, 2013.
- [2] Pinelli, J.-P., Pita, G., Gurley, K., Torkian, B., Hamid, S., Subramanian, C., "Damage Characterization: Application to Florida Public Hurricane Loss Model," *ASCE Natural Hazard Review*, Vol. 12, No. 4, pp. 190-195, 2011.
- [3] D. Mileti, *Disasters by Design: A Reassessment of Natural Hazards in the United States*, Joseph Henry Press, 1999.
- [4] J. W. van de Lindt, A. Graettinger, R. Gupta, T. Skaggs, S. Pryor and K. J. Fridley, "Performance of wood-frame structures during Hurricane Katrina," *Journal of Performance of Constructed Facilities*, no. American Society of Civil Engineers, 2007.
- [5] A. C. Best, "The size distribution of raindrops," *Quarterly Journal of the Royal Meteorological Society*, , , vol. 76(327), pp. 16-36, 1950.
- [6] A. Waldvogel, "The N 0 jump of raindrop spectra," *Journal of the Atmospheric Sciences*, vol. 31, no. 4, pp. 1067--1078, 1974.
- [7] Y. Mualem and S. Assouline, "Mathematical model for rain drop distribution and rainfall kinetic energy," *Transactions of the ASAE-American Society of Agricultural Engineers (USA)*, 1986.
- [8] N. Dingle and Y. Lee, "Terminal fallspeeds of raindrops," *Journal of Applied Meteorology*, vol. 11, no. 5, pp. 877-879, 1972.
- [9] R. E. Lacy, "Climate and building in Britain," Her majesty's stationery office, 1977.

- [10] E. C. Choi, "Wind-driven rain on building faces and the driving-rain index," *Journal of Wind Engineering and Industrial Aerodynamics*, vol. 79, no. 1, pp. 105-122, 1999.
- [11] B. Blocken and J. Carmeliet, "Spatial and temporal distribution of driving rain on a low-rise building," *Wind and Structures*, vol. 5, no. 5, pp. 441-462, 2002.
- [12] J. Straube and E. Burnett, "Simplified prediction of driving rain on buildings," in *Proceedings of the international building physics conference*, Eindhoven, Netherlands, 2000.
- [13] ISO, Hygrothermal performance of buildings - Calculation and presentation of climatic data. Part 3: calculation of a driving rain index for vertical surfaces from hourly wind and rain data, Finnish Standards Association SFS Helsinki, 2009.
- [14] ASTM, ASTM E331-00 Standard test method for water penetration of exterior windows, curtain walls, and doors by uniform static air pressure difference, West Conshohocken, PA: American Society for Testing and Materials, 2009.
- [15] ASTM, ASTM E547-00 Standard test method for water penetration of exterior windows, curtain walls, and doors by cyclic static air pressure difference, West Conshohocken, PA: American Society for Testing and Materials, 2009b.
- [16] V. Korsgaard and C. Rode, "Laboratory and practical experience with a novel water-permeable vapor retarder," in *Thermal Performance of the Exterior Envelopes of Buildings, Conference Proceeding*, Clearwater Beach, Florida, 1992.
- [17] G. A. Tsongas, D. P. Govan and J. A. McGillis, "Field observations and laboratory tests of water migration in walls with shiplap hardboard siding," *Thermal envelopes VII/Moisture-practices*, pp. 469-483, 1998.
- [18] H. Hens and A. M. Fatin, Heat-air-moisture design of masonry cavity walls: Theoretical and experimental results and practice, Atlanta, GA: American Society of Heating, Refrigerating and Air-Conditioning Engineers, Inc., 1995.
- [19] A. M. Aly, A. G. Chowdhury and G. Bitsuamlak, "Wind profile management and blockage assessment for a new 12-fan Wall of Wind facility at FIU," *Wind & Structures*, vol. 14, no. 4, p. 285-300, 2011.
- [20] T. Baheru, Development of Test-Based Wind-Driven Rain Intrusion Model for Hurricane-Induced Building Interior and Contents Damage, Miami, Florida: Florida International University, 2014.
- [21] C. R. Lopez, Measurement, analysis, and simulation of wind driven rain, Gainesville, Florida: University of Florida, 2011.
- [22] A. Tokay, D. B. Wolff and W. A. Petersen, "Evaluation of the new version of the laser-optical disdrometer, OTT Parsivel2," *Journal of Atmospheric and Oceanic Technology*, vol. 31, no. 6, pp. 1276-1288, 2014.
- [23] M. A. Lacasse, T. O'Connor, N. S. C and P. Beaulieu, "Report from Task 6 of MEWS Project: Experimental Assessment of Water Penetration and Entry into Wood-Frame Wall Specimens-Final Report," Institute for Research in Construction, 2003.

[24] M. Taggart, Performance based design of woodframe structures for flooding, Fort Collins, Colorado: Colorado State University, 2007.



*A Resource for the State of Florida*

*SECTION 5*

**Education and Outreach Programs to Convey the  
Benefits of Various Hurricane Loss Mitigation  
Devices and Techniques**

A Report Submitted to:  
The State of Florida Division of Emergency Management

*Prepared By:*  
Erik Salna  
Consultant: Jamie Edwards

The International Hurricane Research Center (IHRC)  
Florida International University

July 31, 2017

## **Executive Summary:**

Erik Salna, IHRC Associate Director, with assistance from consultant Jamie Edwards, developed and coordinated educational partnerships, community events, and outreach programs. This work promoted hurricane-loss mitigation and the objectives of the RCMP.

### ***Hurricane Andrew Anniversary Museum Exhibit – May 19th, 2017***

The Museum of Discovery & Science (MODS), located in Fort Lauderdale, FL, assisted the IHRC in developing and coordinating a new *Hurricane Andrew Anniversary* exhibit, which included a video showing original TV news and weather reports before, during and after the storm. Local officials and media attended a ribbon-cutting ceremony to debut the new exhibit on May 19<sup>th</sup>.

- Local media in attendance for ribbon-cutting: WSVN-TV (FOX), WPLG-TV (ABC) and WTVJ-TV (NBC)
- Combined local media coverage of the exhibit ribbon-cutting and *Eye of the Storm* museum event resulted in a Total Publicity Value amounting to \$8,989.
- MODS averages 450,000 visitors annually, including thousands of local area school children.

### ***Hurricane (Science, Mitigation & Preparedness) Event: Eye of the Storm – May 20th, 2017***

The Museum of Discovery & Science (MODS), located in Fort Lauderdale, FL, assisted the IHRC in planning, coordinating and facilitating this public education event that showcased special hands-on, interactive activities and demonstrations teaching hurricane science, mitigation and preparedness.

- Over 2,000 people attended *Eye of the Storm*.
- 34 South Florida agencies and organizations participated.
- Total Social Media Impressions: 15,637
- Combined local media coverage of the exhibit ribbon-cutting and *Eye of the Storm* museum event resulted in a Total Publicity Value amounting to \$8,989.

### ***Hurricane Preparedness Spanish Website – June 15<sup>th</sup>, 2017***

The IHRC, in partnership with NOAA's National Hurricane Center (NHC), enhanced the Spanish language website (<https://hurricanes.fiu.edu/>) with new static and live content. The goal of the website is to help the Spanish-speaking community be better educated, informed and prepared for hurricanes, including safe-guarding their families, homes and businesses.

### ***NOAA Hurricane Awareness Tour – May 12th, 2017***

In conjunction with NOAA's National Hurricane Preparedness Week, IHRC joined the NOAA Hurricane Awareness Tour at the Miami-Opa Locka Executive Airport.

- As a kick-off to the event, IHRC participated as a speaker in the media conference.
- Media conference was attended by almost 20 local, national and international media outlets.
- "Hurricane Hunter" aircraft were on display and toured by close to 600 South Florida area students and approximately 400 public residents.

***Get Ready, America! The National Hurricane Survival Initiative:***

The annual hurricane preparedness campaign, including the national hurricane preparedness television program was cancelled due to lack of sponsorship.

**Education and Outreach Programs:**

***Hurricane Andrew Anniversary Museum Exhibit – May 19th, 2017***

The Museum of Discovery & Science (MODS), located in Fort Lauderdale, FL, assisted the IHRC in developing and coordinating a new *Hurricane Andrew Anniversary* exhibit, which included a video showing original TV news and weather reports before, during and after the storm. The exhibit recounts the tremendous impact it had on the Miami-Dade County community 25 years ago on August 24<sup>th</sup>, 1992, and promotes mitigation and preparedness moving forward. MODS averages 450,000 visitors annually, including thousands of local area school children. Local officials and media attended a ribbon-cutting ceremony to debut the new exhibit on May 19<sup>th</sup>, including WSVN-TV (FOX), WPLG-TV (ABC) and WTVJ-TV (NBC). Combined local media coverage of the exhibit ribbon-cutting and *Eye of the Storm* museum event resulted in a Total Publicity Value amounting to \$8,989. This resulted in great positive visibility in the community for IHRC, FIU and FDEM’s message of mitigation.

*Hurricane Andrew Remembered* Video: <https://www.youtube.com/watch?v=aQDZxnuKCTc>



*Broward County EM & Ft. Lauderdale EM at Ribbon-Cutting Event.*



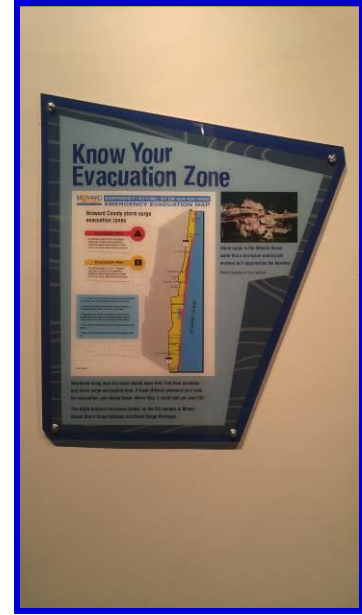
*New Andrew Anniversary Exhibit*



*Famous Andrew Picture*



*Mitigation Do's and Don'ts*



*Know Your Zone*

***Hurricane (Science, Mitigation & Preparedness) Event: Eye of the Storm – May 20th, 2017***

The Museum of Discovery & Science (MODS), located in Fort Lauderdale, FL, assisted the IHRC in planning, coordinating and facilitating this public education event. Over 2,000 people attended *Eye of the Storm*, showcasing the new Hurricane Andrew Anniversary exhibit, and special hands-on, interactive activities and demonstrations teaching hurricane science, mitigation and preparedness. This included special learning activities for parents and children providing family fun throughout the day. This collaborative community education outreach project partnered the IHRC with the Florida Division of Emergency Management, Broward County Emergency Management, City of Fort Lauderdale Emergency Management, NOAA's National Hurricane Center, NOAA's Miami Office of the National Weather Service and NOAA's Atlantic Oceanographic and Meteorological Laboratory-Hurricane Research Division. Great support was provided by Miami Dade College, the International Hurricane Protection Association, local media and 34 South Florida agencies and organizations, including the local American Red Cross.

2017 *Eye of the Storm* Video: [https://youtu.be/xu\\_lIoMjWk](https://youtu.be/xu_lIoMjWk)

Special interactive exhibits and demonstrations included:

- New Hurricane Andrew Anniversary Exhibit
- Live Air Cannon Debris Impact Testing of Shutters
- Tsunami Tim
- How the Weather Works
- Weather Jeopardy
- TV Hurricane Broadcast Center – Miami Dade College
- Live Tropical Weather Briefings by NOAA's National Hurricane Center and National Weather Service
- FIU Engineering on Wheels & FIU Wall of Wind Exhibit

Various distinguished hurricane experts participated:

- Daniel Brown, Senior Hurricane Specialist, NOAA's National Hurricane Center
- John Cangialosi, Hurricane Specialist, NOAA's National Hurricane Center
- Todd Kimberlain, Hurricane Specialist, NOAA's National Hurricane Center
- Robert Molleda, Warning Coordination Meteorologist, National Weather Service-Miami
- Dr. Pablo Santos, Meteorologist In Charge, National Weather Service-Miami
- Dr. Frank D. Marks, Director of Hurricane Research Division, NOAA/AOML/HRD
- Neal Dorst, Hurricane Researcher, NOAA/AOML/HRD
- Stanley B. Goldenberg, Research Meteorologist, NOAA/AOML/HRD
- Erica Rule, Communications and Outreach, NOAA/AOML/HRD

Special guests and presentations:

- Miguel Ascarrunz, Director of Broward County Emergency Management
- Hurricane Hunter Researchers – NOAA's AOML-HRD
- Broward County CERT Teams
- NOAA/NWS *Owlie Skywarn* Mascot
- Miami Dade College *Finn* Mascot
- City of Fort Lauderdale Emergency Management *Sparky the Fire Dog* Mascot
- Museum of Discovery and Science *Joey the Otter* Mascot

Special live interactive theater presentations:

- NOAA/NWS *Owlie Skywarn*
- *Tsunami Tim – Kids Get A Plan*

This event received great attendance and coverage by the South Florida media. Combined local media coverage of the Andrew exhibit ribbon-cutting and *Eye of the Storm* museum event resulted in a Total Publicity Value amounting to \$8,989. This resulted in great positive visibility in the community for IHRC, FIU and FDEM's message of mitigation.

The following media representatives participated:

- Natacha Lang, WSVN-TV Channel 7 (FOX)
- Betty Davis, WPLG-TV (ABC)

Total Social Media Impressions: 15,637

- Facebook: 11,014 people reached
- Twitter: 1,755 impressions
- Instagram: 2,868 impressions

**FREE MUSEUM ADMISSION**  
**Saturday, May 20, 2017**  
**10 a.m. to 5 p.m.**

# Eye of the Storm

Hurricane Science Mitigation and Preparedness

**EVENT ACTIVITIES**

**SPONSORS**  
 FIU  
 PLANI  
 BROWARD  
 FPL  
 MDC

**PARTNERS**  
 NOAA  
 NWS  
 MDC

**INTERACTIVE DEMONSTRATIONS**  
 • Tropical Weather Briefings  
 • Hurricane Hunters

**PRESENTATIONS BY HURRICANE EXPERTS**  
 • FIU Wall of Wind Researchers

**EXPLORE THE MUSEUM'S STORM CENTER**  
 • Meet our local TV meteorologists and do a hurricane broadcast together.  
 • Watch a report from the Miami Dade College TV Studio

**LIVE THEATER SHOWS FOR ALL AGES**  
 • Owlie Skywarn  
 • Tsunami Tim  
 • How the Weather Works

**Event Parking**  
 City Hall Garage • 100 North Andrews Ave.  
 Rate: \$1.00 per hour Payment: Pay by Call # 82327  
 City Hall Garage (2/F) • 100 SE 2nd Street  
 Rate: \$1.25 per hour Payment: Coins, Credit Cards, Bills

**Other Parking in the area**  
 County Lot # • SW 1 Ave and Broward Blvd.  
 North side of Government Center  
 International Village • SW 2nd Street and  
 SW 2nd Ave., SW 3rd Ave., SW 4th Ave.

**MUSEUM OF DISCOVERY & SCIENCE**  
 401 SW Second Street • Fort Lauderdale, FL • www.mds.org



*Fort Lauderdale CERT Team*



*NOAA/NWS Owlie Skywarn Live Theater Show*



*NOAA's NHC-AOML-NWS*



*FIU Wall of Wind Exhibit*



*Broward County Emergency Management*



*Weather Jeopardy NHC-NWS Celebrity Hosts*



*Fort Lauderdale EM Celebrity Weathercasters*



*American Red Cross*



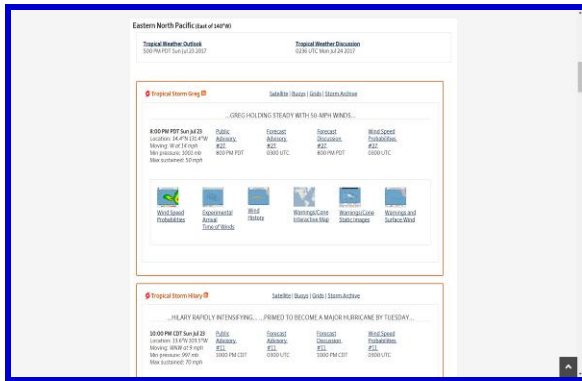
*IHPA Shutter Products Display Area*



*IHPA Live Air Cannon Missile Demonstrations*

## Hurricane Preparedness Spanish Website – June 15<sup>th</sup>, 2017

The IHRC, in partnership with NOAA’s National Hurricane Center (NHC), enhanced the Spanish language website (<https://huracanes.fiu.edu/>) with new static and live content. Hosted by FIU, the website educates and informs the public about hurricane awareness, preparedness and mitigation and includes information on hurricane science, residential mitigation strategies and descriptions of NHC information products, including tropical cyclone advisories. The goal of the website is to help the Spanish-speaking community be better educated, informed and prepared for hurricanes, including safe-guarding their families, homes and businesses. Information was collected from a variety of partners, including the Federal Alliance for Safe Homes (FLASH). The website was originally designed by FIU Digital Communications in 2015.



*New “Live” NHC Tropical Advisories*



*New “Live” NHC Tropical Weather Outlooks*



*New Storm Surge Watch & Warning Information*



*New Potential Storm Surge Flooding Map*



*New Special Needs Information*



*New Homeowner's Insurance Guide*

***NOAA Hurricane Awareness Tour – May 12th, 2017***

In conjunction with NOAA's National Hurricane Preparedness Week, IHRC joined the NOAA Hurricane Awareness Tour at the Miami-Opa Locka Executive Airport. As a kick-off to the event, IHRC participated as a speaker in the media conference which was attended by almost 20 local, national and international media outlets. NOAA's P3 Orion "Hurricane Hunter" aircraft and a U.S. Air Force Reserve WC-130J "Hurricane Hunter" aircraft were on display and toured by close to 600 South Florida area students and approximately 400 public residents. The IHRC shared information about the FIU Wall of Wind research, hurricane wind mitigation and resiliency and ways to protect your home from hurricane force winds.

**Media Conference Speakers:**

- Bryan Koon, Director of Florida Division of Emergency Management
- Rick Knabb, Ph.D., Former Director, NOAA's National Hurricane Center
- Pablo Santos, Ph.D., Meteorologist-In-Charge, National Weather Service, Miami
- Capt. Todd Lutes, Commanding Officer, U.S. Coast Guard Air Station, Miami
- Curt Sommerhoff, Director, Miami-Dade County Emergency Management
- Erik Salna, Associate Director, Extreme Events Institute, IHRC, FIU



*NOAA's WP-3D Orion Hurricane Hunter*



*U.S.A.F. Reserve WC-130J Hurricane Hunter*



*Students at FIU Wall of Wind Booth*



*Bryan Koon, FDEM Dir. and Erik Salna, IHRC*